NHSH CR-166,479

NASA-CR-166479
19860014097

A Reproduced Copy

OF

NASA CR-166,479

Reproduced for NASA

by the

NASA Scientific and Technical Information Facility

NASA CONTRACTOR REPORT 166479

Investigation to Advance Prediction Techniques of the Low-Speed Aerodynamics of V/STOL Aircraft

B. Maskew
D. Strash
J. Nathman
F. A. Dvorak

CONTRACT NAS2-11169
February 1983

NASA

NASA CONTRACTOR REPORT 166479

Investigation to Advance Prediction Techniques of the Low-Speed Aerodynamics of V/STOL Aircraft

B. Maskew
D. Strash
J. Nathman
F. A. Dvorak
Analytical Methods, Inc.
2047 - 152nd Avenue N.E.
Redmond, Washington 98052

Prepared for
Ames Research Center
under Contract NAS2-11169

National Aeronautics and
Space Administration

Ames Research Center
Moffett Field, California 94035

ABSTRACT

A computer program, VSAERO, has been applied to a number of V/STOL configurations with a view to advancing prediction techniques for the low-speed aerodynamic characteristics. The program couples a low-order panel method with surface streamline calculation and integral boundary layer procedures. The panel method--which uses piecewise constant source and doublet panels--includes an iterative procedure for wake shape and models boundary layer displacement effect using the source transpiration technique. Certain improvements to a basic "vortex tube" jet model were installed in the code prior to evaluation.

Very promising results were obtained for surface pressures near a jet issuing at 90° from a flat plate. A solid core model was used in the initial part of the jet with a simple entrainment model. Preliminary representation of the downstream separation zone significantly improved the correlation.

The program accurately predicted the pressure distribution inside the inlet on the Grumman 698-411 design at a range of flight conditions. Furthermore, coupled viscous/potential flow calculations gave very close correlation with experimentally determined operational boundaries dictated by the onset of separation inside the inlet. Experimentally observed degradation of these operational boundaries between nacelle-alone tests and tests on the full configuration were also indicated by the calculation.

Application of the program to the General Dynamics STOL fighter design were equally encouraging. Very close agreement was observed between experiment and calculation for the effects of power on pressure distribution, lift and lift curve slope. In an absolute sense the basic lift curve slope predicted by the program was lower than experiment, primarily because the leading-edge vortices, which occur at the higher angles of attack were not modelled at this stage. The wake-relaxation capability in the VSAERO code was especially important in obtaining good correlation with experimental wing pressure distributions in the presence of the canard wake.

Overall, these initial applications of the VSAERO program to the prediction of aerodynamic characteristics of V/STOL configurations has been most successful and promise further potential improvements in the future. Furthermore, it has been demonstrated that these V/STOL calculations are both practical and economical in computing time.

TABLE OF CONTENTS

TABLE OF CONTENTS (Concluded)

LIST OF FIGURES

LIST OF FIGURES (Continued)

LIST OF FIGURES (Continued)

LIST OF FIGURES (Continued)

LIST OF FIGURES (Continued)

LIST OF FIGURES (Concluded)

1.0 INTRODUCTION

Predicting the low-speed aerodynamic characteristics of vertical and short take-off and landing (V/STOL) aircraft requires the analysis of complex configurations in the presence of multi-energy regions embedded in the general onset flow. The problem is highly nonlinear due to the mutual interaction between free wakes, jets and the airframe and also due to viscous effects and edge vortices at the high angles of attack. Many reviews of both V/STOL prediction techniques and the jet-in-crossflow interaction problems can be found in the literature (1) through (6). Panel methods still offer the most successful basis for predicting characteristics for the general configurations. These use surface singularity distributions based on the Green's Identity formulation (7). The singularity integrals are performed in a piecewise manner over a large number of panels (8). The present report investigates the application of such a program, VSAERO (9), developed at Analytical Methods, Inc., Redmond, Washington, to V/STOL cases with a view to advancing these aerodynamic prediction techniques.

The VSAERO program includes a general potential flow panel method with a wake-relaxation iterative scheme and simple "vortex-tube" jet modelling capability; this is coupled with a surface-streamline tracing routine and with integral boundary layer methods. In the viscous/potential flow iteration cycle, boundary layer displacement effects are modelled using the source transpiration technique.

The versatility of panel methods in their ability to represent complex geometries fills a basic requirement for modelling general V/STOL configurations. In the past, however, there have been drawbacks in such applications. First, earlier panel methods based primarily on source panels with external Neumann boundary condition (e.g., (8)) suffered severely from "leakage" in flows inside inlet ducts and narrow channels. Secondly, the more recent generation of high-order panel methods (e.g., (10)) has lost some of the earlier versatility for general application and ease of data preparation; moreover, computation costs for these methods have risen to such an extent that the necessary iterative approach for solving the nonlinear problems of V/STOL configurations is no longer practical. On the other hand, the VSAERO program is essentially a second generation low-order panel method which maintains and even exceeds the versatility and ease of data preparation of earlier low-order panel methods. Also, the low running cost has been maintained making it practical for application to iterative solutions. Furthermore, the program has essentially overcome the deficiencies associated with earlier low-order panel methods (9).

In the present report the results of a background literature survey are described in Section 2. Section 3 gives a brief description of changes made in the VSAERO model during the course of the work; it includes a description of a two-dimensional pilot

code version of VSAERO used for checking the model changes prior to installation in the full program. In Section 4 the VSAERO program is evaluated in application to basic jets in crossflow situations. In Section 5, the program is applied to two full V/STOL configurations, the Grumman Design 698-411 tilt-nacelle, V/STOL aircraft and the General Dynamics powered STOL fighter model. Finally, in Section 6, the effectiveness of the VSAERO jet model is validated subsequent to a wake relaxation for three V/STOL related configurations

2.0 BACKGROUND

A literature survey was undertaken to identify and review past and ongoing related work in the areas of theoretical and empirical prediction techniques and experimental and flight-test results on V/STOL configurations. The review was conducted with a threefold objective: first, existing theoretical and empirical prediction methods were examined with a view to incorporating existing "good" techniques into the VSAERO code. Secondly, experimental and flight test data were examined for suitable correlation cases and, finally, information on jet flow characteristics was examined with a view to developing a more physically accurate yet practical mathematical model of the turbulent jet in crossflow. Specifically, the existing simple vortex-tube jet model in VSAERO required improvement for the treatment of inclined jets and for close jet/surface interactions.

Many reviews of both V/STOL prediction techniques and the jet crossflow interaction problem can be found in the literature. The work prior to 1970 has been summarized by Margason (1) and reviews by Wooler et al. (2), M.F. Platzer (3) and (4), D.R. Chapman (5), and D.H. Hickey (6) treat the status of more recent V/STOL prediction techniques. This section gives a brief but concise overview of the condition of V/STOL prediction techniques and how they relate to the present effort. Review of the existing prediction techniques is divided into four main classifications.

* Inviscid Potential Flow Methods
* Empirical Prediction Techniques
* Patched Potential Flow Viscous Flow Methods
* Viscous Flow Methods

2.1 Inviscid Potential Flow Methods

Flow conditions dominated by large areas of attached flow are treated with much success by these prediction techniques which are commonly called "panel methods". Several variations of this method currently exist in industry which utilize singularity distributions such as doublets, sources and vortices in the form of panels to model the desired configuration. An integral equation of the second kind can be formulated using Green's Identities (7) to solve for the singularity distribution on the body.

Typical examples of such methods applicable to subsonic flows are the Hess code (8), program VSAERO (9), and Pan Air (10), which are all three-dimensional panel methods. These methods are applicable to subsonic flows while recent success in the transonic regime is realized in the work by Boppe (11). This code will calculate the flow about wing-body-pylon-nacelle configurations with reasonabally good correlation with experiment.

There exist many theoretical treatments dealing with the subject of jet-induced pressures and loads which fall under the category of inviscid potential flow methods. Early work by Spence (12) treated the jet-flap case taking into account the momentum of the jet to determine the jet radius of curvature. Shollenberger (13) and (14), has formulated a flow singularity model for wing/jet interaction analysis. This technique uses an iterative scheme to determine the proper jet vorticity and the jet boundary location based on the tangential flow boundary condition along the jet.

The analysis of P.T. Wooler (15) et al. utilizes the continuity and momentum equations to provide the jet path. The constants of integration for the jet equations of motion are determined by reference to experimentally determined jet trajectories. The characteristic kidney shape is approximated by an ellipse and the jet entrainment is approximated by distributing sinks along the ellipse major axis. The blockage effect of the jet is represented by a distribution of doublets along the jet axis. The sink strengths are made proportional to the mass of air entrained and the doublet strengths are determined from the jet geometry.

Combining Wooler's jet momentum interpretation with Shollenberger's geometric model and providing for an iterative solution to the jet trajectory and boundary distortion is one of the proposed improvements in the VSAERO jet model.

2.2 Empirical Prediction Techniques

A complete treatment of these methods is not practical within a limited space due to their inherent limited range of application. Related empirical studies dealing with the jet-crossflow interaction problem and a few V/STOL configurations chosen for analysis are presented in Section 2.5 of this report.

The importance of empirical prediction methods to V/STOL aircraft design and development cannot be overlooked. In the analysis of specific V/STOL configurations, wind tunnel testing is necessary to predict or verify the overall performance capabilities of the design as well as to visualize local regions of viscous, turbulent and separated flow present in most V/STOL applications.

An empirical model of the jet centerline (16) has been employed in the present work to set up the initial mathematical model of the jet to reduce the number of iterations needed for convergence. Also, a vorticity decay model (17), (18) is applicable to represent the diffusion of the jet.

2.3 Patched Potential Flow Viscous Flow Methods

Work in this area has primarily concentrated on the coupling of a boundary layer analysis with a potential flow method to determine overall aircraft drag or the performance of flap systems (4).

Boundary layer methods can be generally separated into two categories: finite-difference methods and integral methods. The integral method is primarily for the analysis of two-dimensional flows due to the need for a velocity profile model. In two-dimensional flows the velocity profile is described by a family of curves whereas in three-dimensional flows the velocity profile on the body does not conform to a general model. The advantage of using the integral method in boundary layer analysis is the relatively low computing costs when compared to the other methods. The finite-difference method solves the boundary layer equations directly through discretization without assuming a velocity profile (19).

An integral method is currently being used in Program VSAERO in a fully coupled viscid/inviscid iterative procedure. This is applicable to both the external and inlet-duct regions of the V/STOL configurations.

2.4 Viscous Flow Methods

Solutions under this category are based on various forms of the Navier-Stokes equations which thus far have no applications to practical aircraft configurations. The major effort in computational viscous flow solutions is being concentrated on two-dimensional flow problems such as blunt-body flows, leading-edge flows and shock-wave/boundary layer interactions (20), (21), with very limited success in the area of three-dimensional flow problems (18). This apparent restriction is a result of the inability at this time to accurately predict such regions as those exhibiting large flow gradients, turbulence, unsteadiness, three dimensionality and separated flow zones.

Restrictions placed on the grid size for the computational domain are directly related to the available computer memory capacity. With recent developments in the field of computer technology (22), the analysis of practical three-dimensional wing-body configurations with the full Reynolds averaged Navier-Stokes equations could be possible in the near future (5), but at the present time the large computer run times are a very real impediment.

The possibility exists that future work could call for the coupling of VSAERO with a Navier-Stokes technique for zonal flow analysis in critical regions characteristic of V/STOL configurations.

More detailed information concerning viscous flow methods can be found in recent reviews by Graves (22) and Chapman (5), and in an earlier report by Platzer and Margason (18).

2.5 Experimental Work and Flight Test Results

The objective of Section 2.5 is to present pertinent sources of information that may be used for data correlation purposes in the present work. A number of excellent reviews currently exist which summarize presently available work on the subject of V/STOL aircraft, and, more specifically, in the area of jets in a subsonic crossflow (23). The work by D.H. Hickey (6) on the subject of V/STOL configurations and the work by Margason (1) and (4), Wooler (2) and Platzer (3) and (4) on the subject of jets in a crossflow are all excellent reviews.

The V/STOL configurations outlined in this section include the very simple flat plate and body of revolution test cases analyzed using the proposed potential flow pilot code, as well as the full V/STOL configurations examined using the potential flow code, VSAERO, with improved jet model.

2.5.1 Jets in a Subsonic Crosswind

(15) "Pressure Distribution on a Rectangular Wing with a Jet Exhausting Normally into an Air Stream", Wooler, P.T., Burghart, G.H. and Gallagher, J.T.

A theoretical model of the flow is presented which utilizes continuity and momentum as an initial step to determine the jet path in a crosswind. The velocity field induced by the jet is simulated by replacing the jet with a sink-doublet distribution in such a manner as to model both the blockage effects (doublet) and the entrainment effects (sink) of the jet. the expected kidney-shaped jet cross section is approximated by an ellipse downstream of the orifice with the sink distribution located along the major axis as shown in Figure 1.

Due to the effective treatment of important physical considerations the correlation with experiment is good for a 10% thick straight wing with AR=3.

(14) "Three-Dimensional Wing/Jet Interaction Analysis Including Jet Distortion Influences", Shollenberger, C.A.

A theoretical model of the flow is presented which employs the vortex-lattice formulation to describe both the wing and jet boundaries. The wing is divided into chordwise divisions and spanwise strips such that the entire lifting surface is composed of quadrilateral panels which may be nonplanar. The jet boundary is modelled in a similar fashion with the jet cross vorticity component located along the mid-panel line as opposed to the quarter panel line in the lifting-surface case, as shown in Figure 2. An iterative procedure is employed to determine the shape and location of the jet boundary through successive application of the tangential flow boundary condition at the jet panel corners.

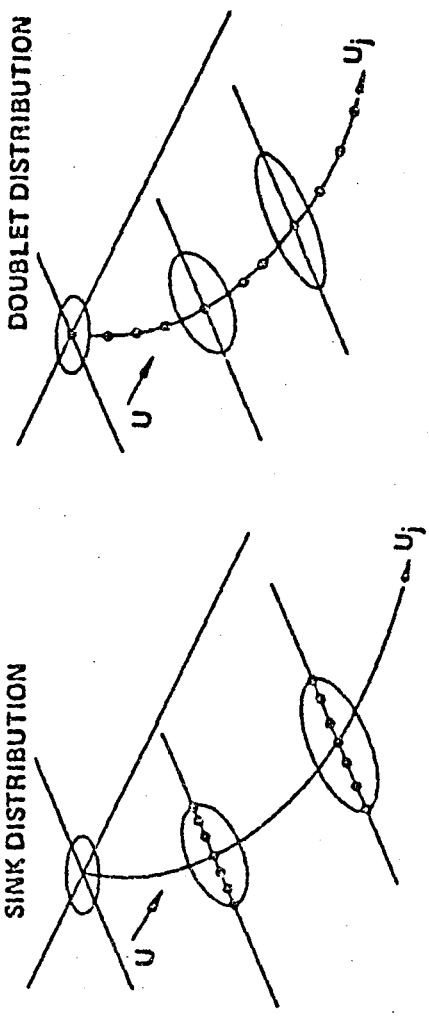

Figure 1. Wooler Sink/Doublet Distribution (Ref. 15).

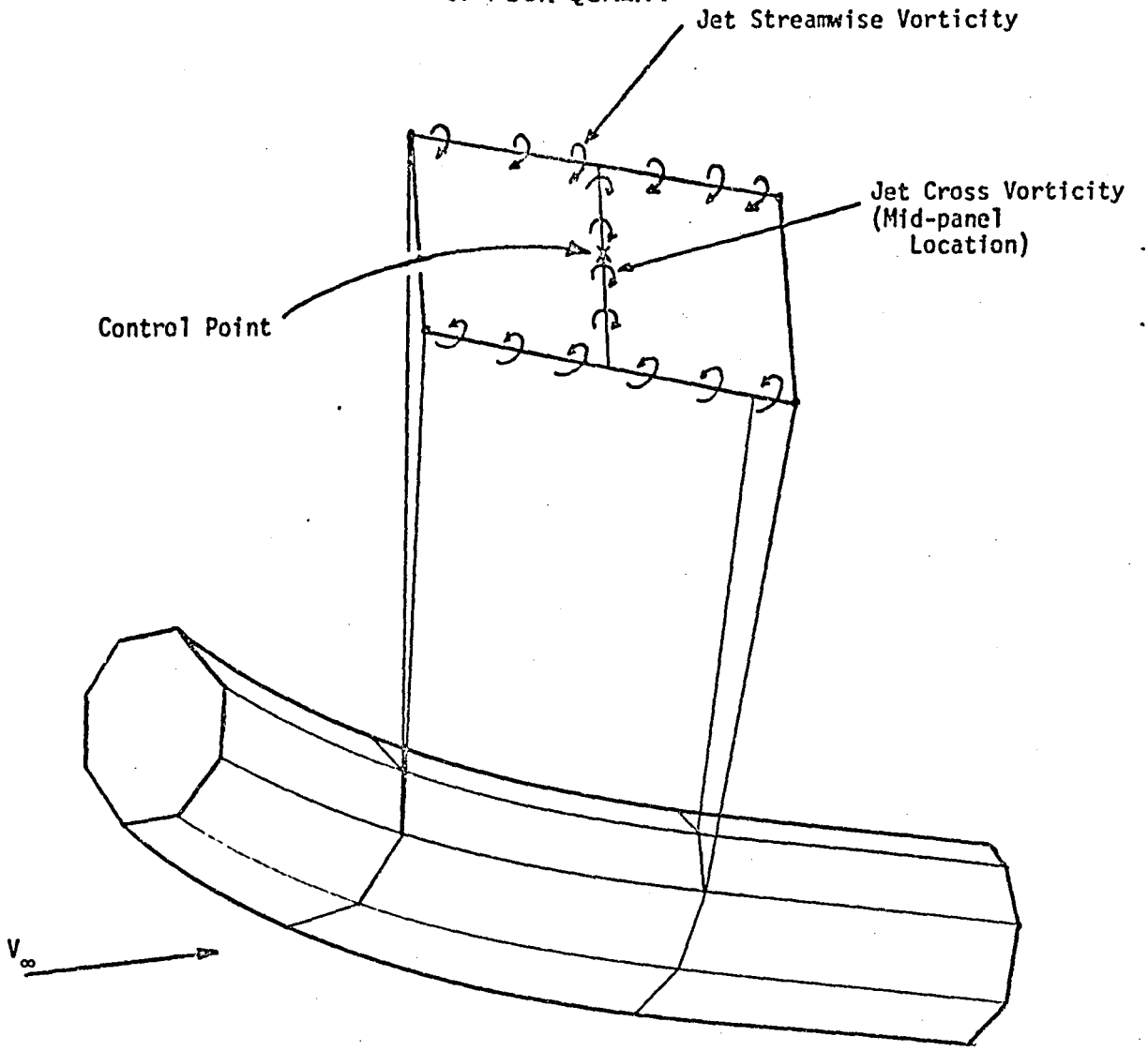

Figure 2. Shollenberger Jet Boundary--Vortex Panel Arrangement (Ref. 14).

Reasonably good correlation with previous methods is observed, but more importantly, the model can be used as a general method which lends itself to further modification.

(17) "Vorticity Associated with a Jet in a Cross Flow", Fearn, R., and Weston, R.P.

An experimental investigation is presented which examines the characteristics of the pair of contrarotating vortices associated with a round, turbulent jet directed normally through a flat plate into a subsonic cross flow. The analysis represents the first quantitative description of the pair of contrarotating vortices and includes their location, strength and diffuseness for jet-to-cross-flow velocity ratios of $3 \leq R \leq 10$. Two vortex models are introduced to give a quantitative description of the vortices. The simpler model employs the measured upwash velocity along the local vertical axis in the plane perpendicular to the jet (see Figure 3) to determine the strength and location of two infinite vortex filaments. The more complex model assumes a Gaussian distribution of vorticity which defines the strength, location and diffuseness of the vortex pair given all the measured upwash velocities in that cross section.

A least squares curve fit of the jet centerline and vortex curve locations is presented along with very useful observations into the physical aspects of the dominant features of a jet in a cross flow.

(16) "The Path of a Jet Directed at Large Angles to a Subsonic Free Stream", Margason, R.J.

An experimental investigation is presented which examines the path of the jet centerline, defined as the locus of points of maximum jet velocity. The best empirical fit to the data is determined and is presented as a function of velocity ratio and jet deflection angle (see Figure 3). The jet deflection angles ranged in 30° increments from 30° to 180° from the free stream and effective velocity ratios in the range of $1.2 \leq R \leq 10$.

(18) "Experimental Investigation of Effect of Jet Decay Rate on Jet-Induced Pressures on a Flat Plate", Kuhlman, J.M., Ousterhout, D.S. and Warcup, R.W.

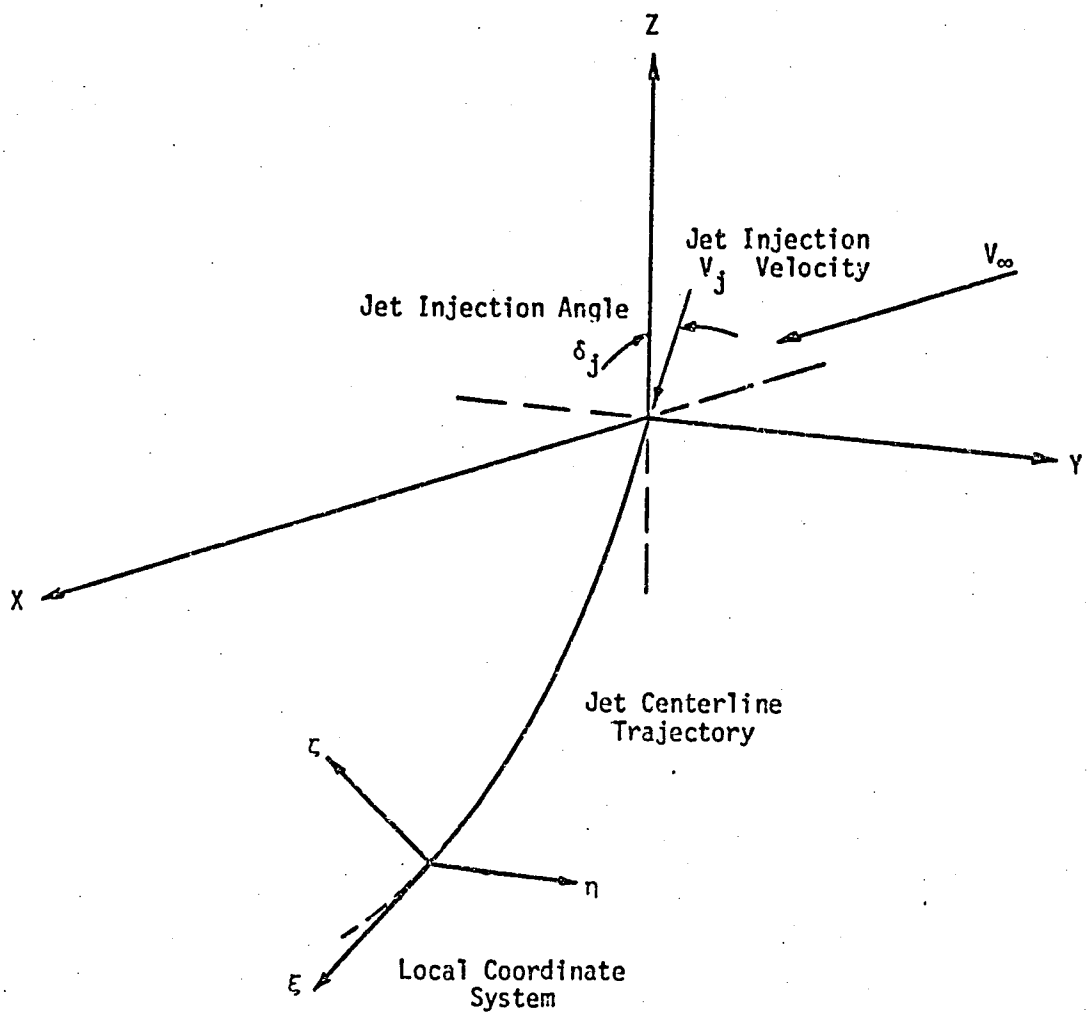

Figure 3. Jet Coordinate Axis Definition.

An experimental investigation into the effects of jet decay rate on the induced flat plate pressures is presented for the case of an unheated, subsonic circular jet exiting normally from a flat plate in a subsonic cross flow as shown in Figure 4. The jet decay rate was varied through use of cylindrical centerbodies submerged at various depths below the jet exit plane for jet-to-crossflow velocity ratios of $2.2 \leq R \leq 10$.

A volume of tabulated data from the experimental investigation is compiled in a separate report presented by the same authors.

(24) "Induced Pressure Distribution of a Jet in a Cross Flow", Fearn, R.L. and Weston, R.P.

An experimental investigation is presented which examines the pressure distribution on a flat plate with a four-inch diameter, subsonic jet exiting normal to the plate. Detailed pressure measurements are presented in tabular and graphical form with an extensive summary of conclusions which examines the effects of varying the velocity ratio from 2 to 10 on the flat plate pressure distribution.

(25) "Experimental Investigation of Jet Inclined to a Subsonic Cross Flow", Aoyagi, K. and Snyder, P.K.

An experimental investigation is presented which examines the flow field close to a jet issuing from a flat plate and a body of revolution at several nozzle injection angles as shown in Figures 5 and 6. Flat plate pressures were obtained for a single round jet inclined to the cross flow and the pressure distribution for the body of revolution was obtained for the case of two round jets spaced to six nozzle diameters apart as well as a single jet configuration.

Mean velocity measurements were obtained with laser velocimeter surveys near the jet orifice to more fully understand the entrainment mechanism.

2.5.2 V/STOL Configurations

(26) "Evaluation of Pressure and Thermal Data from a Wind Tunnel Test of a Large-Scale, Powered STOL Fighter Model", Howell, G.A., Crosthwait, E.L. and Witte, M.C.

The wind tunnel test program of a large-scale STOL fighter model, shown in Figures 7 and 8, is presented. The investigation was conducted by Ames Research Center in the NASA/Ames 40- x 80-foot wind tunnel. General Dynamics, Fort Worth Division, provided the lines for the model under contract with NASA Ames.

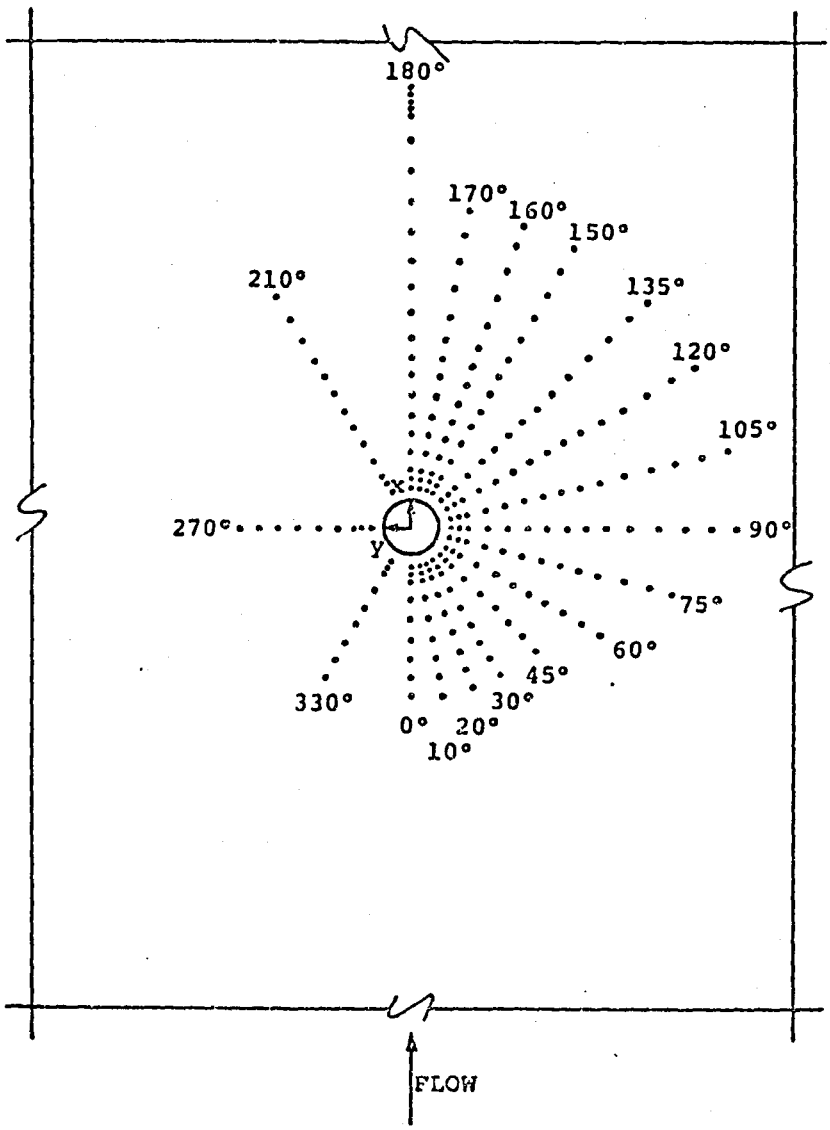

Plate pressure port distribution.

Figure 4. Kuhlman et al. Experimental Set-Up (Flat Plate), Ref. 18.

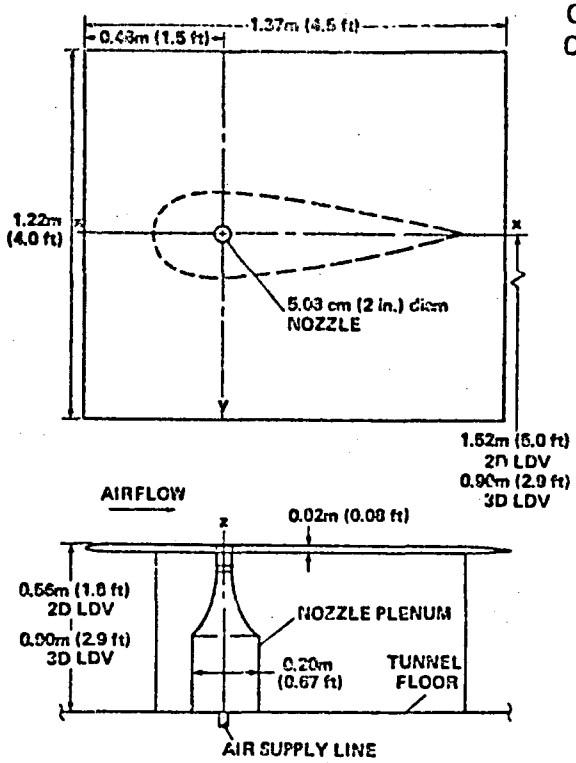

Jet in a crossflow model used with 2D and 3D laser-doppler velocimeter.

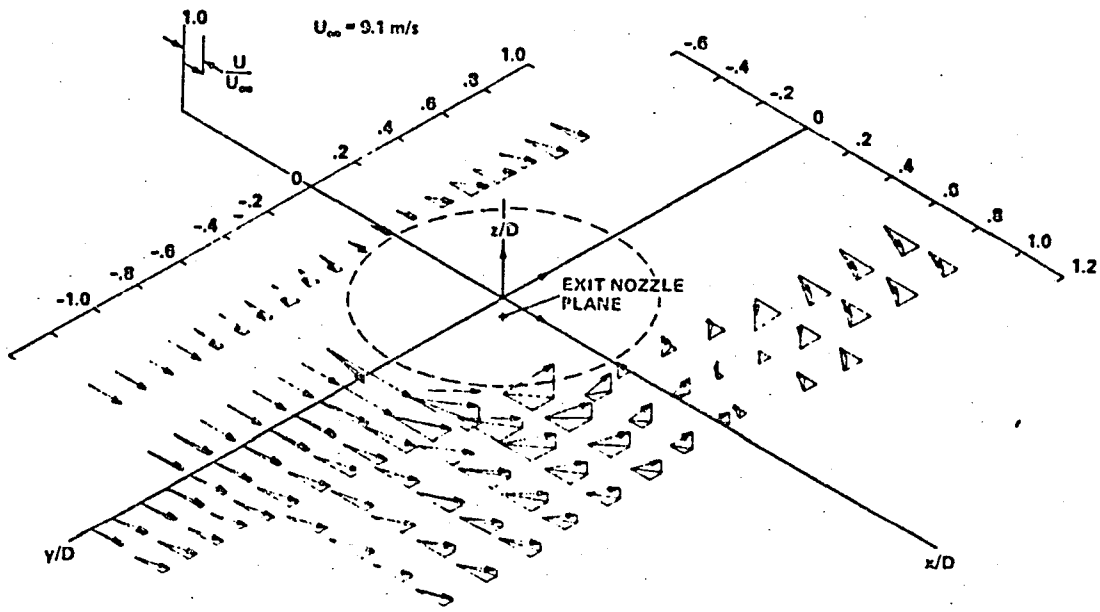

Mean velocity vector plot from 3D LDV data; z/D = 0.71, R = 7.6, jet velocity 69.3 m/sec.

Figure 5. Aoyagi et al. Experimental Set-Up (Flat Plate), Ref. 25.

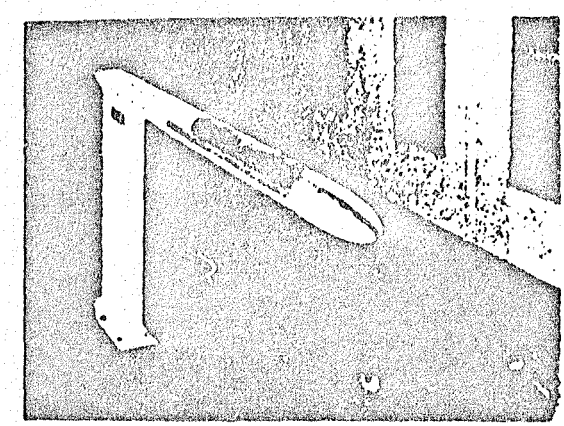

Body of revolution model as mounted in the NASA Ames 7- by 10-Foot Wind Tunnel.

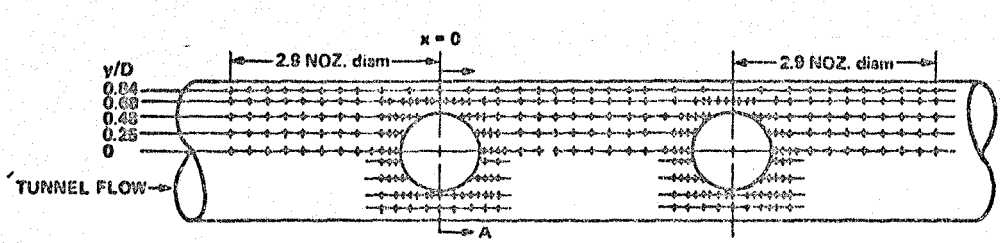

PLAN VIEW WITH SURFACE PRESSURE LAYOUT

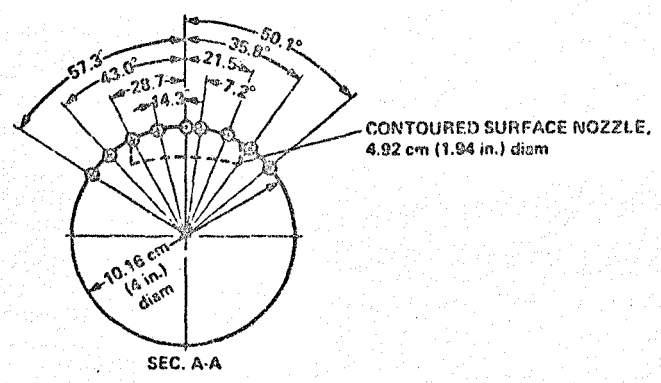

SEC. A-A

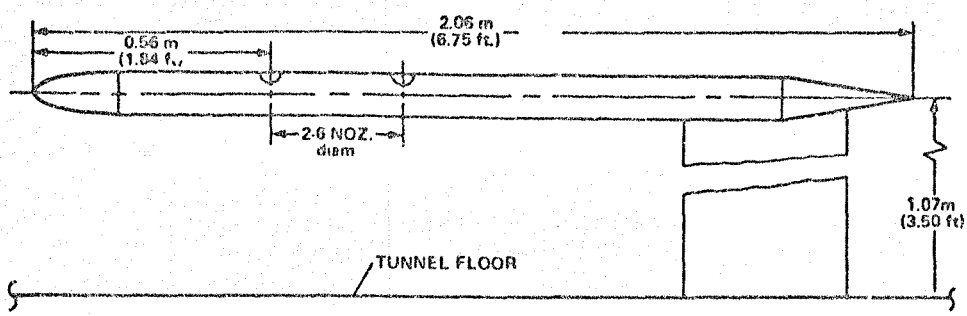

Body of revolution model with surface pressure layout.

Figure 6. Aoyagi et al. Experimental Set-Up (Body of Revolution), Ref. 25.

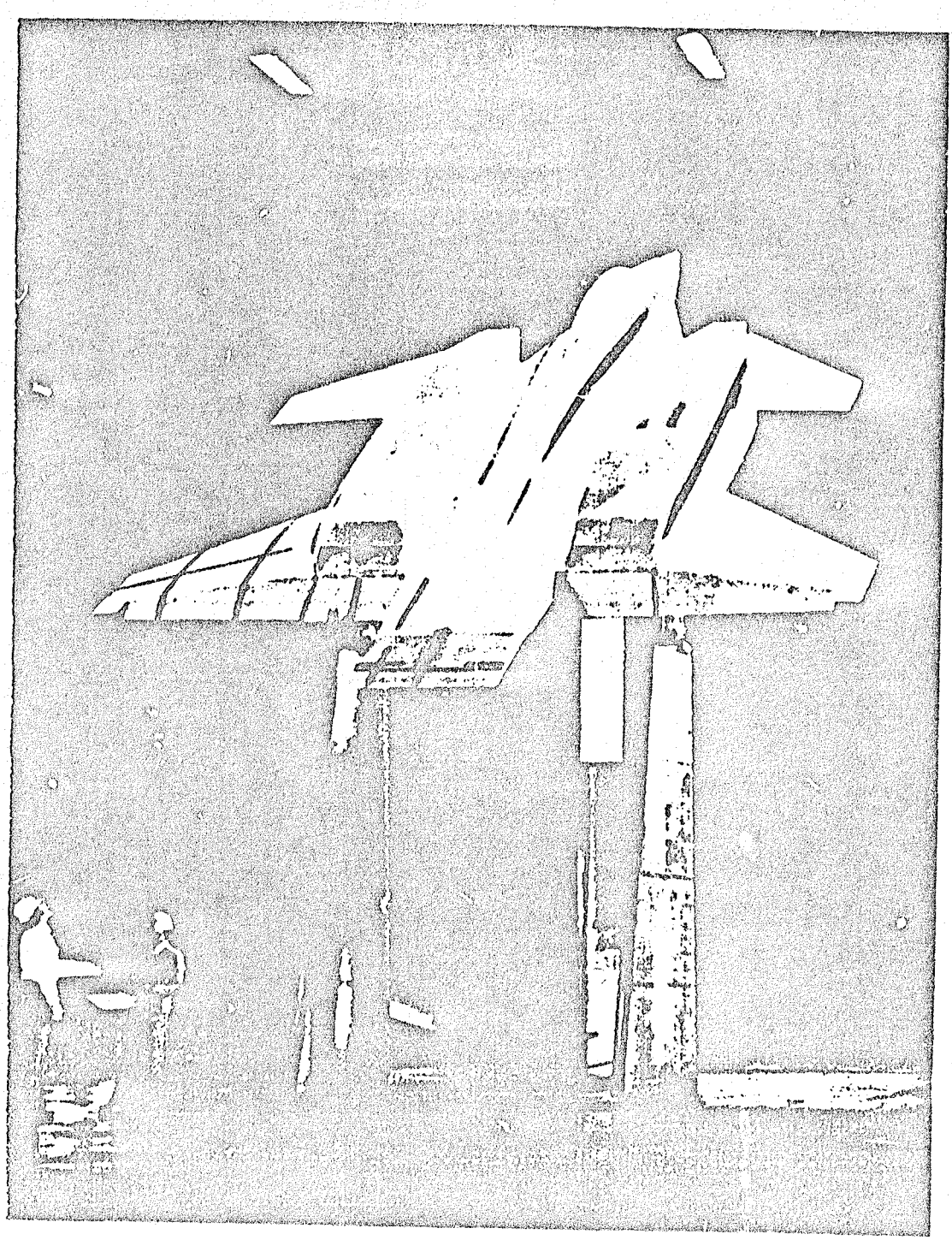

Figure 7. STOL Fighter Model in NASA/Ames 40- x 80-Foot Wind Tunel, Upper View (Ref. 26).

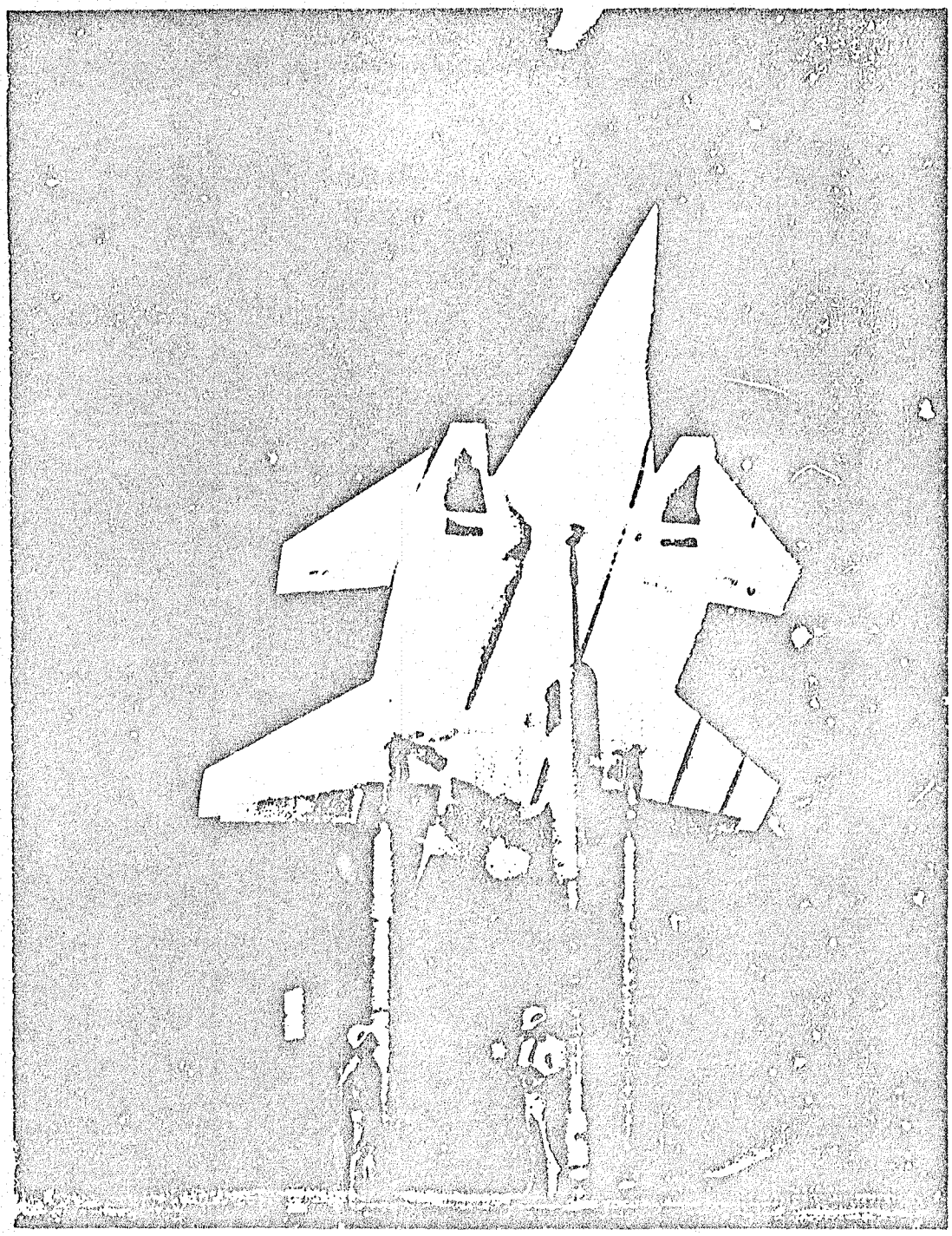

Figure 8. STOL Fighter Model in NASA/Ames 40- x 80-Foot Wind Tunnel, Lower View (Ref. 26).

The model was approximately 3/4-scale of an operational fighter and was powered by two General Electric J-97 turbojet engines. The effects of spanwise blowing and control-surface deflection were examined with limited pressure and thermal instrumentation.

(27) "Full Scale Tests of Grumman Design 698-411 Tilt Nacelle V/STOL Model at the NASA Ames Research Center", Grumman Aerospace Corporation.

The wind tunnel and static stand test program of a full-scale powered model of a high-performance, subsonic tilt-nacelle V/STOL concept, shown in Figures 9 and 10, is presented. The tests were conducted by NASA and Grumman Aerospace Corporation at the NASA Ames 40- x 80-foot wind tunnel and the NASA Ames outdoor Static Stand for a joint NASA/Naval Air Systems Command and Grumman Aerospace Corporation program. The transition speed range of the V/STOL concept was examined by utilizing a large-scale model with an 11.2 m wing span and two TF-34 turbofan engines.

(28) "Large-Scale Wind Tunnel Tests of a Sting-Supported VATOL Fighter Model at High Angles of Attack", Stoll, F. and Minter, E.A.

In the first use of the new sting model support developed for the NASA Ames 40- x 80-foot wind tunnel, a 0.4-scale model of a VATOL fighter, shown in Figure 11 was tested to angles of attack exceeding 90o. The model was based on a two-engine fighter configuration developed by the Vought Corporation under a NASA/Navy jointly sponsored contract.

The wind tunnel pressure data is available in a previous report which includes an overall analysis of the design (29).

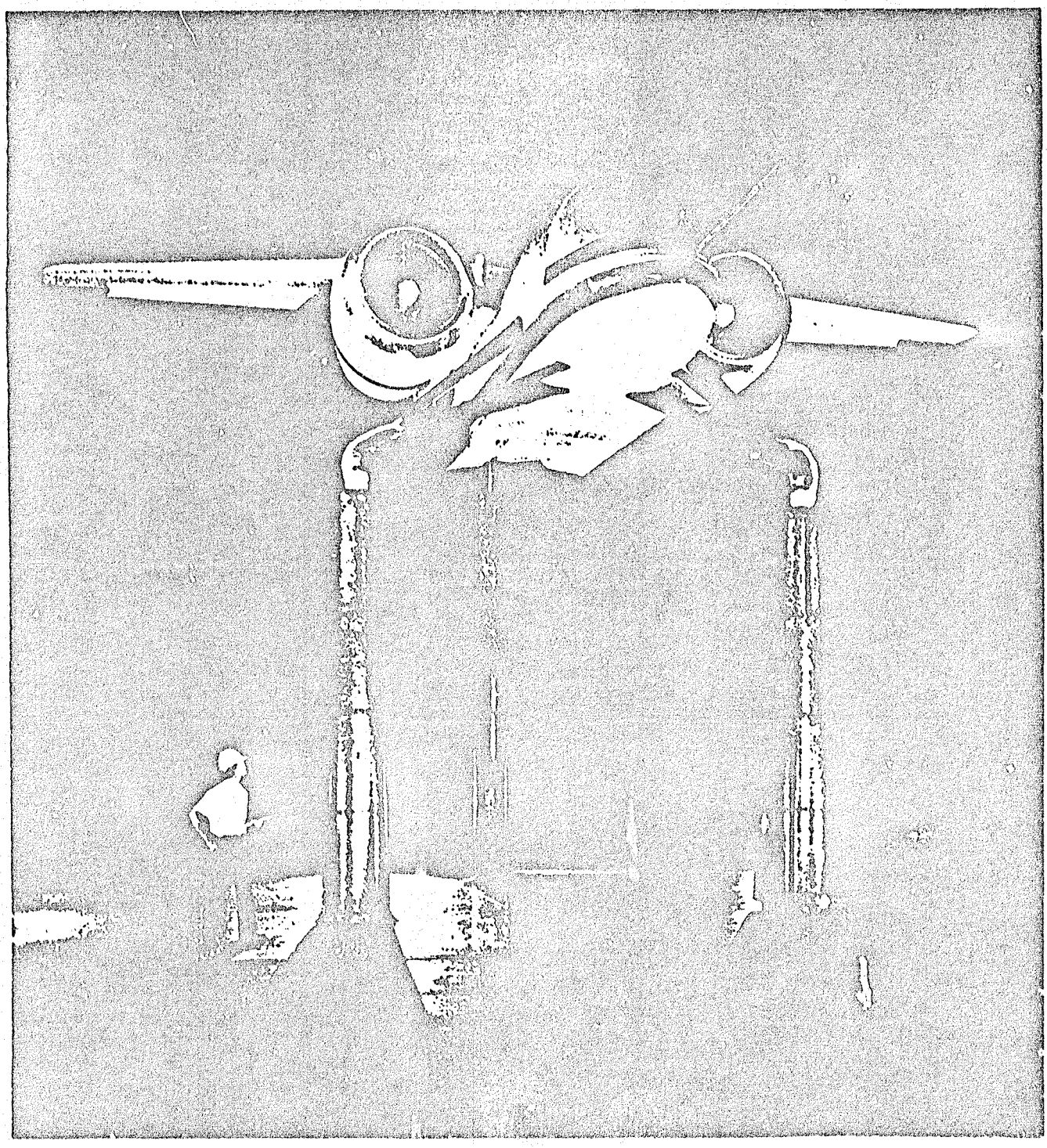

Figure 9. Grumman Design 698-411 Full-Scale, Tilt-Nacelle V/STOL Model, Ref. 27.

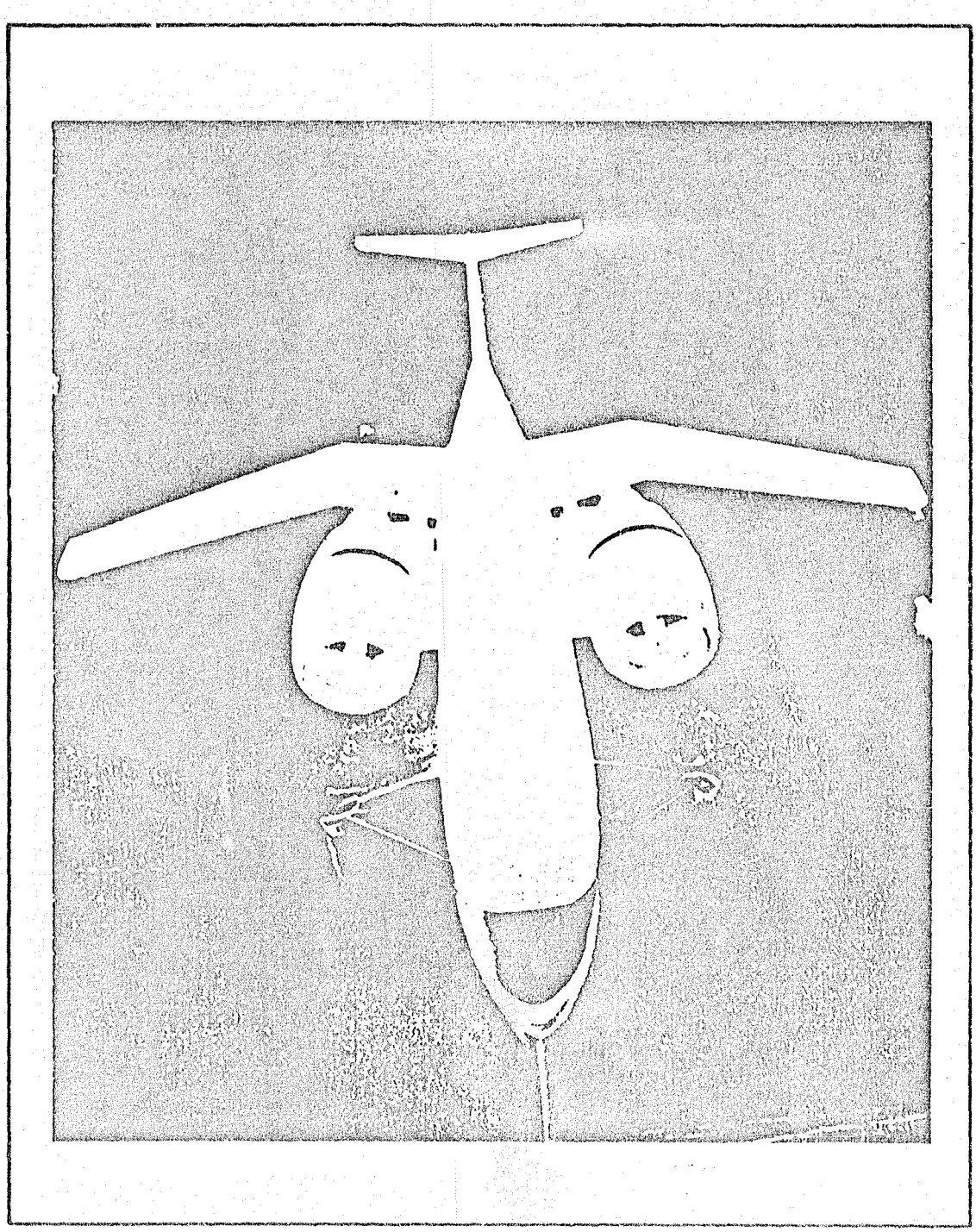

Figure 10. Grumman Design 698-411 Full-Scale, Tilt-Nacelle V/STOL Model (Ref. 27).

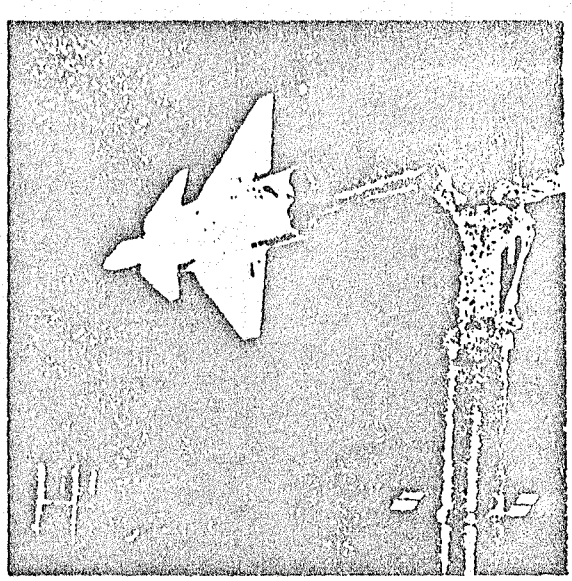

Model installed.

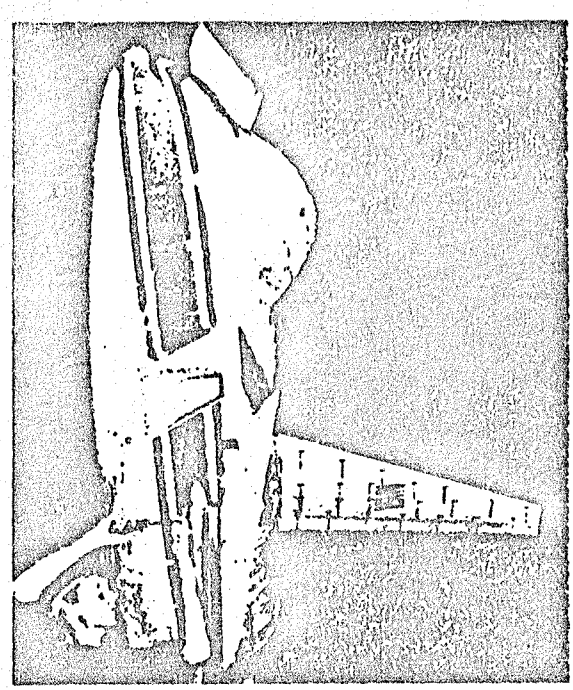

Front view of model.

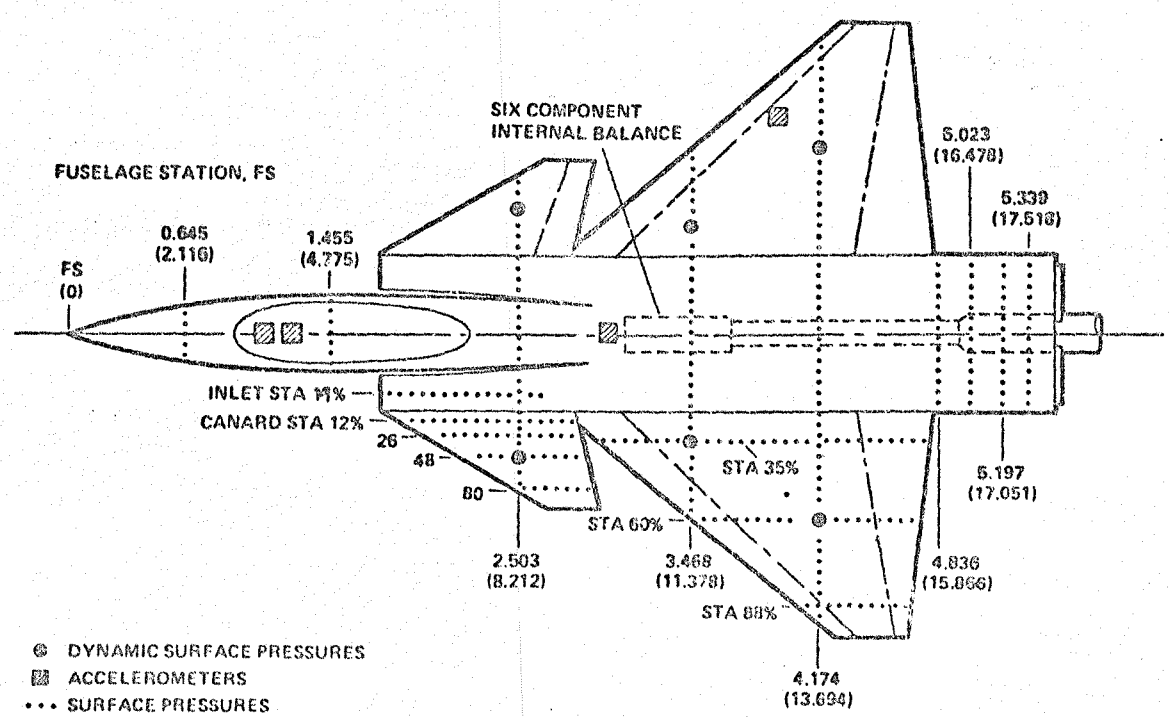

Figure 11(a). Large-Scale VATOL Fighter Model (Ref. 29).

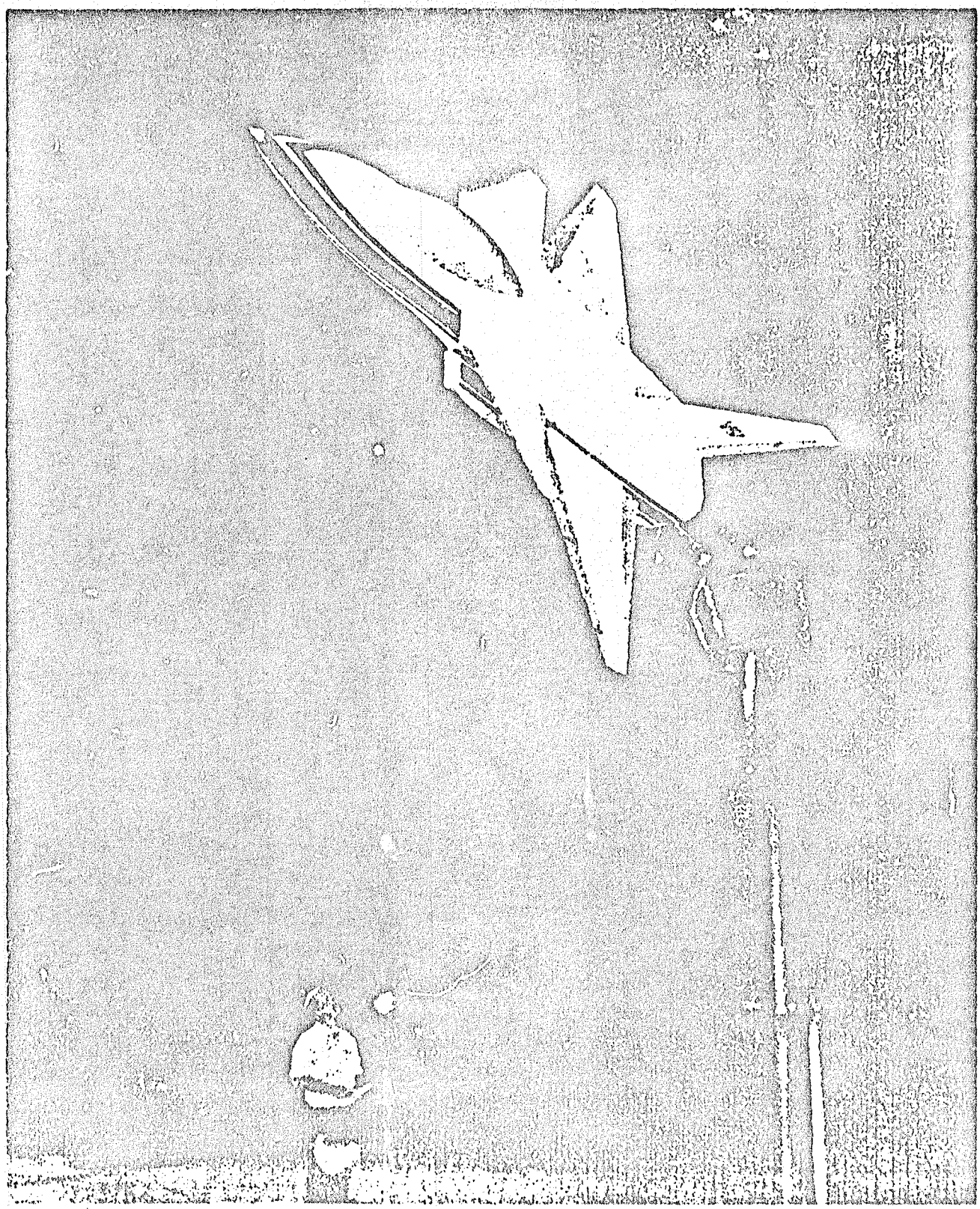

Figure 11(b). Large-Scale VATOL Fighter Model (Ref. 29).

2.6 Characteristics of a Jet in a Subsonic Crosswind

Section 2.6 consists of a summary of results compiled from several experimental investigations into the characteristics of a round, subsonic jet exiting at large angles to a subsonic crosswind. These characteristics are an important consideration when developing a physically accurate theoretical model for the jet-crosswind interaction problem. A complete treatment of turbulent jets has been written by Abramovich (30) and should be consulted for theoretical background.

2.6.1 General Description

A considerable amount of information is available in the literature which deals with the important physical aspects of a jet in a cross flow (Refs. 31 through 40). The dominant characteristics common to many analyses are the two modes of entrainment which, as shown by Kamotani and Greber (36), (41), act independently to control the rate of entrainment. One mode is similar to that of the free jet, which appears due to the relative velocity difference between the jet and stream fluid. This shear layer creates a turbulent mixing layer around the jet periphery which effectively grows in the jet flow direction, thus entraining main stream fluid. The second mode of entrainment is a result of the pair of contrarotating vortices which are produced by the interaction between the free stream and the jet component normal to the free stream.

The vorticity generation will reach a maximum within the curvilinar region of the jet (23), (42) and diffuse at a rate which is a function of the arc length along the vortex curve, but which is a weak function of the effective velocity ratio (17). The vortices gradually weaken each other by the diffusion of vorticity across the plane of symmetry at a rate which is much slower than the jet velocity decay rate. As shown by Fearn and Weston (17), the pair of contrarotating vortices are easily detectable 45 jet diameters while Pratte and Baines (43) reported that the vortices were detected up to 1,000 jet diameters downstream of the jet orifice. In comparison, the jet centerline, defined by the locus of points of maximum jet velocity in the symmetry plane, was detected only up to 15 jet diameters downstream, beyond which no detectable difference between the jet velocity and the freestream flow was measured (17). It should be noted that the jet-to-freestream velocity ratio was varied from 3 to 10 in this analysis.

2.6.2 Zonal Flow Definition

An effective and analytically convenient description of a round jet issuing at angles near 90° is described by J.F. Keffer (23). The jet is separated into three regions of influence:

1. Source Flow Zone
2. Curvilinear Zone
3. Far-Field Zone

The source flow zone is marked by a conical shaped core of potential fluid near the jet orifice with the length, as shown by R.L. Fearn (24), following a second-order variation with velocity ratio. Within this region the fluid is considered to have a negligible degree of turbulence when compared to the fully developed turbulent flow of the other two zones. For velocity ratios greater than about four, the potential core possesses a sufficient amount of axial momentum to resist appreciable deflection by the cross flow. The fluid on the sides of the jet tends to deflect due to the lateral shearing action to form the characteristic kidney-shaped cross section at the end of the potential core zone.

The curvilinear zone is dominated by two modes of entrainment, as described above, with the combined effect of dispersing axial momentum over a steadily increasing area and thus deflecting the jet downwind. At the beginning of the curvilinear zone, the velocity profile taken in the streamwise direction (i.e., normal to the jet cross section), is more or less Gaussian (26). The flow at this point is fully developed with a separated flow region downstream of the jet and the jet blockage effect felt upstream of the jet in the form of a positive pressure region.

The far-field zone consists of flow dominated by the pair of contrarotating vortices with the axial jet velocity reaching a negligible magnitude. The rate of entrainment and the amount of jet spread falls off dramatically in this zone, as shown by Pratte and Baines (43), (23).

2.6.3 Jet-Induced Effects

Several experimental investigations have treated the jet induced pressures and loads on a flat plate or wing with application to V/STOL aerodynamics. A generally consistent description of the pressure distribution around the jet orifice has resulted from these analyses and is shown for two investigations in Figure 12 (Ref. 18). The flow upstream of the jet orifice is decelerated and thus produces a positive pressure region. A negative pressure region exists to the side and rear of the jet due to entrainment and flow separation downstream of the jet orifice. This negative pressure region acts to reduce the lift force on the flat plate and the asymmetrical pressure distribution fore and aft of the jet tends to produce a nose-up pitching moment. The tendency is for both the pitching moment and the lift loss to increase with increased free stream velocity (18). This result is verified by Fearn and Weston (35), and is apparently due to the growth in the negative pressure area to the side and behind the jet orifice and the decrease in both magnitude and area of

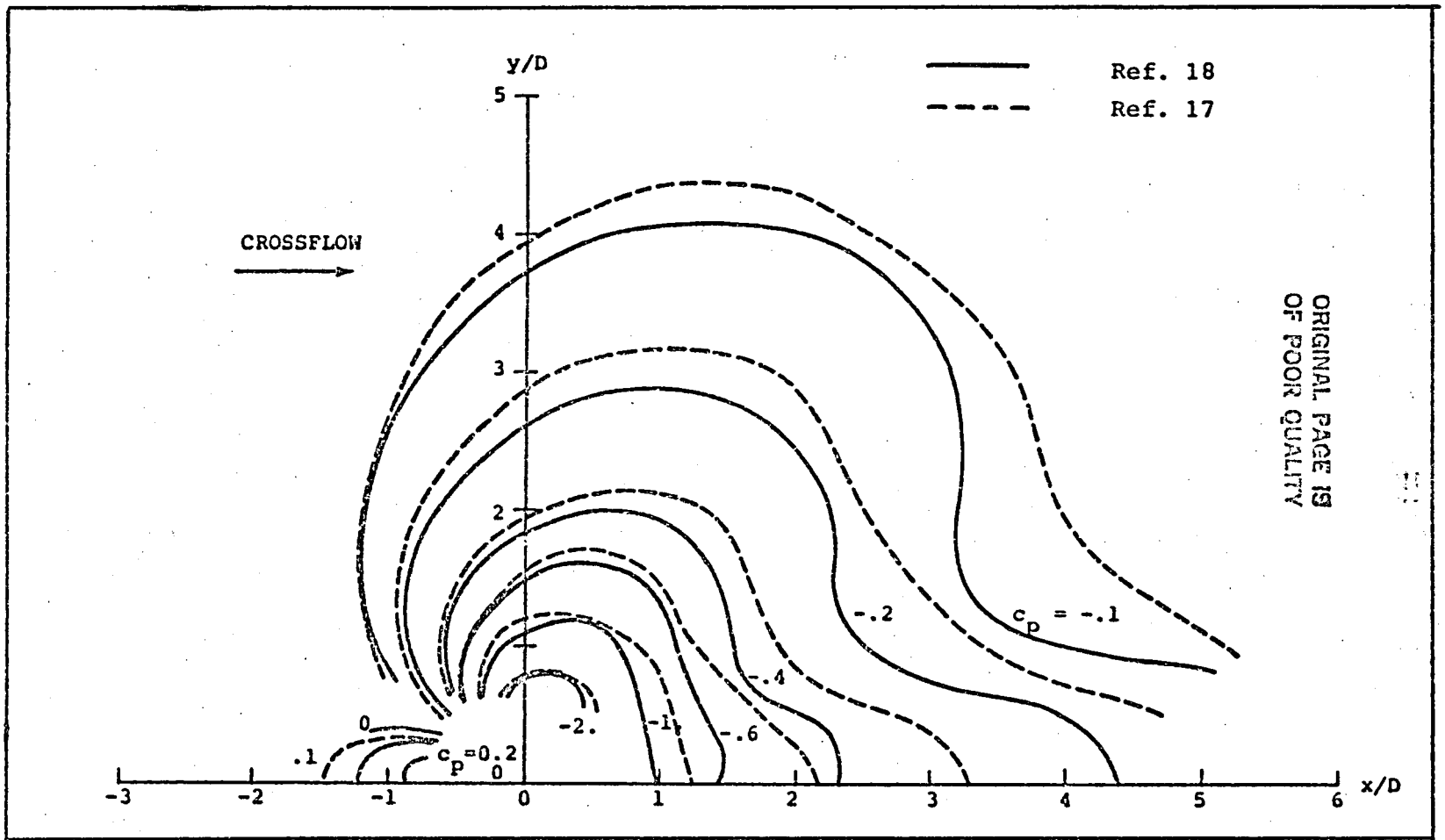

Figure 12. Flat-Plate Constant Pressure Contours with Jet Exiting at 90°, Ref. 18.

the positive pressure region ahead of the jet. Also shown by Fearn and Weston is the existence of "a large radial component of the pressure gradient in the region close to and to the side of the jet". This, as previously mentioned, is a result of the pair of vortices formed by the extreme mixing action on the sides of the jet.

An interesting observation made by both Fearn and Weston (35) (flat plate) and Mikolowsky and McMahon (44) (wing jet) is a "hook" in the surface pressure distribution in the wake region of the jet. As shown by the wing-jet analysis using flow visualizations, the presence of a "standing vortex" is verified for an angle of attack of 90 and a velocity ratio of 2.

As noted by Mikolowsky and McMahon, for a jet exiting normal to a wing lower surface in cross flow (44), the lower surface positive pressure region upstream of the jet increases in size for velocity ratios less than six with no corresponding effect measured in the nonlifting flat plate case. The large pressure region results in a lift augmentation and thus an increased positive pitching moment. For velocity ratios greater than six, the flat plate results and the lifting-surface results correspond closely. The jet induced effect on the wing upper surface was characterized by small induced suction pressures, the level of which was found to be invariant with changes in velocity ratio, jet location and angle of attack. Thus the major contributor to the observed aerodynamic interference behavior is the change in jet induced pressures on the surface exposed to the jet efflux.

3.0 PROGRAM DEVELOPMENT

3.1 General

The basic jet model in the VSAERO program consists of a doublet sheet located on the jet "boundary". The doublet distribution in the jet axial direction is linear--this represents constant vorticity; i.e., it represents the shear in tangential velocity between the inner jet velocity and the external local flow velocity. At the outset, the linear and axial doublet distribution was represented in the program as a stepwise constant model using flat panels with uniform doublet distribution. With this model the solution was often sensitive to jet panel arrangement, especially when the jet was in close proximity to a solid boundary. During the course of this work, therefore, the model was changed so that each jet panel now has a linear doublet distribution in the jet axial direction. The jet panels are still described in a vertical wake-grid-plane structure which is rather restrictive in applications to large cross-flow angles.

The location of the initial jet trajectory was an input in the basic code. While this is reasonable for jets that are essentially streamwise, it is rather tedious for cases with high jet deflection angles. Also, in the latter case, a poor initial jet location could lead to a lengthy iteration process to get a converged solution, or it could even lead to a divergence. During the course of this work, therefore, a procedure has been installed in the code which generates the jet surface geometry around a jet centerline geometry based on Margason's (16) empirical model. The procedure allows an expansion factor to be specified to represent the effects of jet growth as a function of axial distance. This procedure was applied in the cases of the jet issuing from a flat plate (Section 4.1) from a round body (Section 4.2) and in the later runs of the Grumman 698 configuration (Section 5.1).

Further model changes were made during the course of the method evaluation and validation. In particular, the jet potential core region was represented by using a solid boundary model, thus allowing the effects of initial entrainment on surface pressures to be more accurately modelled (see Section 4.1). Guidelines for the height of the solid core model were taken from Fearns correlations with respect to jet velocity ratio. It also allowed the effects of downstream separation behind the jet to be represented. Other detail changes included a modification to the way the jet doublet model allows the shed circulation to be superimposed. These changes significantly improved the calculated results on the STOL fighter configuration, particularly in the presence of the large offset between the upper jet exit lip and the lower jet boundary, leaving the flap trailing edge (Section 5.3). For the most part, such modelling details were first examined in a two-dimensional pilot code (described below) before being installed in the VSAERO program.

Finally, some detail changes were made to the wake relaxation procedure which significantly improved the jet trajectory calculation (Section 6.0); however, the vertical wake-grid-plane structure of the basic method is now the major obstacle in treating jets with large cross-flow angles. New work is planned to install an alternative and more general wake/jet structure in the program to remove this problem.

3.2 Two-Dimensional Pilot Code

The pilot code was generated using the two-dimensional equivalent of the VSAERO program; solid surfaces are represented by flat panels with uniform source and doublet singularity distributions. Jet boundaries are modelled by a number of flat panels each having a linear doublet distribution (i.e., uniform vorticity); the doublet gradient or vorticity value (= $V_{OUTER} - V_{JET}$) is specified by the user. The source values on the solid boundaries are determined by the external Neumann boundary condition. Non-zero normal velocities may be specified to represent the effects of inlet inflow and jet outflow. The doublet values on solid boundaries are determined by solving a set of simultaneous equations specifying zero perturbation potential at a control point underneath each panel center.

The pilot code was utilized to determine the numerical stability of the jet model as well as the accuracy of the calculation. Detailed model changes were first tested in this code prior to being installed in the VSAERO program.

3.3 Two-Dimensional Results

Results from the two-dimensional jet model pilot code are presented for a 12 1/2% thick elliptic cylinder with a slotted jet exiting from the lower-surface trailing edge as shown in Figure 13. The airfoil is at zero degrees angle of attack with the jet at an exit velocity of 1.5 times the freestream velocity and at an injection angle of 31.4° from the horizontal. A comparison is shown with the work done by D.A. Spence using thin airfoil theory including a vortex sheet representation of the jet boundary. A thickness correction has been applied by Spence to correlate with the experimental data.

The correlation between theory and experiment for the two-dimensional pilot code is as good as the Spence theory for the lower surface and shows an improvement over the Spence results for the upper-surface pressures. The discrepancy seen in the lower-surface region near the jet is possibly due to the entrainment of mainstream fluid, which is not modelled in the present treatment. Variation of the wake length proved to be a substantial factor in the overall solution stability. This is due to the fact that in the two-dimensional case the wake in the

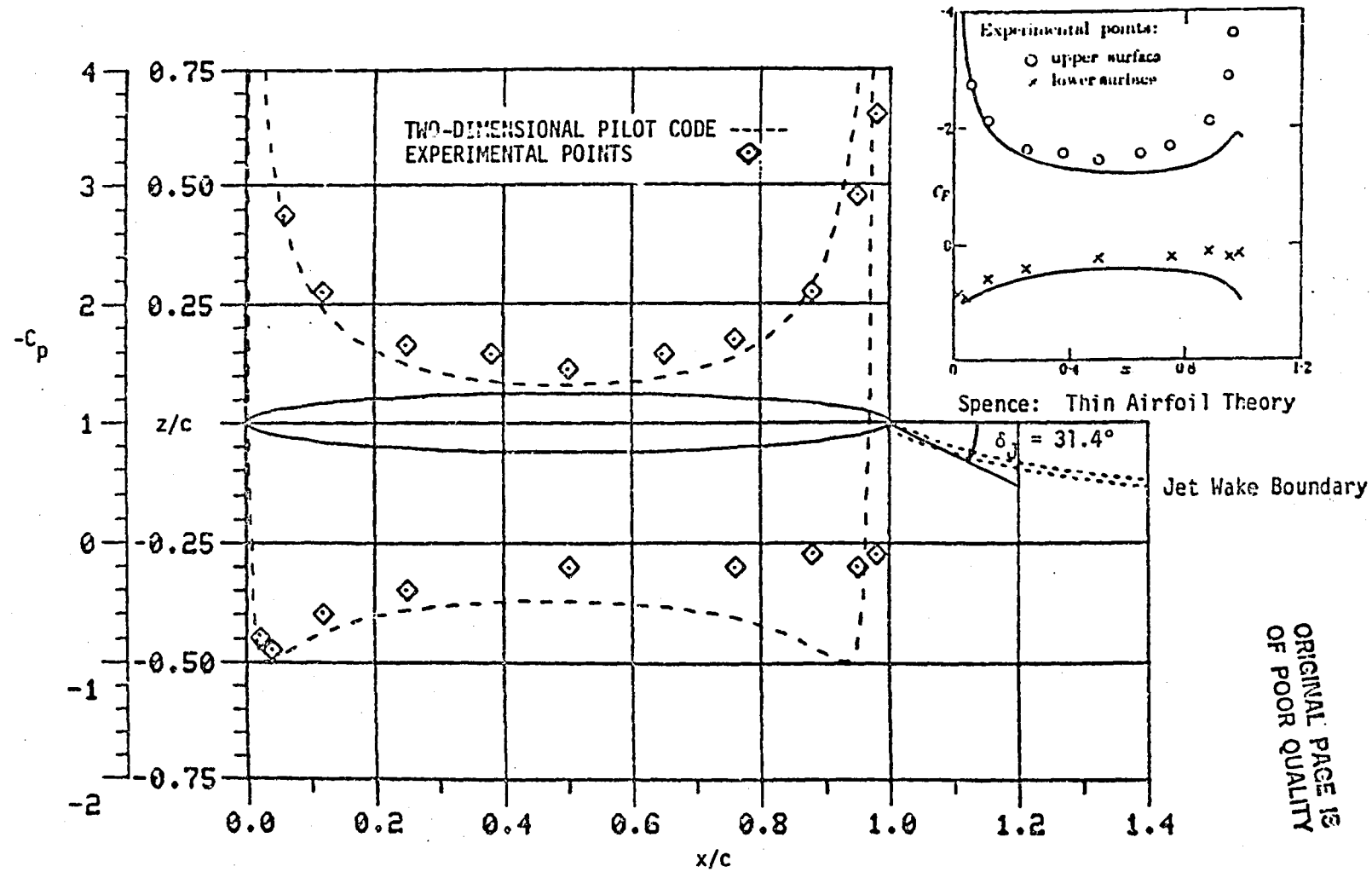

Figure 13. Comparison between Theory and Experiment for a Two-Dimensional Elliptical Airfoil with Slotted Jet.

streamwise direction has been truncated at some finite length, whereas the spanwise component is at infinity. It has been shown by experience with the separated flow problem to be purely a consequence of the two-dimensionality of the model and will disappear when considering the three-dimensional case. A single wake filament is attached at either edge of the slot to model the jet thickness.

4.0 VSAERO METHOD EVALUATION

4.1 Simple Test Case: Flat Plate

Due to the complexity of the jet-in-crossflow problem, namely, the close coupling between the entrainment rate and the separated flow region and how this coupling affects the local pressure distribution, the simple flat plate configuration was employed in this phase of the analysis (see Figure 14).

This configuration was utilized to determine the effects of each modification made in the analysis with VSAERO. Initially, the jet was allowed to exit normal to the surface with the improved jet wake model available in VSAERO. The surface pressures local to the jet orifice did not correlate well with the experimental data due to the form of the wake boundary condition enforced by VSAERO. For the jet-in-crossflow problem, one of the dominant features is the property of the relatively high energy jet to induce local flow tangency. The flow tangency boundary condition implied in the VSAERO wake formulation is not sufficient in the potential core region where the angle between the jet efflux and the onset flow is at or near 90o.

A modification was made to the potential core region (Figure 15), to better enforce this flow tangency boundary condition as well as to allow entrainment and separation to be modelled in the high-energy potential core region of jet development. The advantages of representing the potential core region by a solid "body" panel arrangement have been substantiated by this analysis.

The pressure coefficient was plotted in Figure 16 for the flat plate configuration at a radial distance to nozzle diameter ratio of 0.7 for a jet velocity ratio of 8.0 and an injection angle of 90o. The advantages of the solid body potential core model are clearly shown when comparing the experimental Cp distribution with the VSAERO results. Substantial improvement is seen when an entrainment model is employed as compared to the VSAERO results with no entrainment model. The results with entrainment model indicate a problem with the magnitude of the normal velocity specified on the front face of the potential core. Specifically, the normal velocity on the front face is too low in magnitude resulting in a higher positive Cp than experiment and a lower entrainment rate. Alleviating the cause of this discrepancy is viewed as a refinement to the preliminary entrainment model.

The doublet strength derived by Wooler (see Eqn. (23), Ref. 15) was used to determine the vortex pair normal velocity component in the potential core region; i.e., the peripheral variation of normal velocity, and the source/sink distribution derived by Dietz (see Eqn. (18), Ref. 31) was used to determine the remaining normal velocity component due to the "free-jet" entrainment effect. The "free-jet" entrainment effect is the entrainment of mainstream fluid through turbulent shear resulting

Figure 14.

FLAT PLATE WITH ROUND JET + POTENTIAL CORE UJ=8.0
XVUE= 14.35E+06 YVUE= 14.35E+06 ZVUE= 100.00

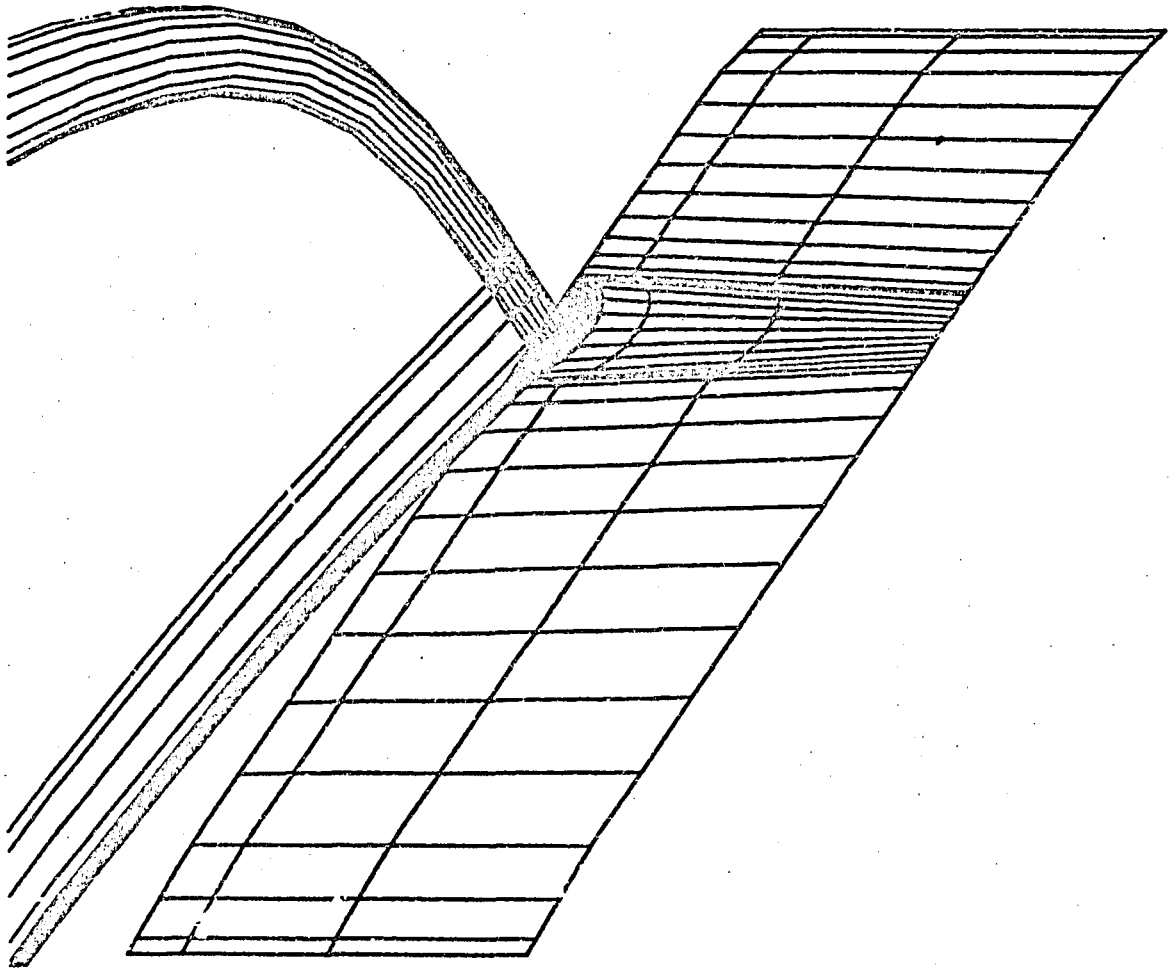

Figure 15.

FLAT PLATE CONFIG. + ENTRAINMENT MODEL + SEPARATED WAKE MODEL VJ=8.0
XVUE=0.14E+08 YVUE=0.14E+08 ZVUE= 100.00

from the difference between the jet velocity and the local mainstream velocity. The source distribution accounts for normal velocity variation along the jet length.

Excellent correlation with experiment is seen in Figure 16 when a separated wake model is coupled with the entrainment model as previously described. The separated wake was attached vertically along the solid potential core at an approximate angle of 130° from the onset flow direction (Figure 17). The pressure peak at $\beta \approx 90°$ was reduced in this configuration when compared to the case with no wake. This is due to the isolation of the rear face of the potential core within the separated zone and thus the loss of some of the rear entrainment effects. This reduction in entrainment rate is related to the front face anomaly, and is expected to improve after further analysis with the coupling of entrainment and separated wake models.

This configuration is examined further in Section 6.0 in connection with jet trajectory calculations.

4.2 Simple Test Case: Body of Revolution

The body of revolution (25) as shown in Figure 18 was analyzed in a similar manner with the exception of the separated wake which was not included with this configuration. As an aid in visualizing the flow characteristics in the neighborhood of the jet, surface velocity vectors have been plotted on the body of revolution in Figure 19. The velocity contours behave in a consistent and accurate manner as verified by the pressure distribution and similar experimental velocity vector plots on the flat plate configuration (25) with the exception of the velocity vectors located at the front of the jet orifice. This is again related to the inaccuracy of the entrainment model on the frontal region of the potential core zone.

A series of pressure cuts were taken parallel to the flow and presented in Figures 20 through 24 with the experimental pressure trends plotted for comparison purposes. The problem with the entrainment model in the frontal area of the potential core is again very evident from the calculated stagnation Cp distribution near the jet orifice. The discrepancy in the rear region of the jet is due to the lack of a separated wake model in this particular configuration. At a y/D of .48 and greater, the correlation with experiment is very good when taking into account the model inadequacies as described above.

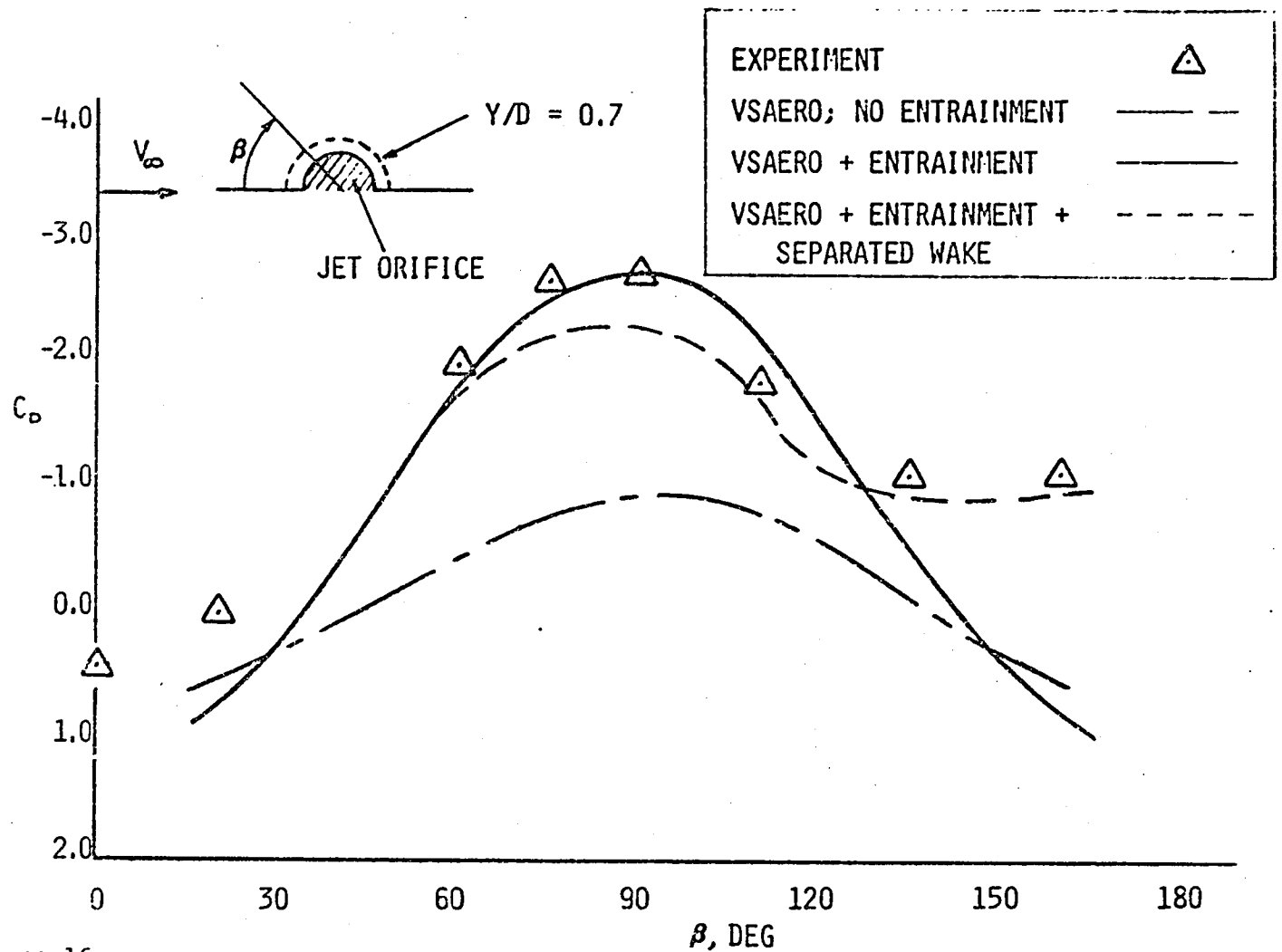

Figure 16.

FLAT PLATE PRESSURE COMPARISON: Y/D = 0.7, V_{JET} = 8.0, δ_J = 90.0.

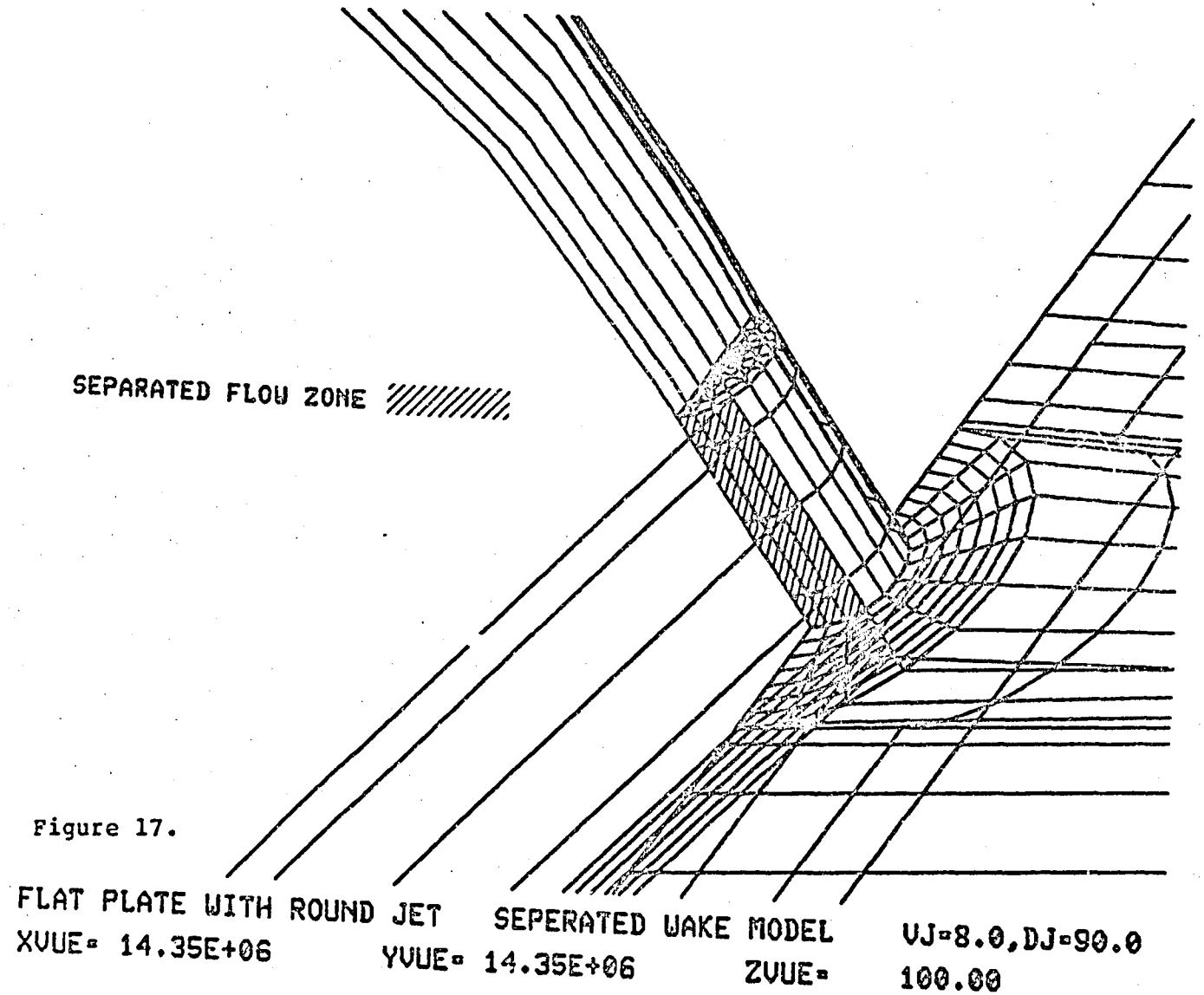

Figure 17.

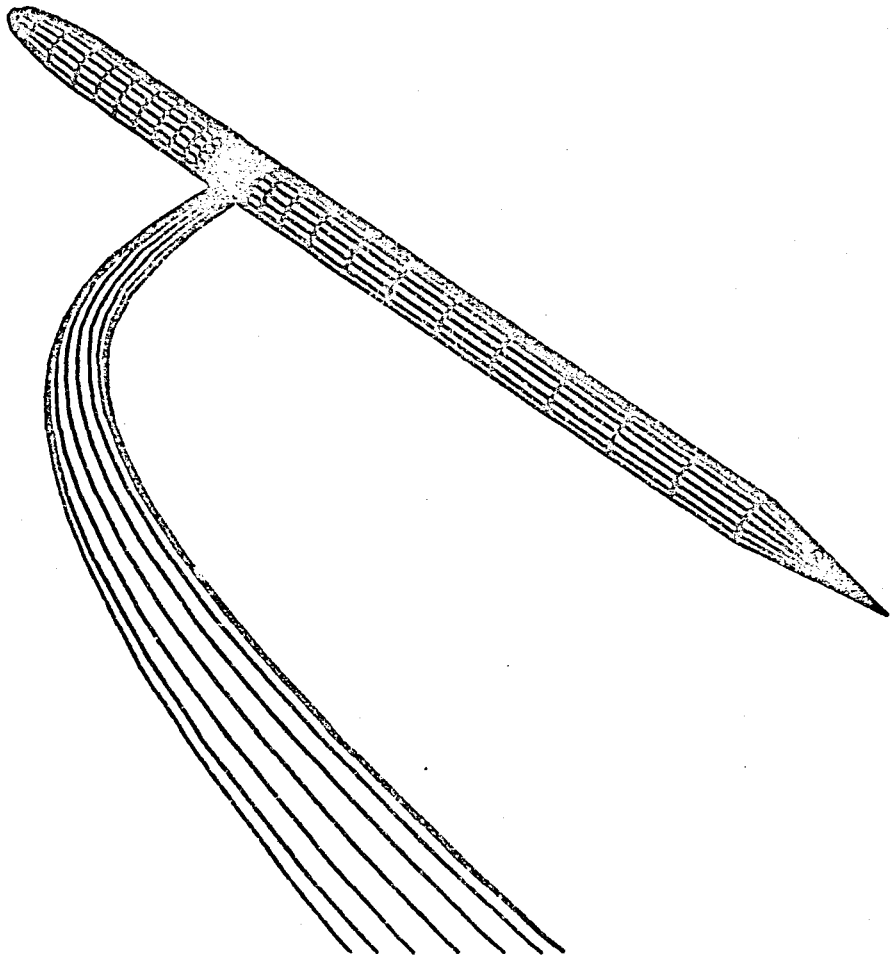

Figure 18. Body of Revolution with Round Jet and Potential Core Model.

Figure 19. Body of Revolution with Round Jet and Entrainment Model; Velocity Vector Contours.

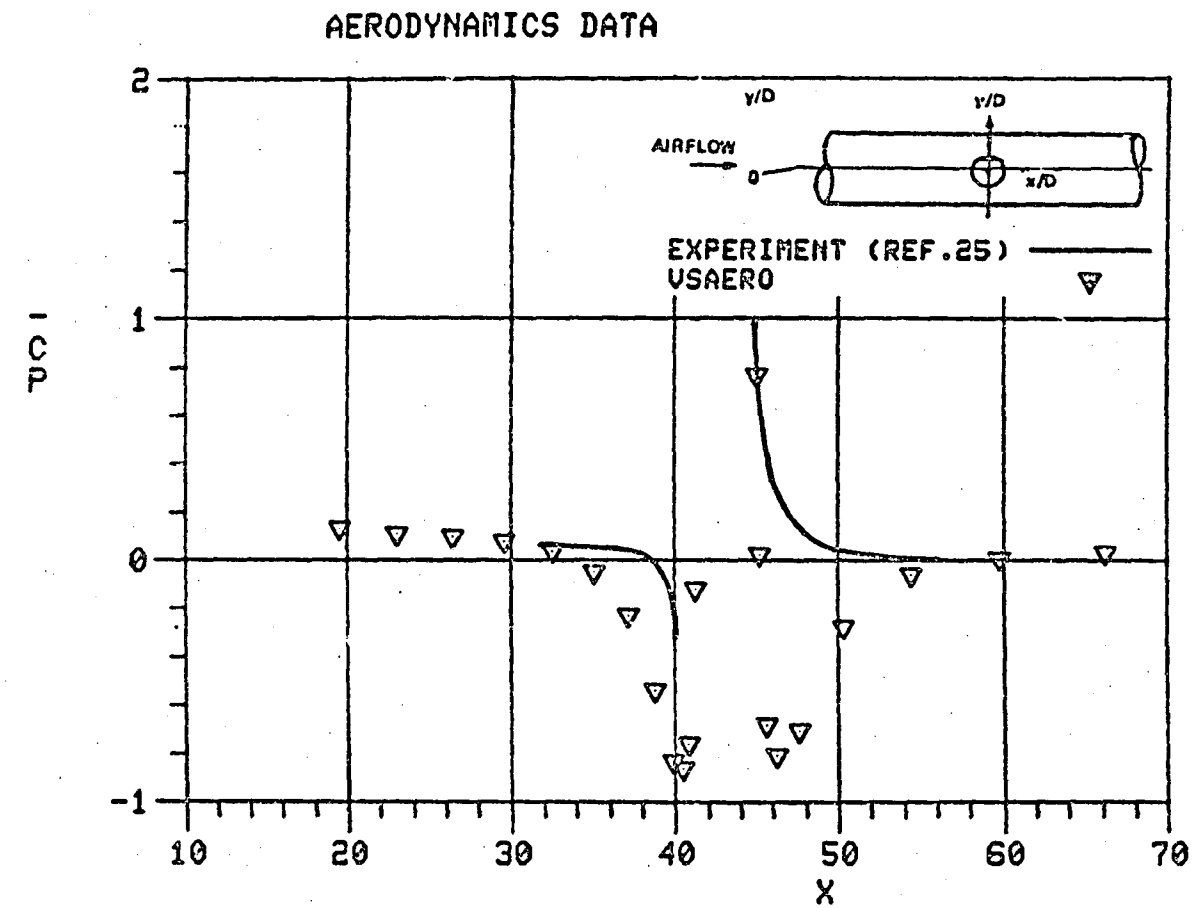

Figure 20. Body of Revolution with Potential Core and Entrainment Model; y/D = 0.0.

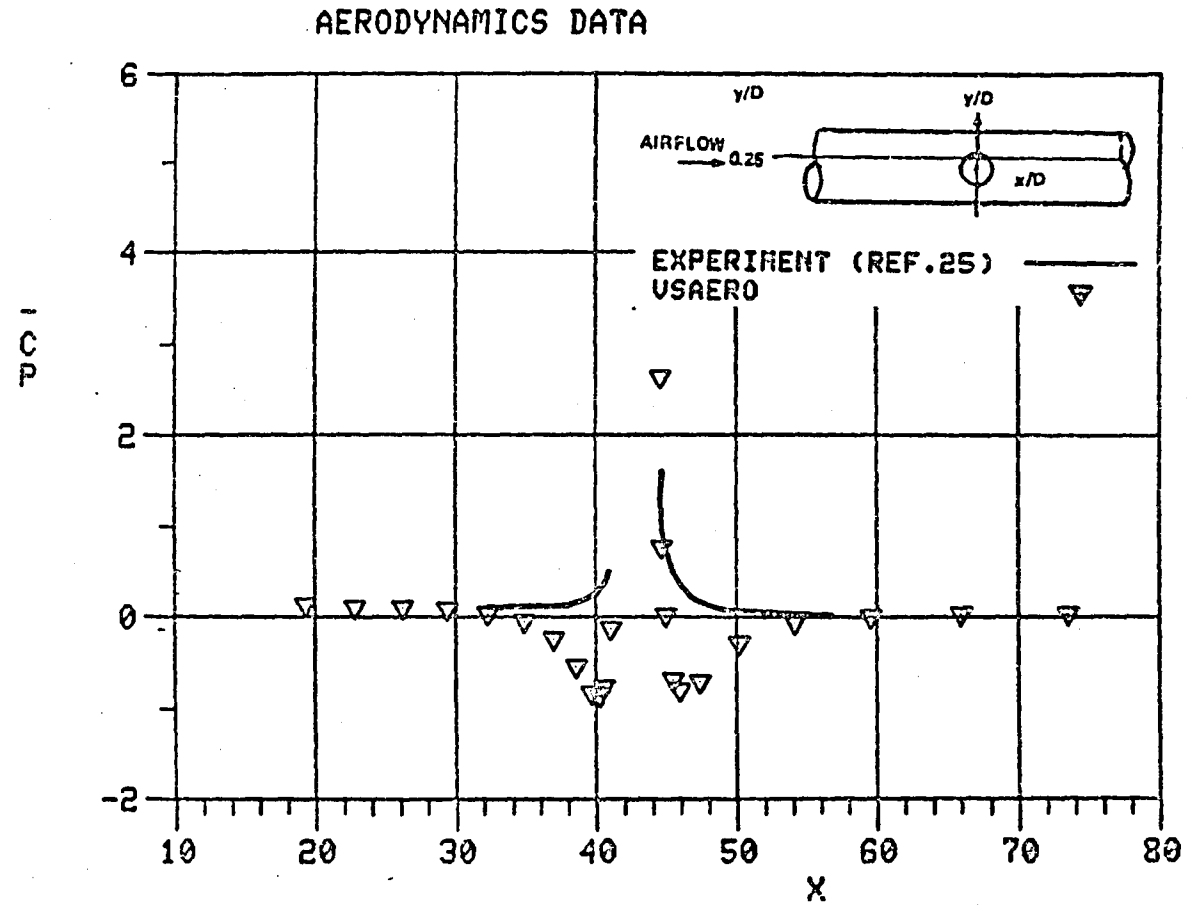

Figure 21. Body of Revolution with Potential Core and Entrainment Model; y/D = 0.25.

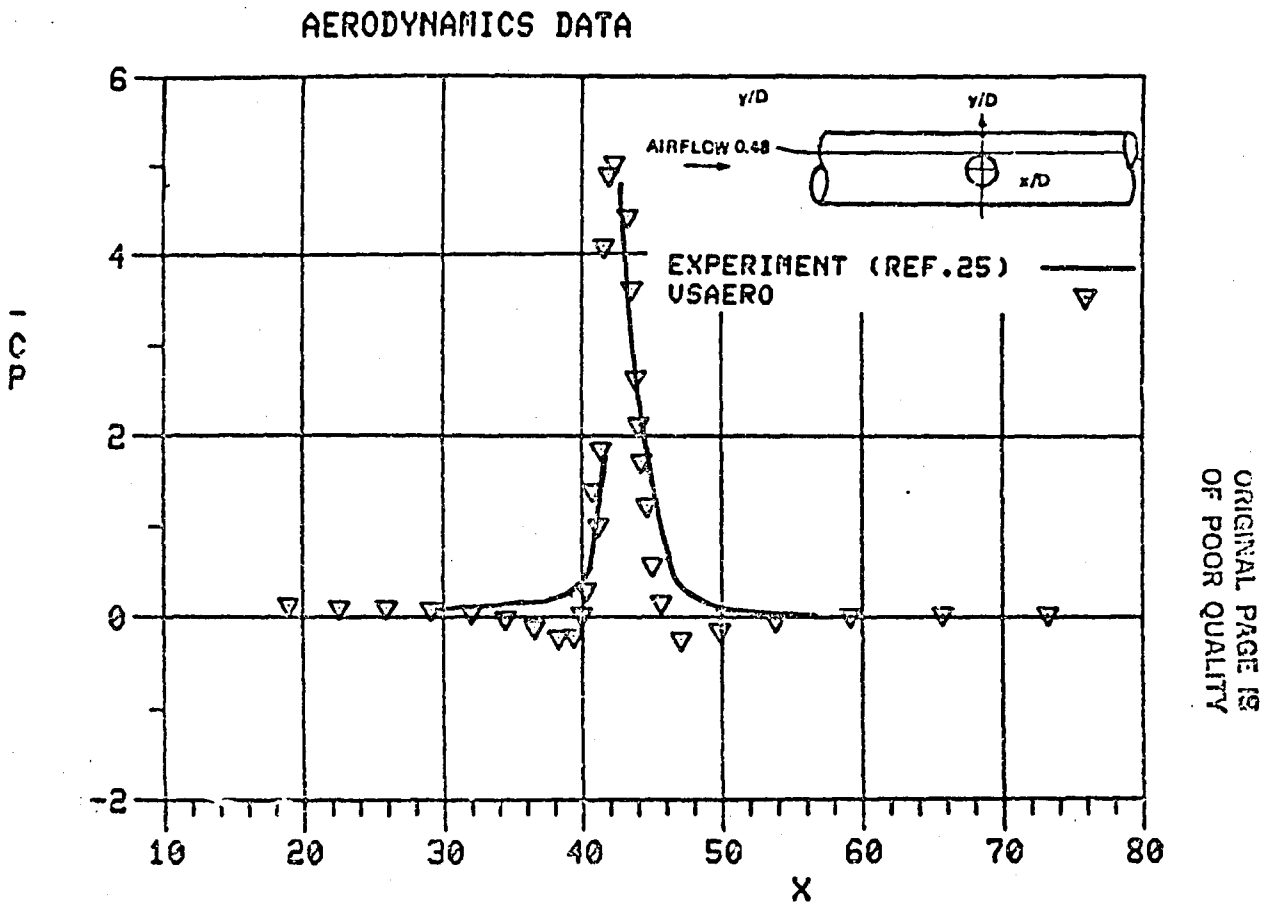

Figure 22. Body of Revolution with Potential Core and Entrainment Model; y/D = 0.48.

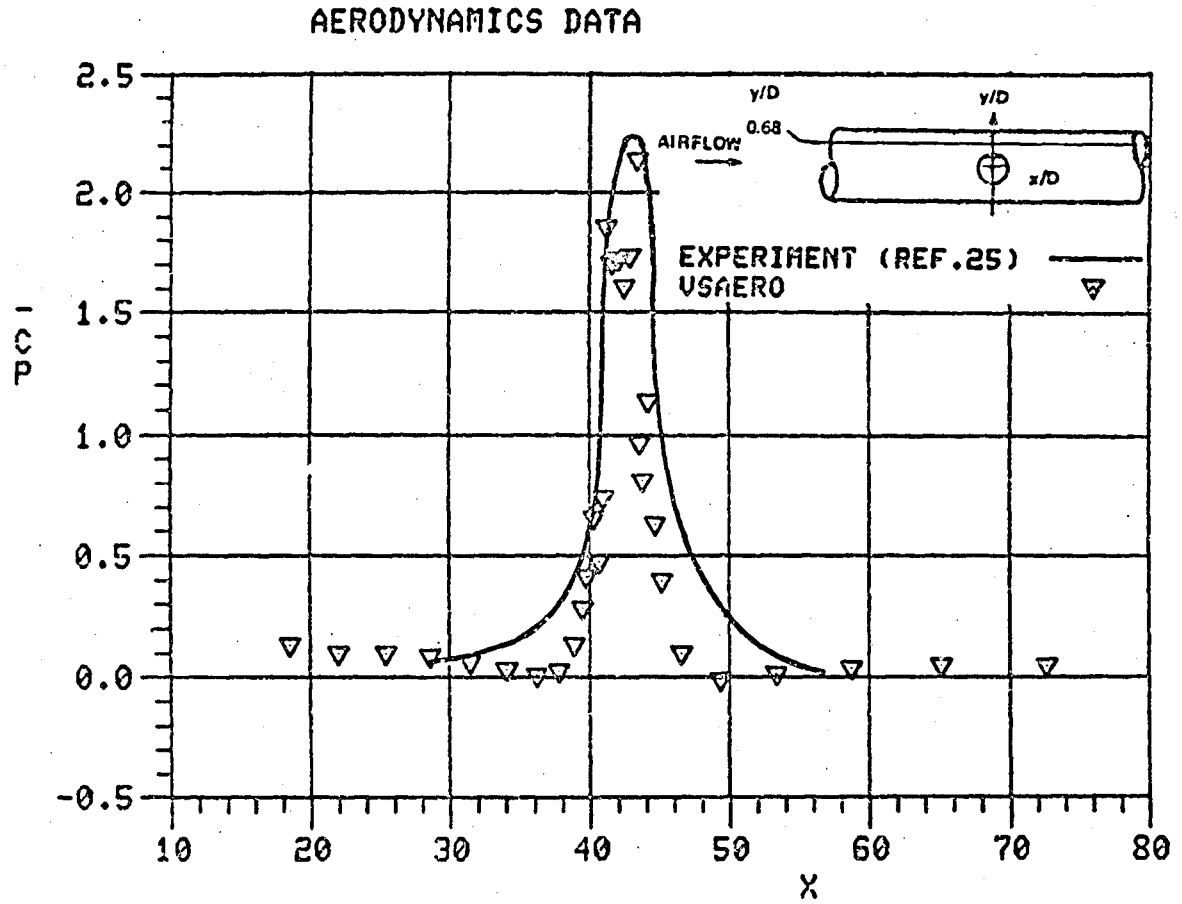

Figure 23. Body of Revolution with Potential Core and Entrainment Model; y/D = 0.68.

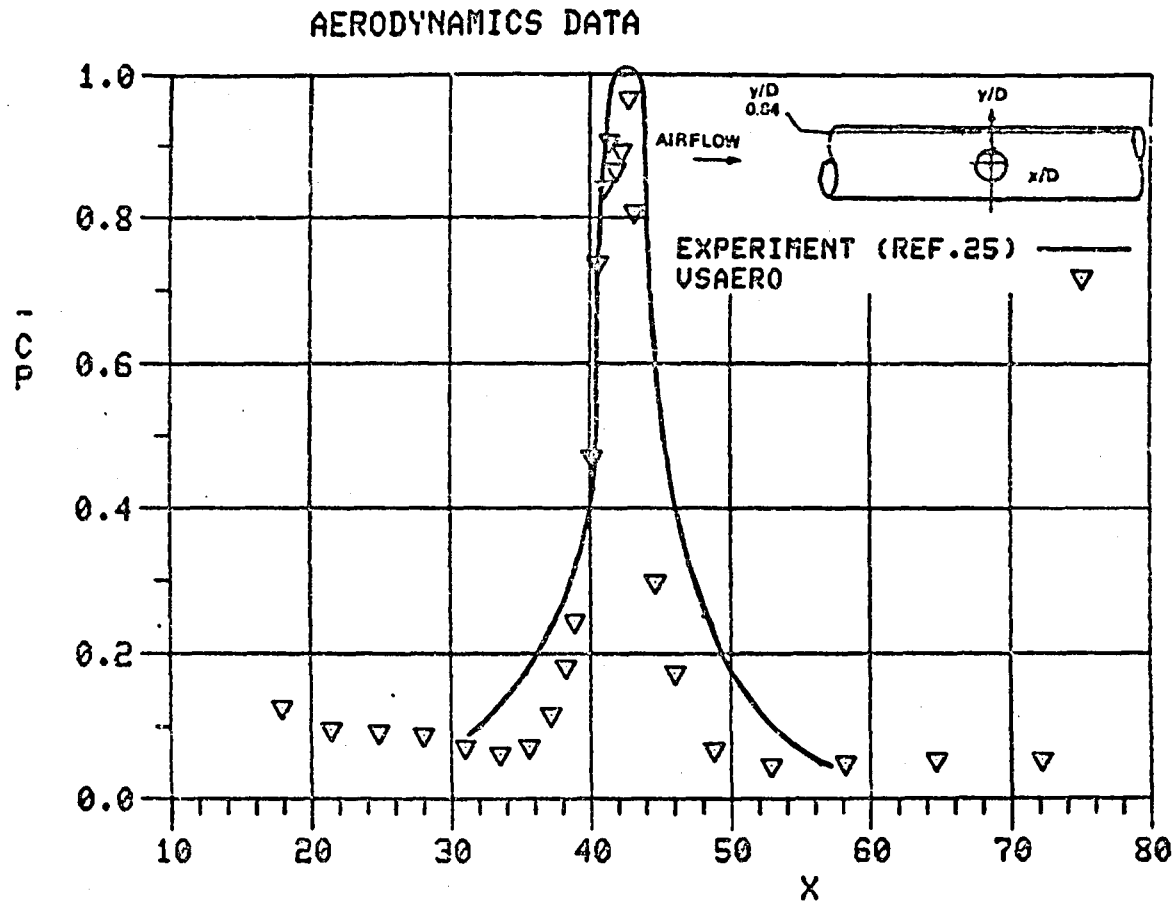

Figure 24. Body of Revolution with Potential Core and Entrainment Model; y/D = 0.84.

4.3 Summary

Further analysis is required with the separated wake and entrainment model combination to improve the correlation in the upstream and downstream region near the jet orifice. The simple configurations utilized in this analysis proved to be very useful for determining the jet-in-crossflow characteristics in a simplified three-dimensional environment.

5.0 PROGRAM VALIDATION

5.1 VSAERO Analysis of Grumman Design 698-411

5.1.1 Configuration

The Grumman design 698-411 full-scale, tilt-nacelle V/STOL model was analyzed using the three-dimensional potential flow program VSAERO. The model was tested at the NASA Ames Research Center in the 40- x 80-foot wind tunnel and the NASA Ames outdoor static stand in 1981 (27).

To help visualize the complexity of this configuration a series of figures are presented which describe the progression of the VSAERO panelling from the relatively "simple" clean configuration to the very complex configuration with nacelles at 50o. This series is presented in Figures 25(a) through (i) with a summary of the configuration specifics presented in Table 1.

LABEL	GENERAL DESCRIPTION	α(DEG)	δ_N(DEG)	V_∞(KTS)	V_F/V_∞
Case A	Fuselage/Wing/Tail	0.0	---	---	---
Case B	Fuselage/Wing/Tail/Nacelle	0.0	5.0	100.5	2.57
Case C	Fuselage/Wing/Tail/Nacelle	12.0	50.0	104.0	2.39
Case D	Fuselage/Wing/Tail/Nacelle	16.5	50.0	100.0	2.30

Table 1. Grumman Design 698-411 Configuration Summary.

The configurations labelled Case A and Case B (which correspond to Figures 25(a), (b), and 25(c), (d), respectively) were used mainly to determine the nacelle-on and nacelle-off characteristics and also to examine the numerical stability of the panelling arrangement. As shown by Figure 25(c), the all movable horizontal tail could pose a problem with regard to the root junction when the horizontal tail angle setting is modified to fit the particular flight condition under analysis. Specifically, the panelling arrangement in the vertical stabilizer/horizontal tail junction would require modification for each tail angle setting. Due to the internal Dirichlet boundary condition of zero perturbation potential "inside" the body as applied in VSAERO (9), this "T" tail design allowed for a rather unique panel arrangement. A simple test case was run using program VSAERO to determine the behavior and numerical stability of a particular wing/body junction which has direct application to the "T" tail junction present in this configuration. For ease in analysis, the vertical tail was panelled up regardless of horizontal tail location. The open end of the horizontal tail was then "butted" up against the vertical tail, as shown by

Figure 25(a). Grumman Design 698-411 Tilt-Nacelle, V/STOL Model; Engine-off Configuration.

Figure 25(b). Grumman Design 698-411 Tilt-Nacelle, V/STOL Model; Engine-off Configuration.

Figure 25(c). Grumman Design 698-411 Tilt-Nacelle, V/STOL Model; Nacelle Installed, Cruise Attitude.

Figure 25(d). Grumman Design 698-411 Tilt-Nacelle, V/STOL Model; Nacelle Installed, Cruise Attitude.

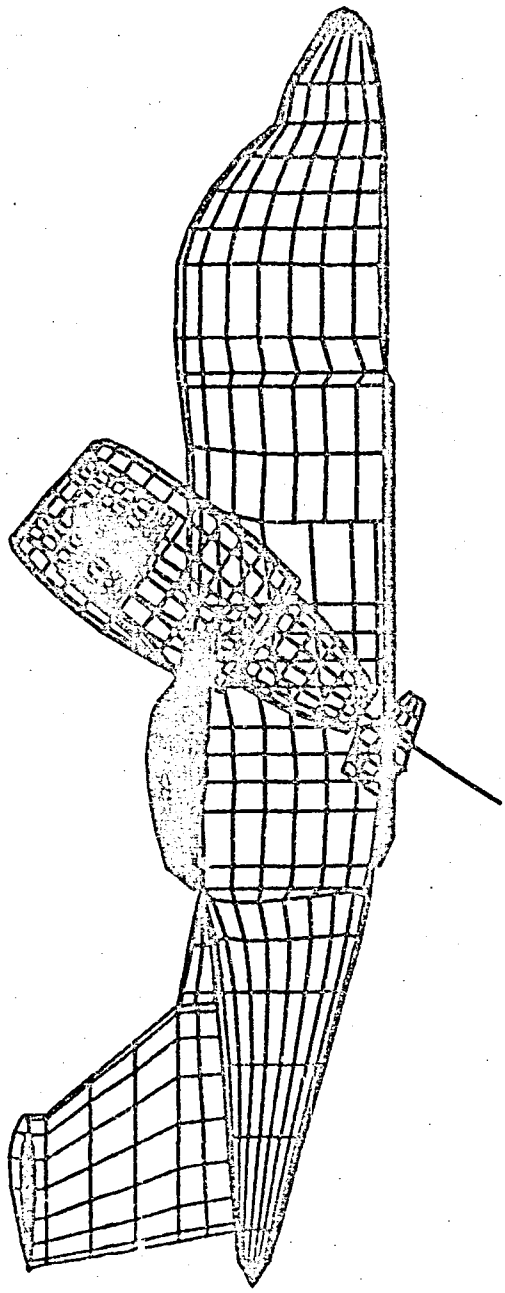

Figure 25(e). Grumman Design 698-411 Tilt-Nacelle, V/STOL Model; Nacelle at 50°, α = 12.00.

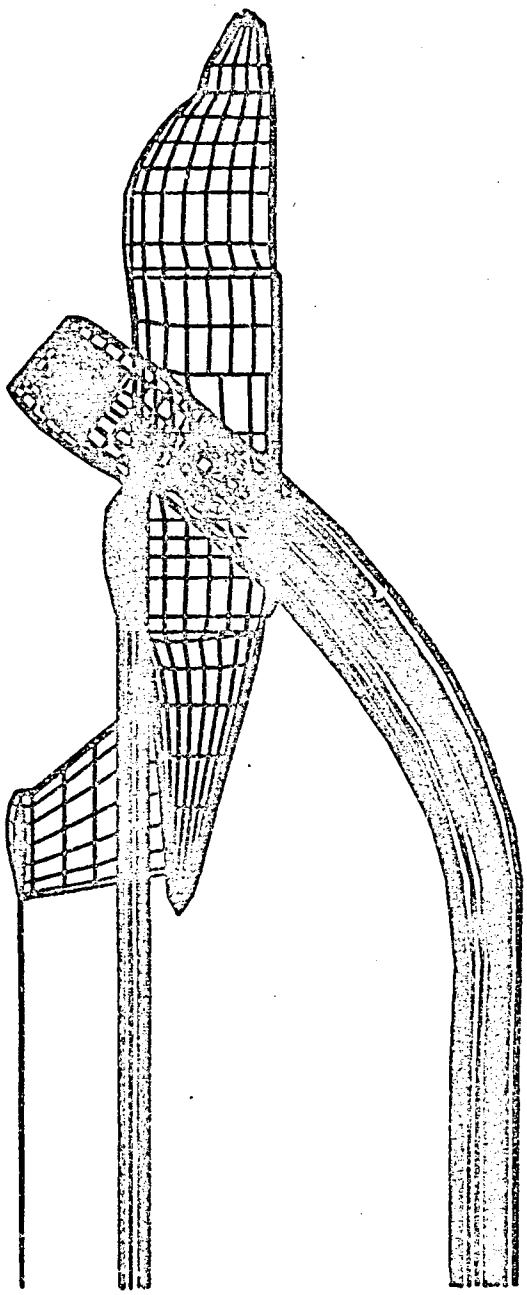

ALPHA=12.0

Figure 25(f). Grumman Design 698-411 Tilt-Nacelle, V/STOL Model; Nacelle at 50°, α = 12.00.

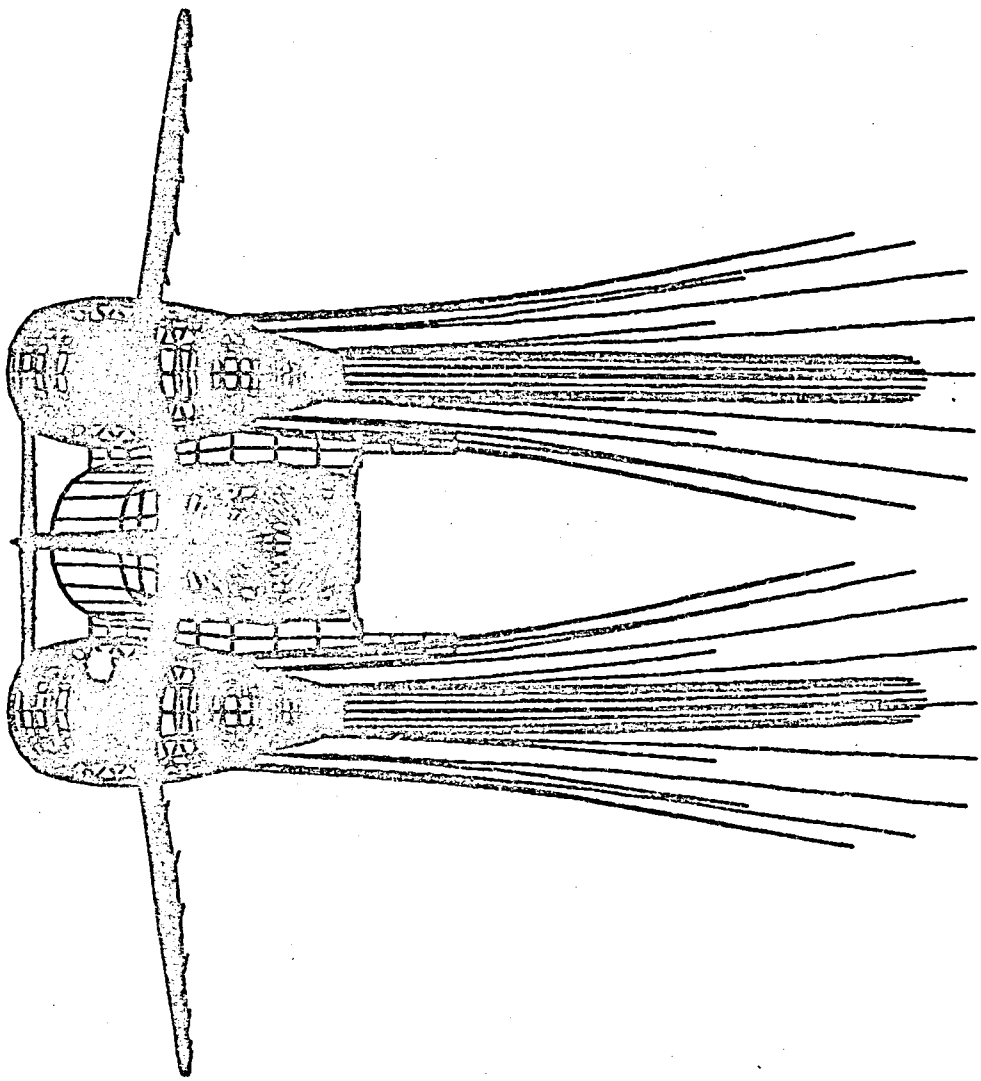

Figure 25(g). GRUMMAN DESIGN 698-411 TILT-NACELLE V/STOL MODEL WITH IMPROVED JET TRAJECTORY.

Figure 25(h).

GRUMMAN DESIGN 698-411 TILT-NACELLE V/STOL MODEL WITH IMPROVED JET TRAJECTORY.

Figure 25(i). GRUMMAN DESIGN 698-411 TILT-NACELLE V/STOL MODEL WITH IMPROVED JET TRAJECTORY.

the inset in Figure 25(c). This simplified arrangement allows for the horizontal tail deflection angle to be changed (depending on the flight condition) with no modification of the "T" tail junction. The stability of this model was verified.

Cases C and D are related in that the nacelle angle in both instances is set at +50°, but for Case D a considerably more realistic jet geometry has been added to the configuration. A subroutine has been added to VSAERO which calculates the jet trajectory and jet geometry based on the initial jet injection angle and jet velocity. The trajectory coordinates are calculated based on an empirical jet centerline equation developed by Margason (16). A linear factor may also be applied to the circular jet diameter at the user's option to expand the jet boundary and thus geometrically simulate entrainment as shown in Figures 25(g) through (i).

5.1.2 Results

Comparison with experiment was limited due to the absence of fuselage or wing experimental pressure measurements except for the fuselage bottom centerline with the model in ground effect. Since the analysis of the Grumman configuration in ground effect was not included in this study, VSAERO was utilized to examine the jet-induced effects of the TF34-100 Turbofan nacelle, which was treated thoroughly in the experimental analysis.

For Case C, with the nacelle at an absolute angle of attack of 62°, (see Figures 25(e), (f)) excellent correlation with experiment was found. The ratio of local static pressure to ambient total pressure was plotted against a nondimensional distance parameter along the bottom centerline of the TF34 engine inlet and is presented in Figure 26(a). Further correlations with experiment are presented in Figures 26(b) and (c) for the TF-34 engine inlet. The TF-34 inlet characteristics under both isolated and installed conditions are documented in the experimental study (27) and are treated in Section 5.2 of this report.

The nacelle-on/nacelle-off characteristics are presented in Figures 27 through 31. A comparison of the wing pressure distribution at a spanwise location of 70.0, which is approximately located at the nacelle centerline, is shown in Figure 27(a) and (b). This Cp distribution indicates a considerable loss in lift for the engine installed configuration. A negative sectional lift coefficient was maintained (as calculated by VSAERO) from the wing root junction to a spanwise location just outboard of the initial flap station for the engine-installed configuration. Due to the forward location of the nacelle with respect to the wing leading edge (see Figure 25(d)), the wing receives a downwash velocity, thus resulting in negative lift throughout the wing inboard stations. This lift degradation present in the close-coupled nacelle/wing region for the cruise configuration

$V_{FAN}/V_\infty = 2.39$ $\alpha = 12°$

$V1/V_\infty = 2.56$ $\delta_{NAC} = 50°$

$V2/V_\infty = 2.73$ $M_{fan} = 0.39$

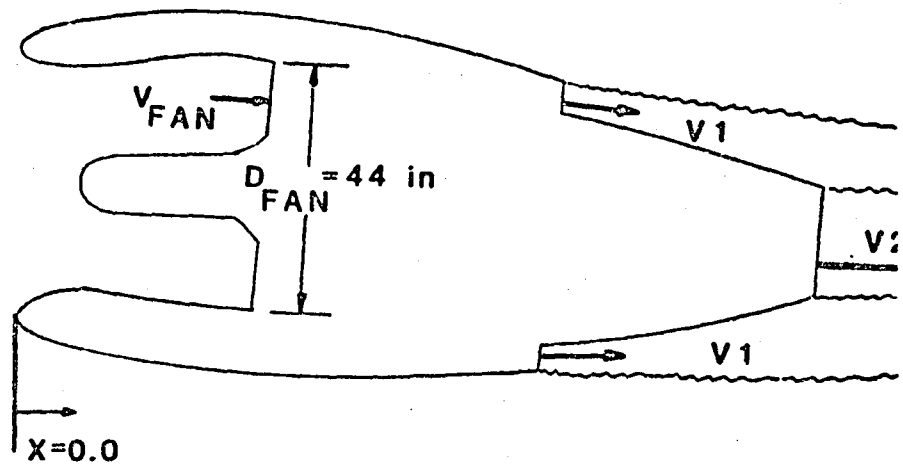

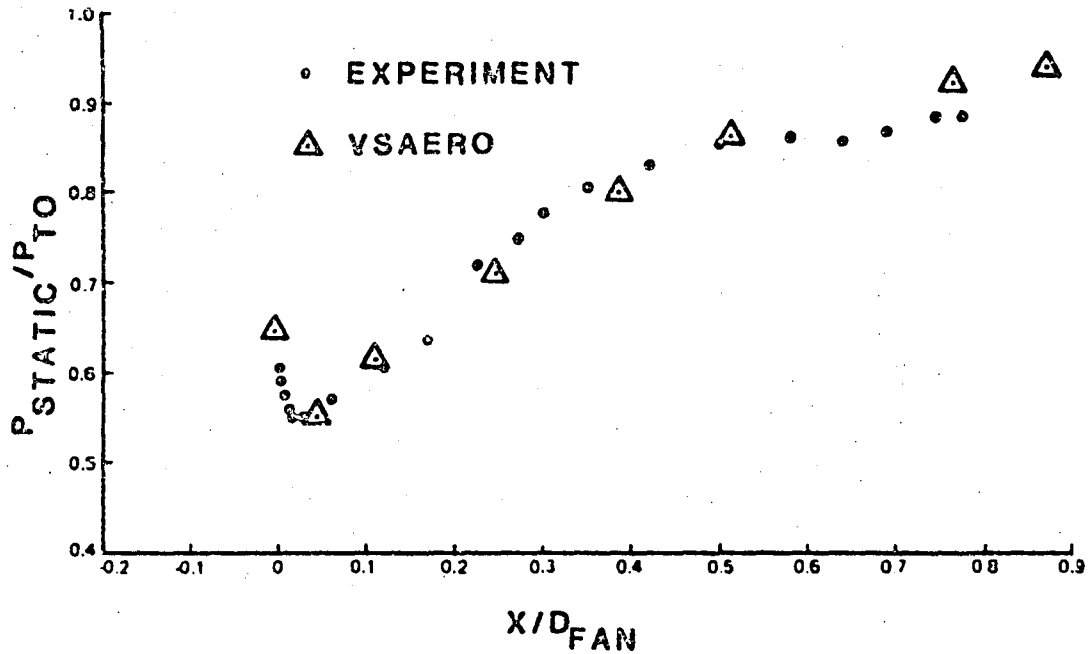

Figure 26. TF34-100 Nacelle Pressure Ratio, Nacelle Inlet Bottom Centerline.

(a) V_∞ = 104 kts., WK = 281 lbs./sec.

$V_{FAN}/V_\infty = 2.36$ $\alpha = 0°$

$V1/V_\infty = 2.52$ $\delta_{NAC} = 62°$

$V2/V_\infty = 2.69$ $M_{fan} = 0.40$

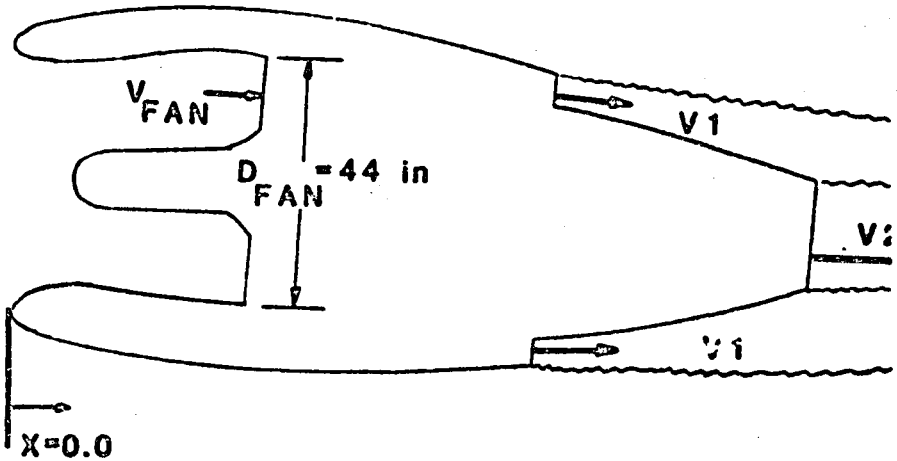

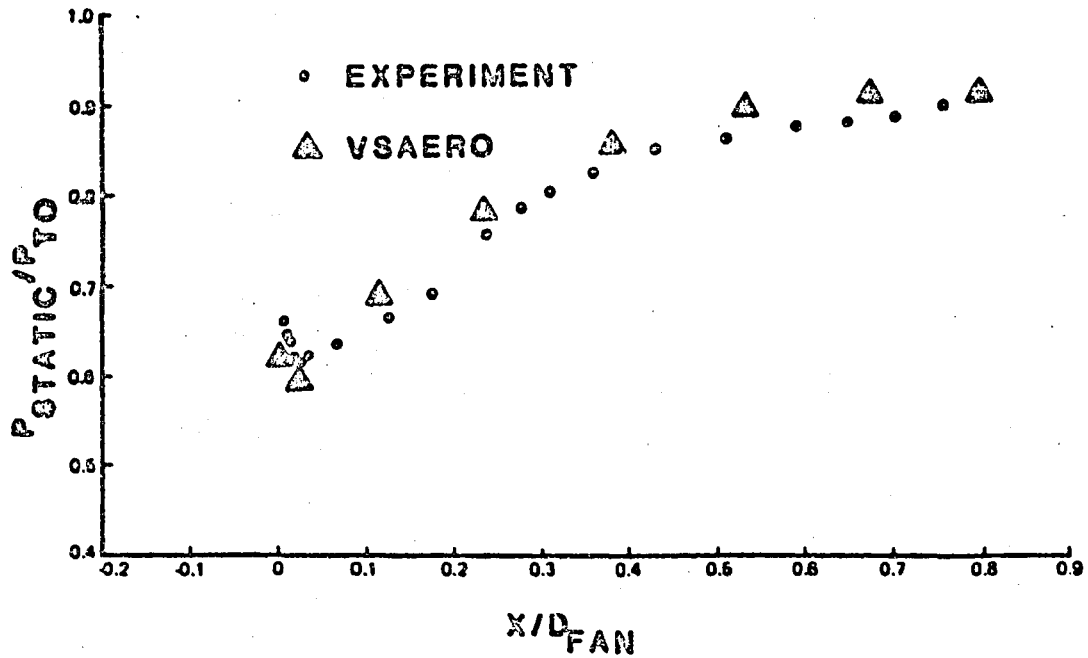

Figure 26. Continued.

(b) V_∞ = 99 kts., WK = 262 lbs./sec.

$V_{FAN}/V_\infty = 2.65$ $\alpha = 0°$

$V1/V_\infty = 2.83$ $\delta_{NAC} = 62°$

$V2/V_\infty = 3.02$ $M_{fan} = 0.32$

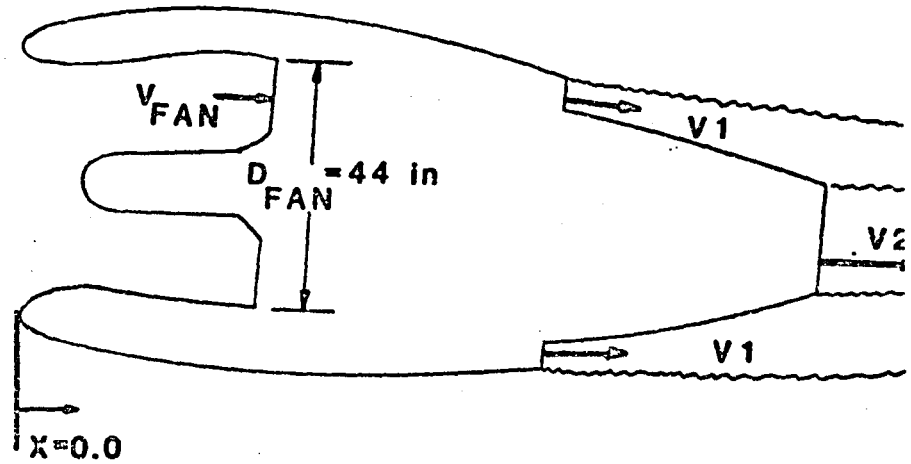

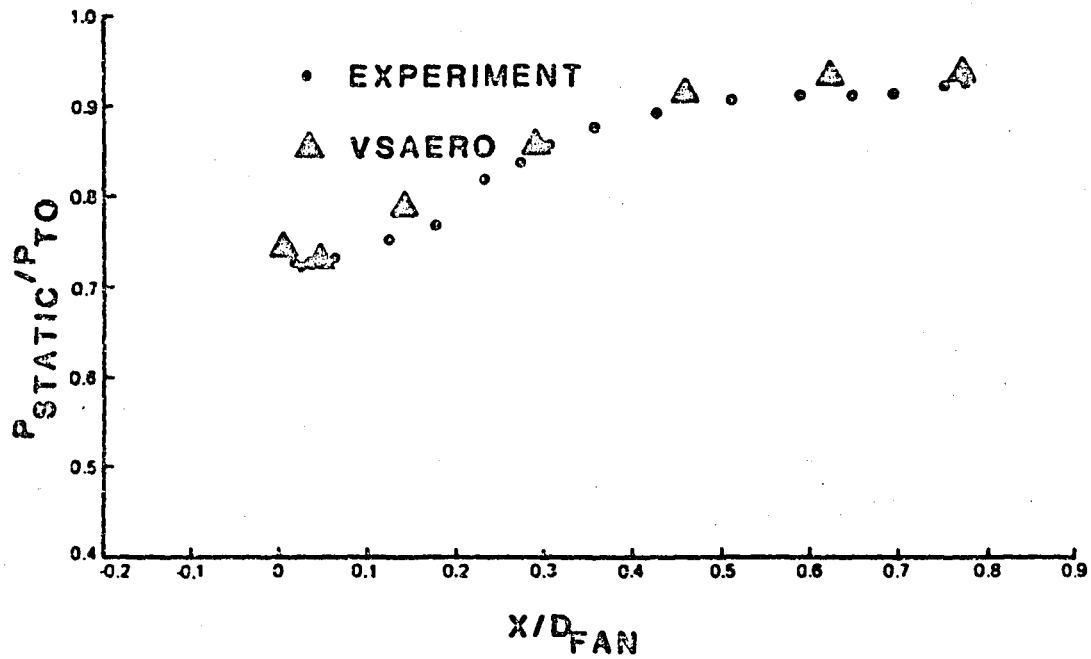

Figure 26. Concluded

(c) V_∞ = 79 kts., WK = 236 lbs./sec.

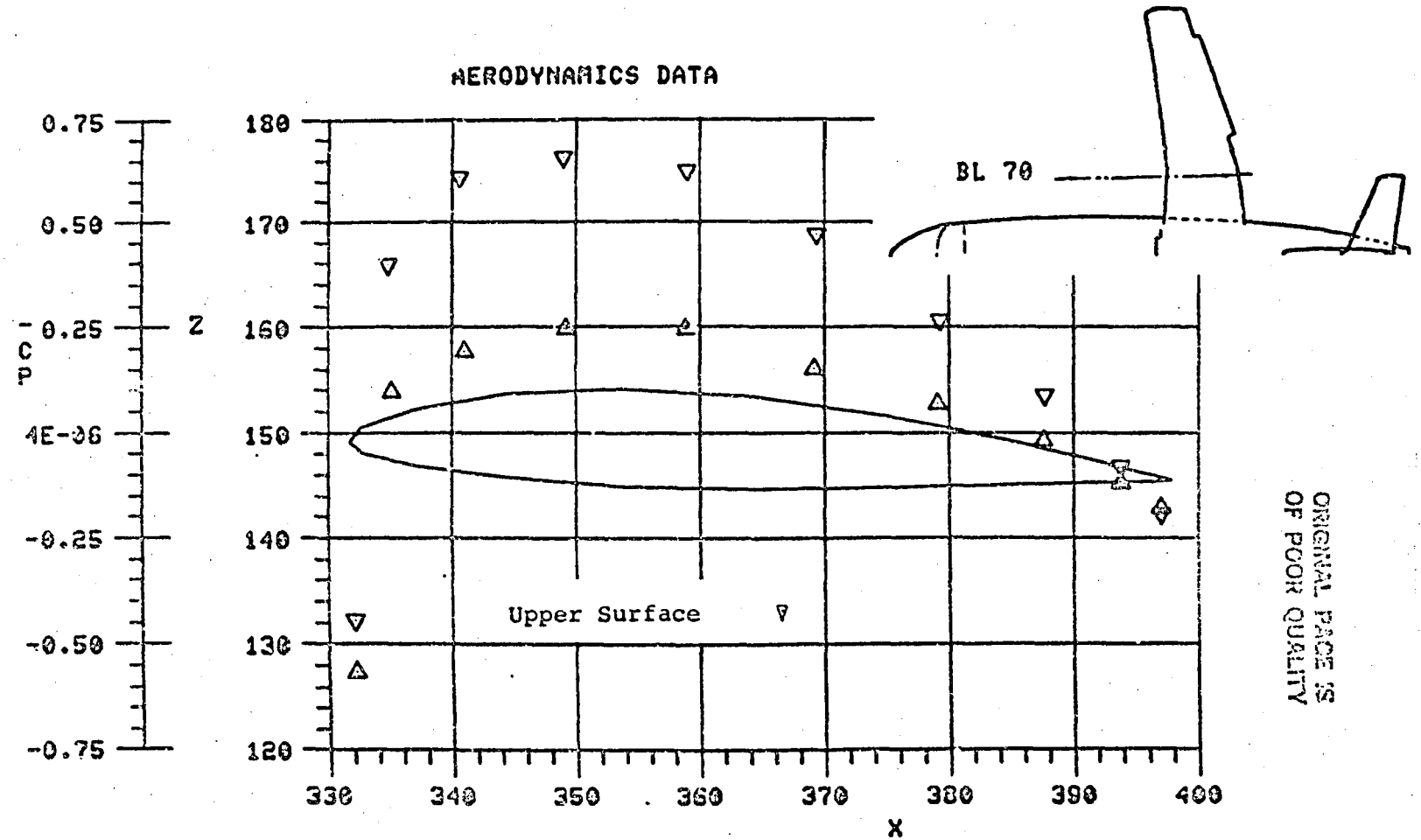

Figure 27(a). Grumman Design 698-411 Tilt-Nacelle, V/STOL Model, Nacelle-off Configuration; $\alpha = 0.0$, Wing Spanwise Pressure Cut y = 70.0.

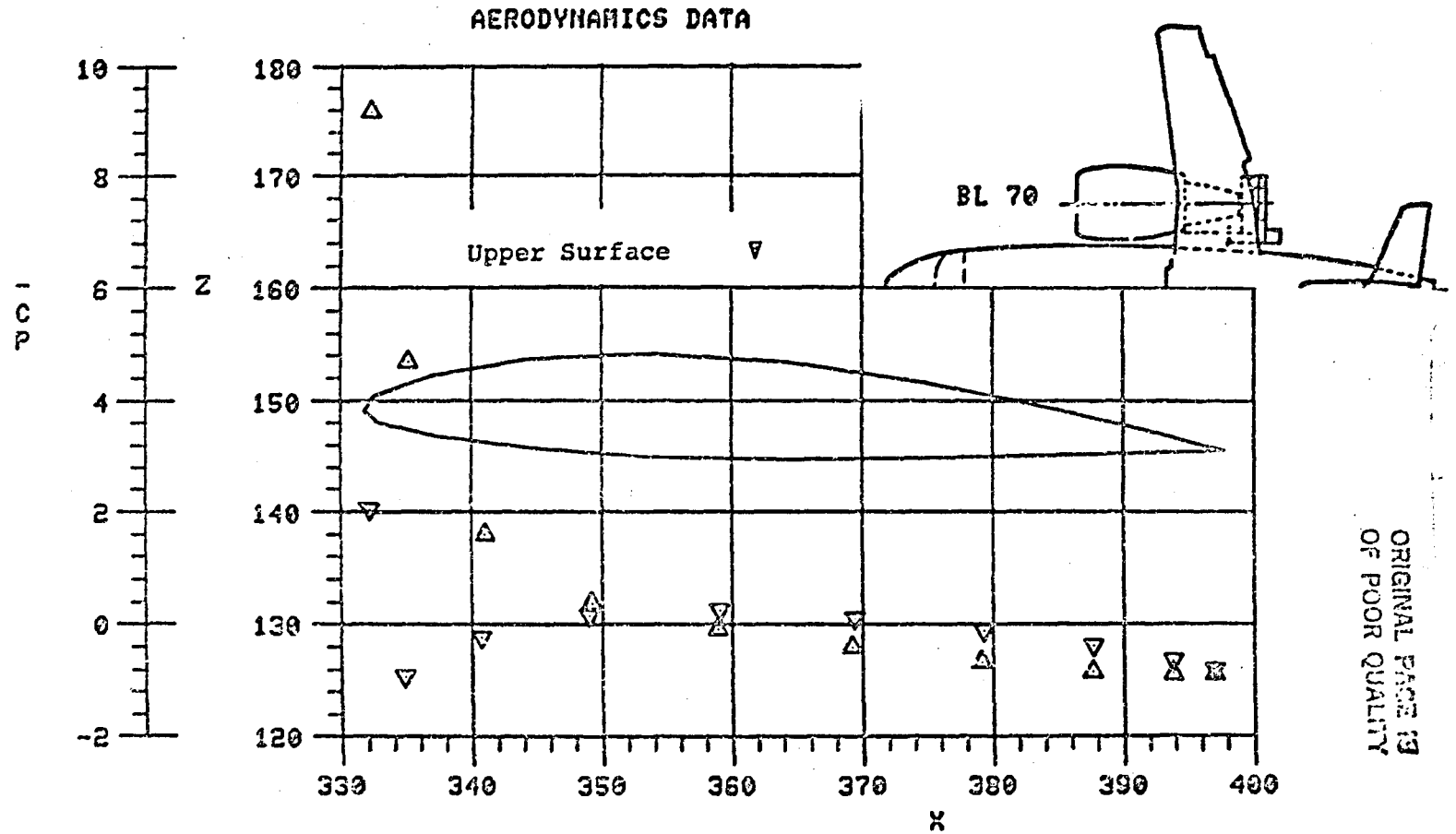

Figure 27(b). Grumman Design 698-411 Tilt-Nacelle, V/STOL Model; Nacelle-on Configuration; δ_N = 5.00, α = 0.0; Wing Spanwise Pressure Cut at y = 70.0.

was not reported in the experimental study due to the absence of wing pressure taps. It should be noted that an analysis of the wing surface pressures and further analysis of the fuselage surface pressures has been proposed for a future experimental study at NASA Ames.

A buttline cut through the symmetrical horizontal tail surface verifies that the tail is set at zero degrees angle of attack as shown by Figure 28(a) for the nacelle-off configuration. The slight downward loading evident on the tail leading edge is possibly caused by wing-induced downwash. The nacelle-on effects (see Figure 28(b)) indicate the presence of an upwash field at the tail producing tail lift. This upwash field is the result of a change in sign of the inboard wing loading (see Figures 27(a) and (b)) which is caused by the presence of the nacelle in the cruise condition ($\delta_N = 5.0^o$).

The fuselage/nacelle interference effects are evident when examining the fuselage upper surface pressure distribution as presented in Figures 29 and 30. This indicates an increase in velocity for the nacelle-installed configuration. The jet-induced effects on the fuselage underside are shown in Figures 31(a) and (b) for nacelle deflection angles of 5 and 50 degrees. The suction peak evident in Figure 31(b) for the nacelle deflection angle of 50^o is induced by the close approach of the jet wake which is passing within one jet diameter of the fuselage centerline as shown by Figure 25(g). The suck-down effect is expected to increase when entrainment of mainstream fluid is included in the jet wake model.

A preliminary comparison between experimental and calculated force and moment is shown in Figure 32 for the power-off configuration. The calculated lift and drag values show the correct trend but are on the low side. The pitching moment looks good at low lift but has a large discrepancy at the higher lift value. Even so, the correlations are encouraging; there are areas of the configuration surface that require more precise geometric definition, e.g., forward fuselage and nacelle support structure, before more serious correlations are attempted. Also, modelling of separated flow areas--predicted by the analysis (e.g., Section 5.2.2)--needs to be pursued.

5.1.3 Summary

Very good correlation with experiment was found for the nacelle inlet conditions at an angle of attack of 62^o to the crossflow for the complete Grumman configuration analyzed with VSAERO. A negative wing loading was calculated by VSAERO for the cruise configuration from the wing root to a spanwise station just outboard of the first flap station. This condition could not be verified due to the absence of experimental wing pressure data, but is justified by the forward location of the nacelle with respect to the wing leading edge.

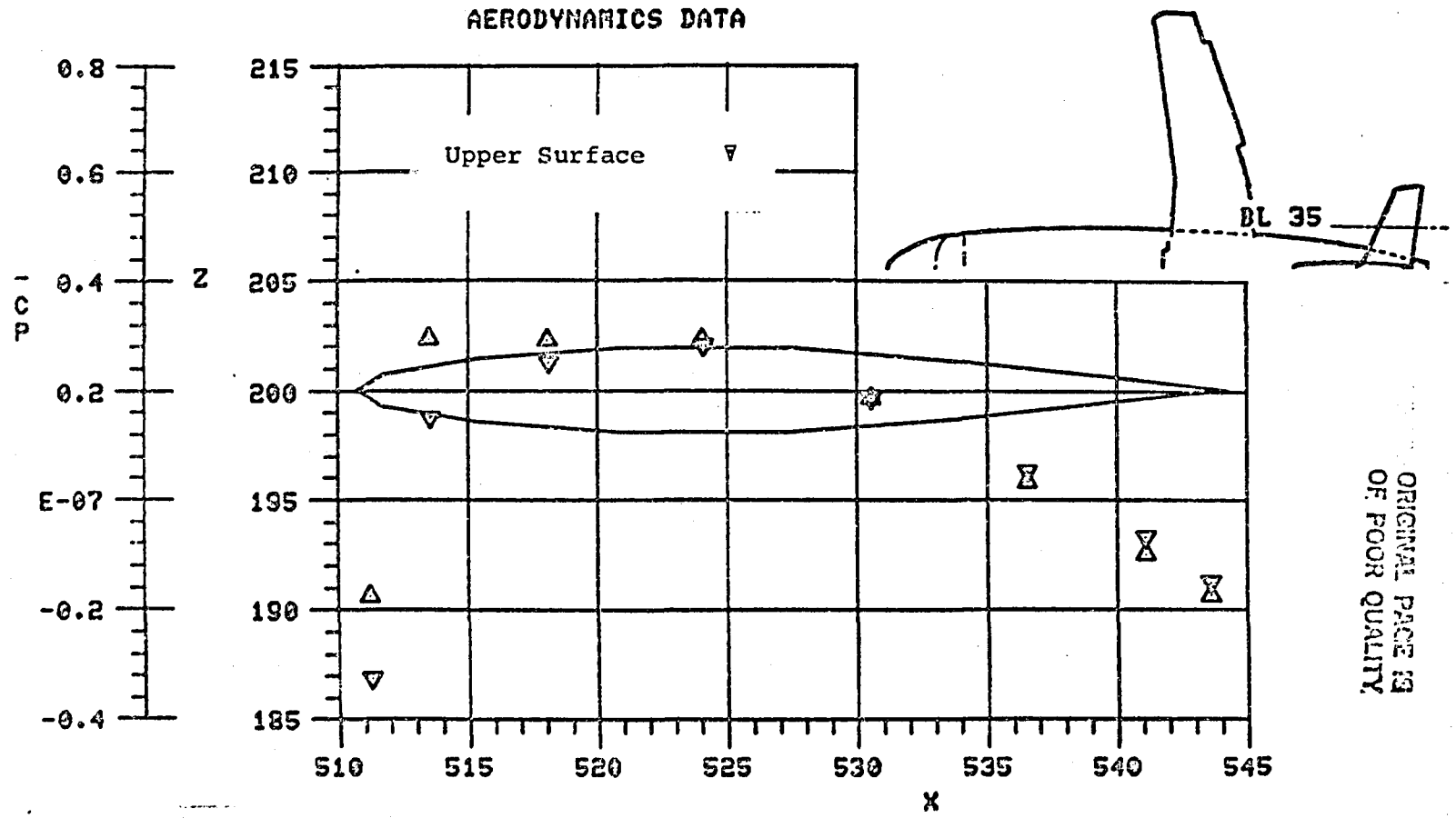

ORIGINAL PAGE IS
OF POOR QUALITY

Figure 28(a). Grumman Design 698-411 Tilt-Nacelle, V/STOL Model; Nacelle-off Configuration; Horizontal Tail Spanwise Pressure Cut at y = 35.0.

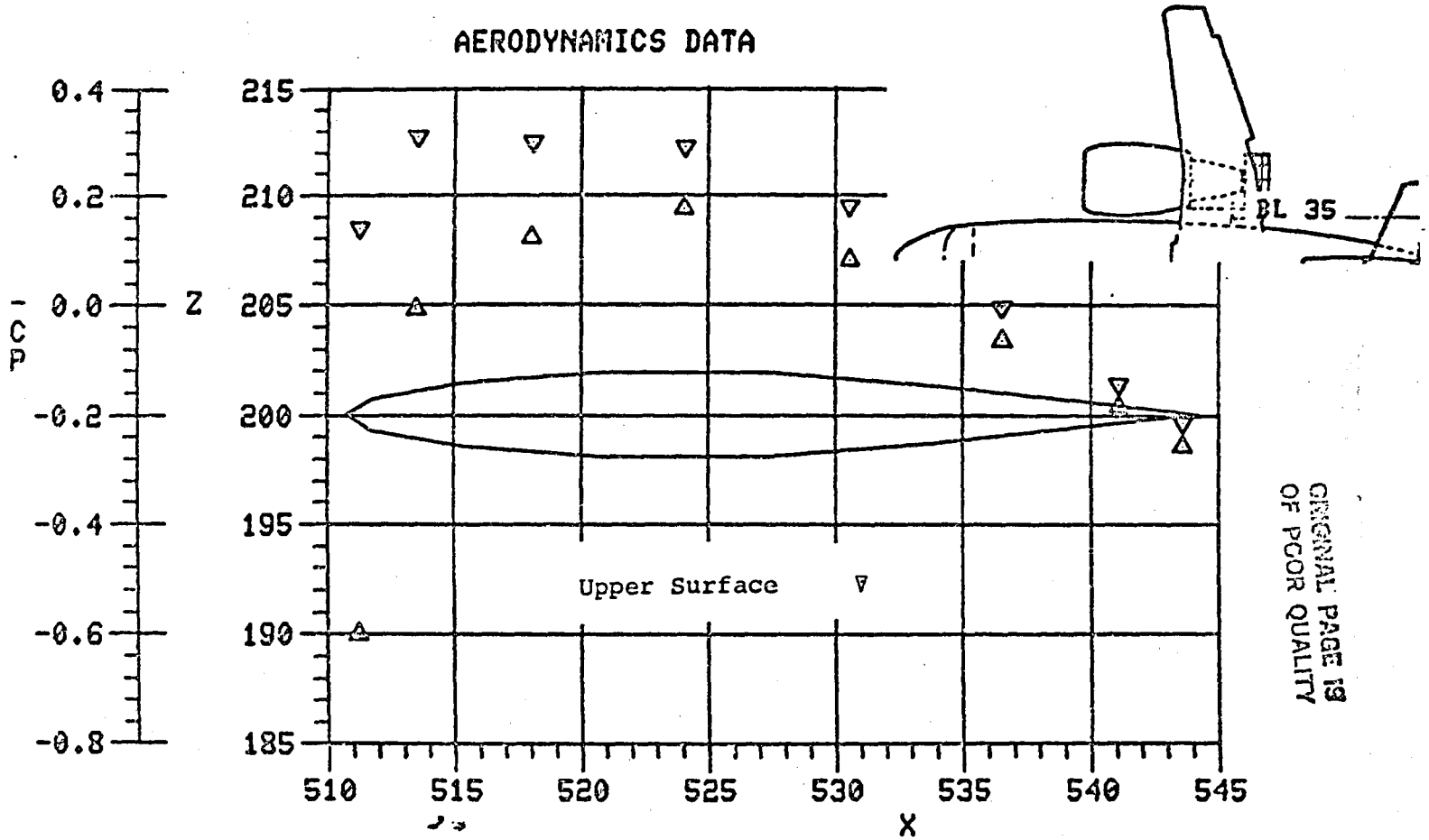

Figure 28(b). Grumman Design 698-411 Tilt-Nacelle, V/STOL Model; Nacelle-on Configuration; CUT '5.0°, α = 0.0; Horizontal Tail Spanwise Pressure Cut at y = 35.0.

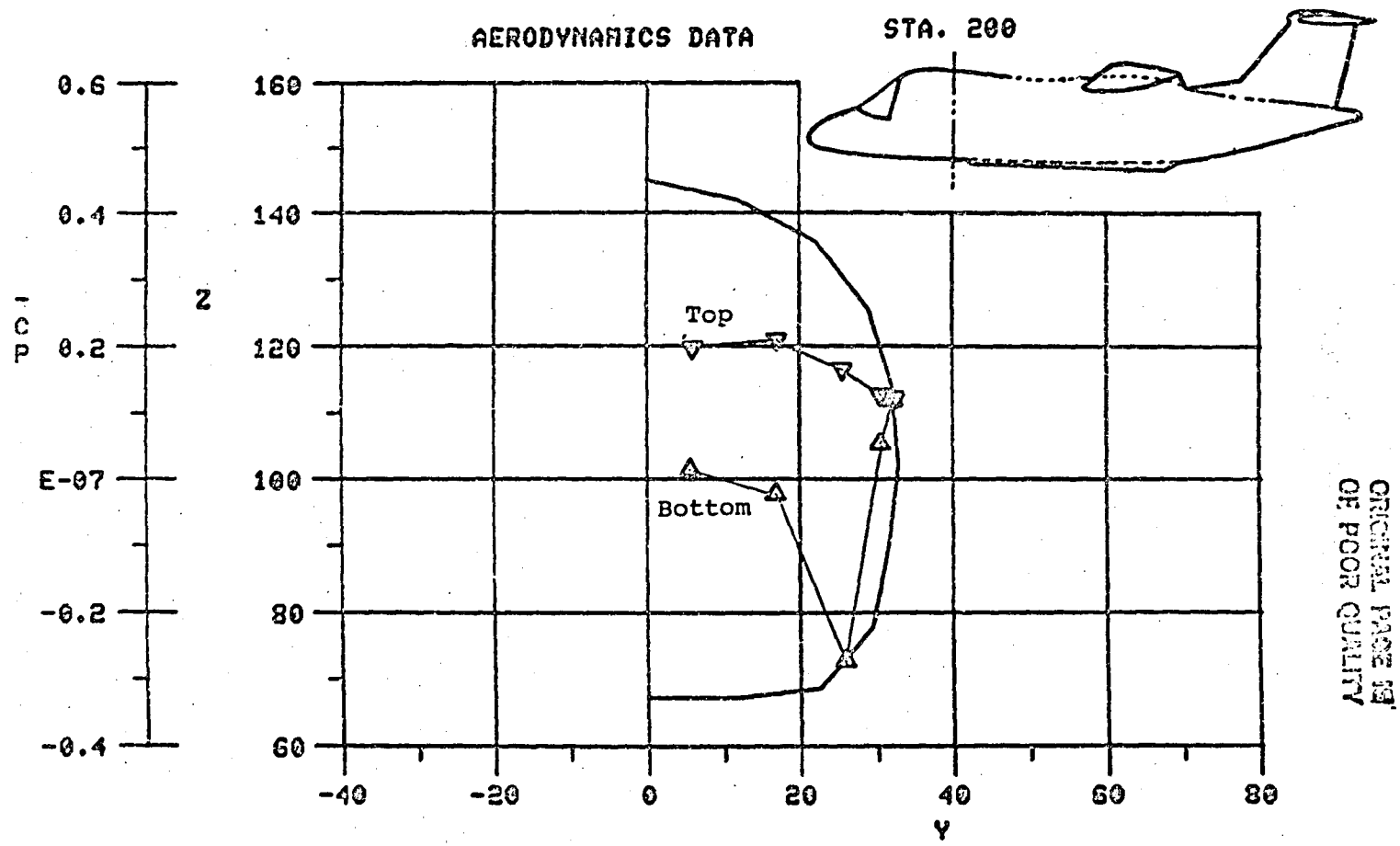

Figure 29(a). Grumman Design 698-411 Tilt-Nacelle, V/STOL Model; Nacelle-off Configuration Station Cut x = 200.0.

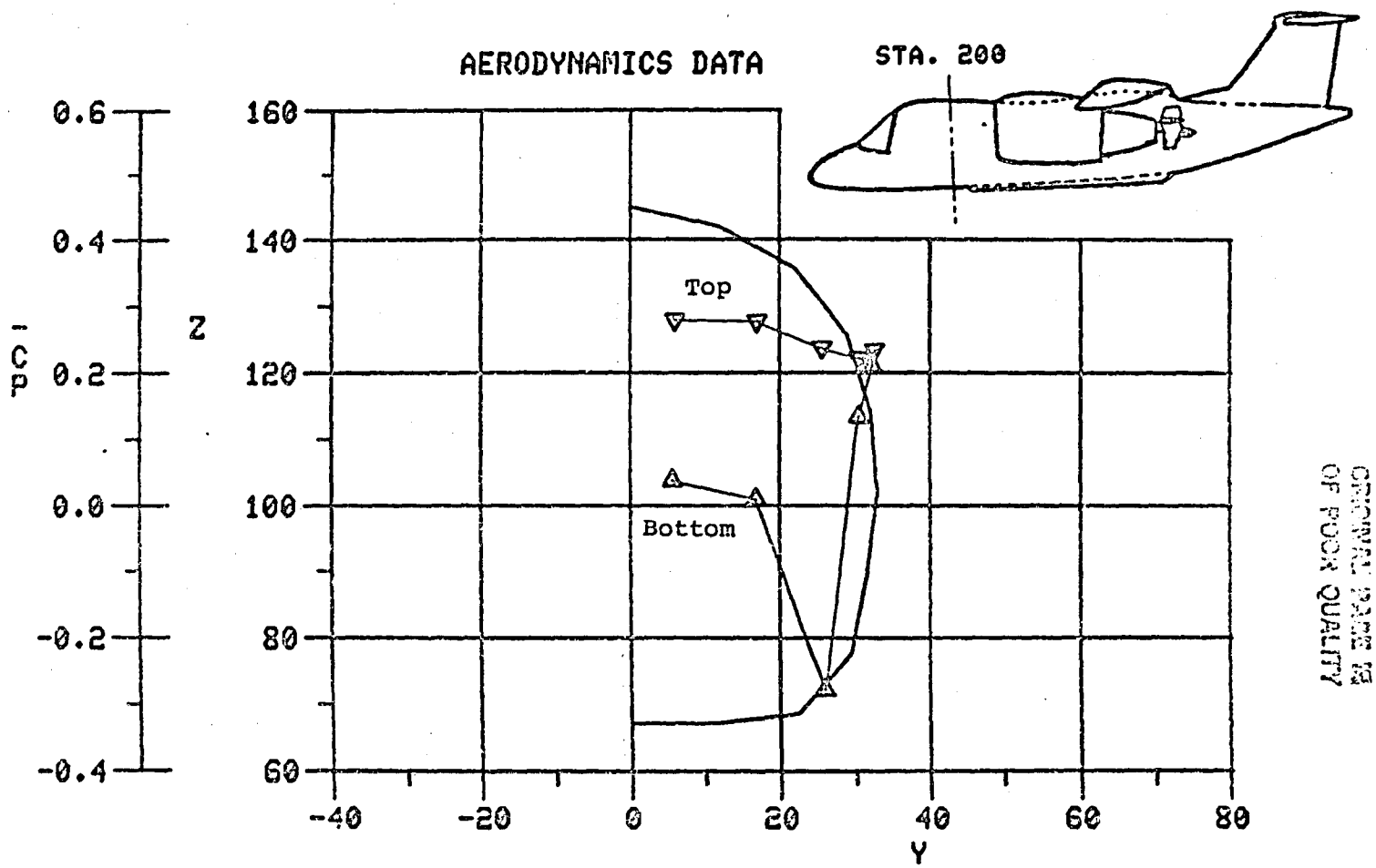

Figure 29(b). Grumman Design 698-411 Tilt-Nacelle, V/STOL Model; $\delta_N = 5.0$, $\alpha = 0.0$; Station Cut x = 200.0.

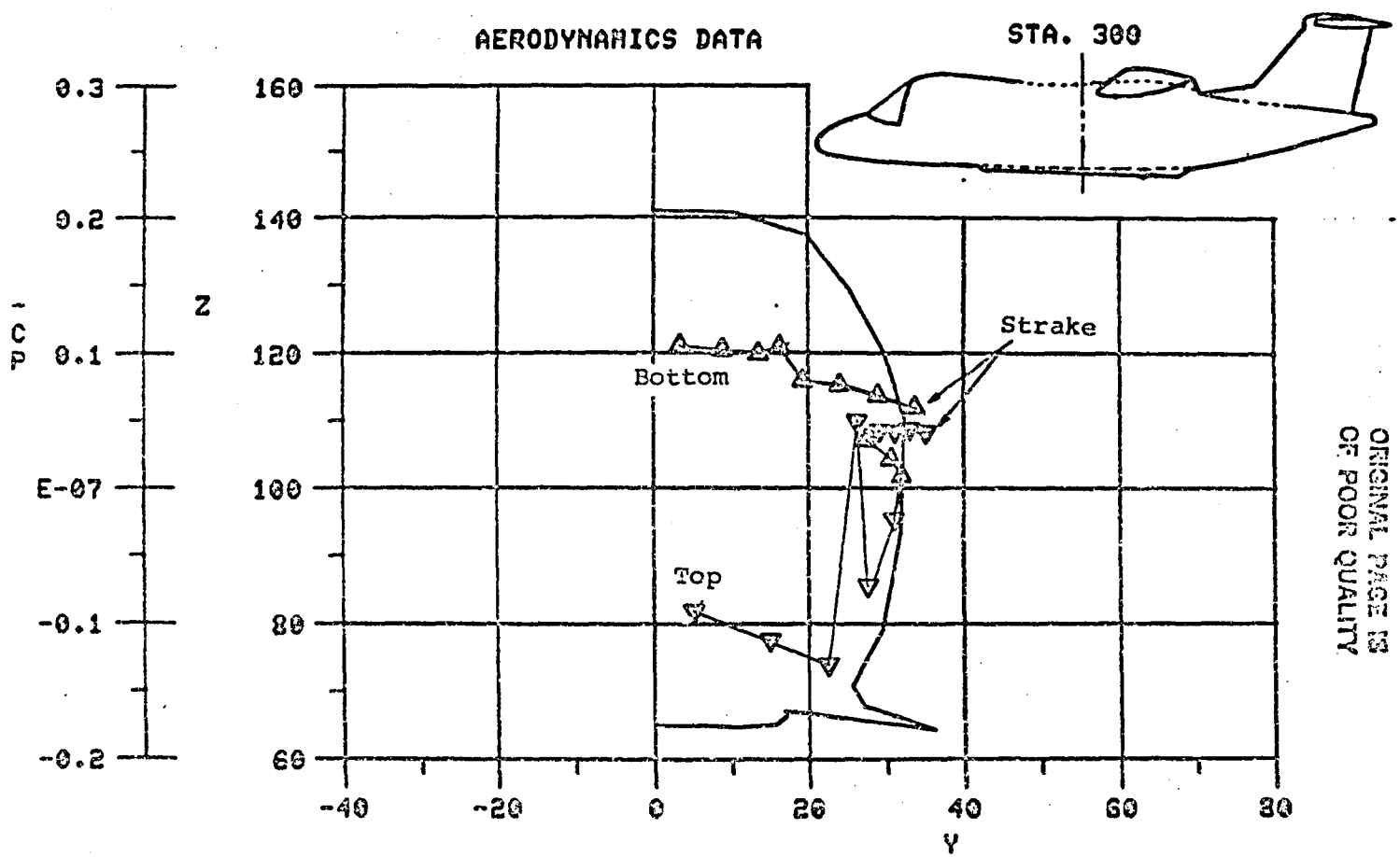

Figure 30(a). Grumman Design 698-411 Tilt-Nacelle, V/STOL Model; Nacelle-off Configuration; Station Cut x = 300.0.

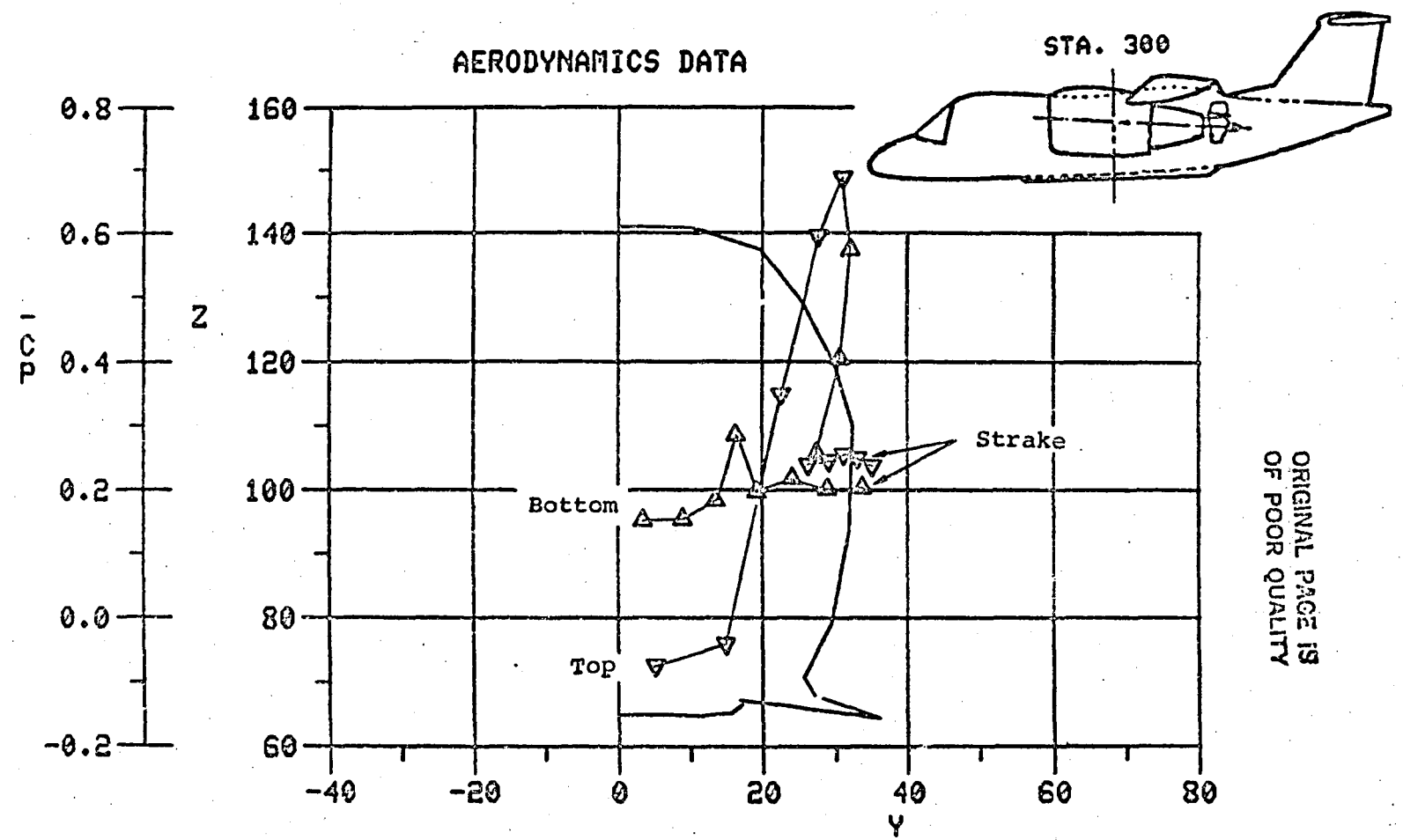

Figure 30(b). Grumman Design 698-411 Tilt-Nacelle, V/STOL Model; Nacelle-on Configuration; $\delta_N = 5.0°, \alpha = 0.0$, Station Cut x = 300.0.

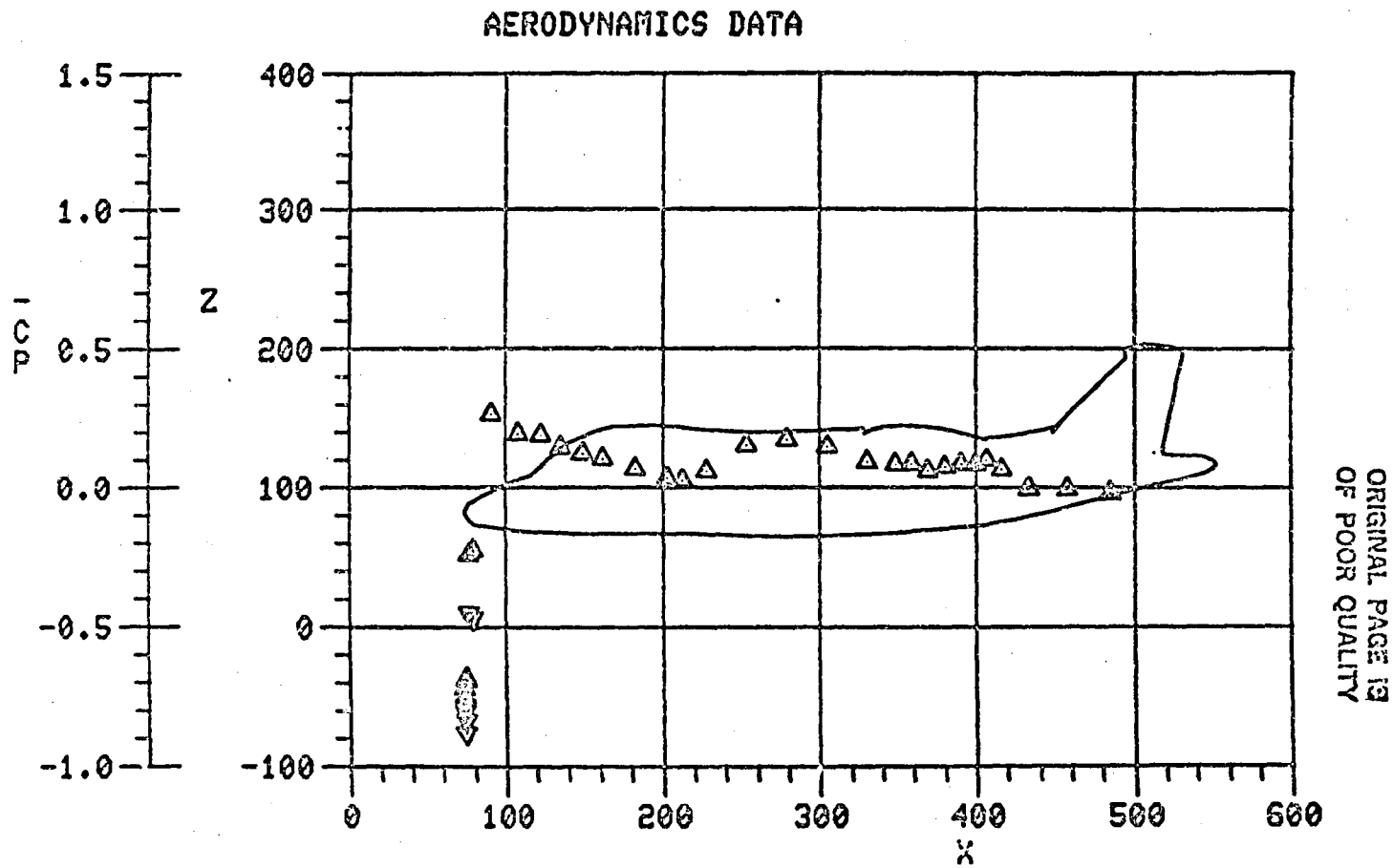

Figure 31(a). Grumman Design 698-411 Tilt-Nacelle, V/STOLModel; $\delta_N = 5.0^\circ$, $\alpha = 0.0$, Fuselage Centerline Lower-Surface Pressures.

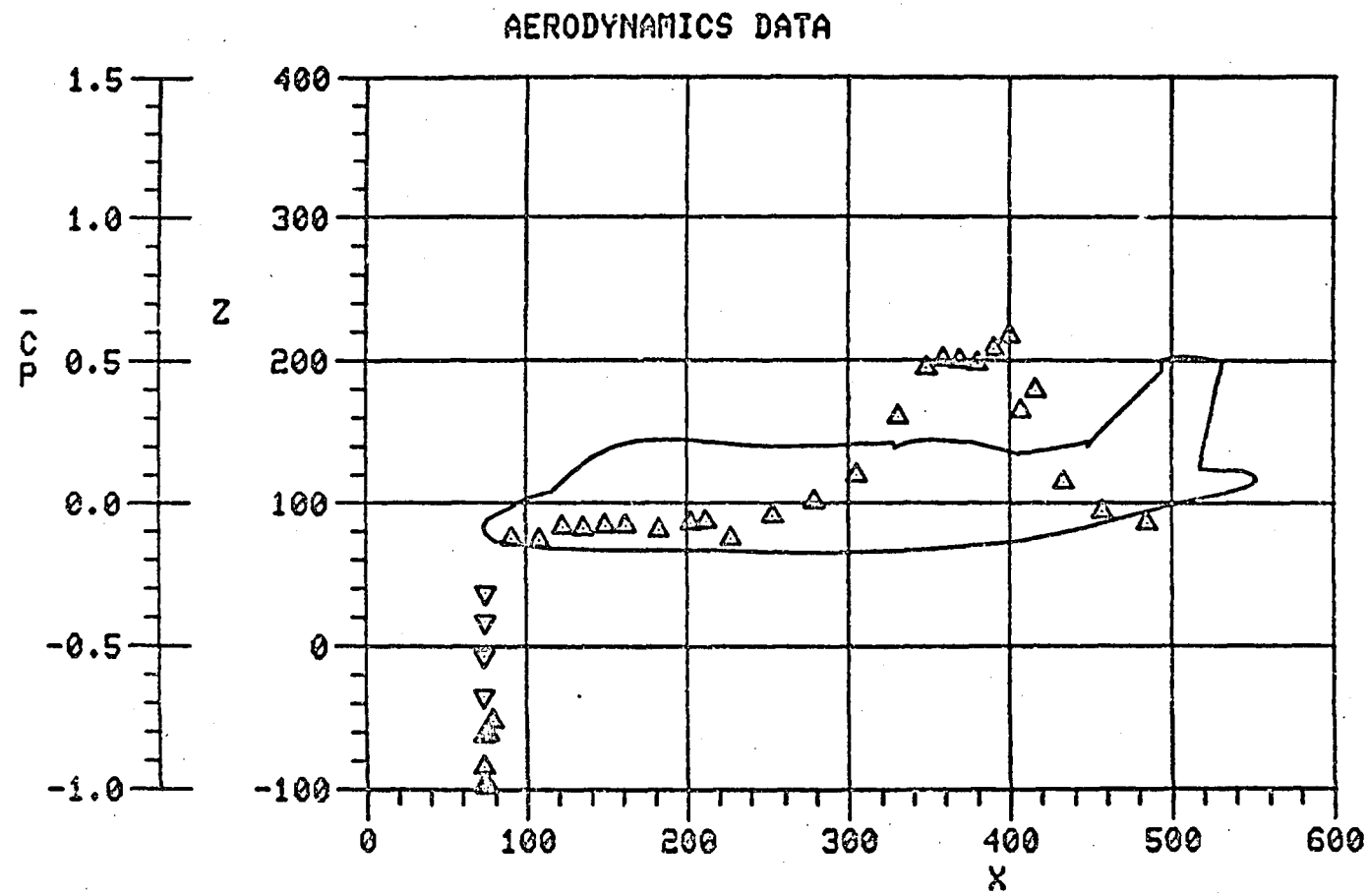

Figure 31(b). Grumman Design 698-411 Tilt-Nacelle, V/STOL Model; $\delta_N = 50.0°$, $\alpha = 16.5$, Fuselage Centerline Lower-Surface Pressures.

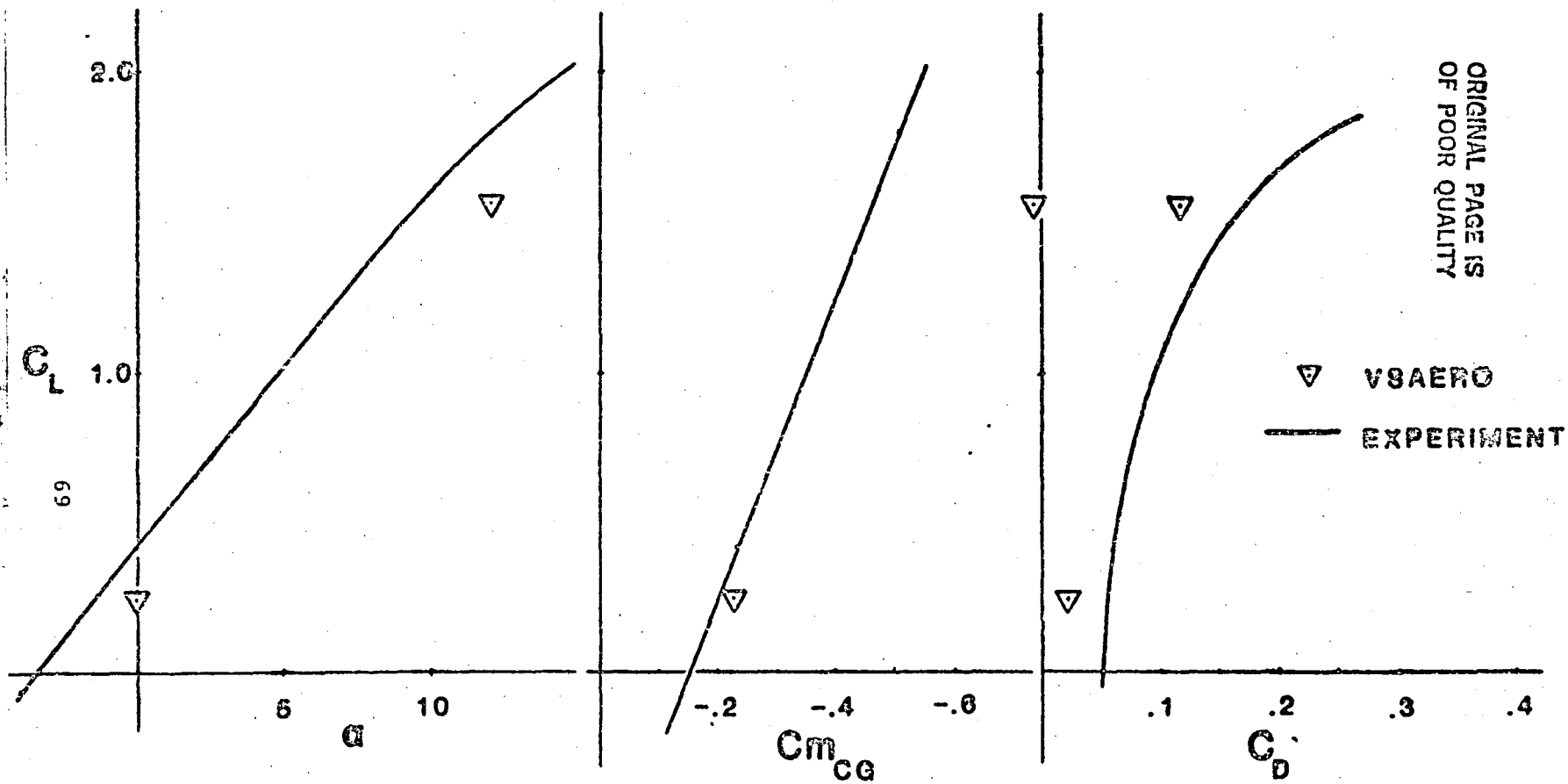

Figure 32. Aerodynamic Characteristics of the Grumman Tilt-Nacelle Configuration (δ_N = 5°; Windmill).

A qualitative picture of the jet-induced effects on the Grumman fuselage were determined by the analysis with VSAERO, but correlation with experiment is limited to lower fuselage centerline pressures in ground effect which was not treated in this study.

The computing time for the complete configuration was 190 seconds on the CRAY 1-S. The calculation involved 1760 surface panels on one side of the plane of symmetry and included 24 streamline and boundary layer calculations (discussed in 5.2).

5.2 TF34-100 Streamline and Boundary Layer Analysis

5.2.1 Configuration

Due to the high angle-of-attack environment present in the Grumman tilt-nacelle V/STOL design, the inlet performance is a critical parameter in determining the transition capabilities of the aircraft. Utilizing the coupled streamline and boundary layer procedure available in VSAERO (45)(46), a preliminary study was undertaken to determine the inlet and external engine cowling boundary layer characteristics for both nacelle-alone and nacelle-installed configurations (see Figures 33 and 34). Although not required in the statement of work, it was determined that the prediction of nacelle inlet performance characteristics with VSAERO warranted a brief but concise examination. The complete test conditions are summarized in Table 2.

Configuration Description	Total Nacelle Angle of Attack (deg)	Specific Airflow ($W_K/ACAP$)	Inlet Fan Velocity Ratio (V_F/V_∞)
Nacelle Alone	45.0	0.14	2.12
	56.5	0.14	2.12
	56.5	0.18	2.73
	76.5	0.20	3.03
Complete Configuration	76.5	0.20	3.03

Table 2. Streamline and Boundary Layer Test Conditions.

ORIGINAL PAGE IS
OF POOR QUALITY

Figure 33. TF34 Tilt-Nacelle/Streamline and Boundary Layer Analysis: TF34 Geometry.

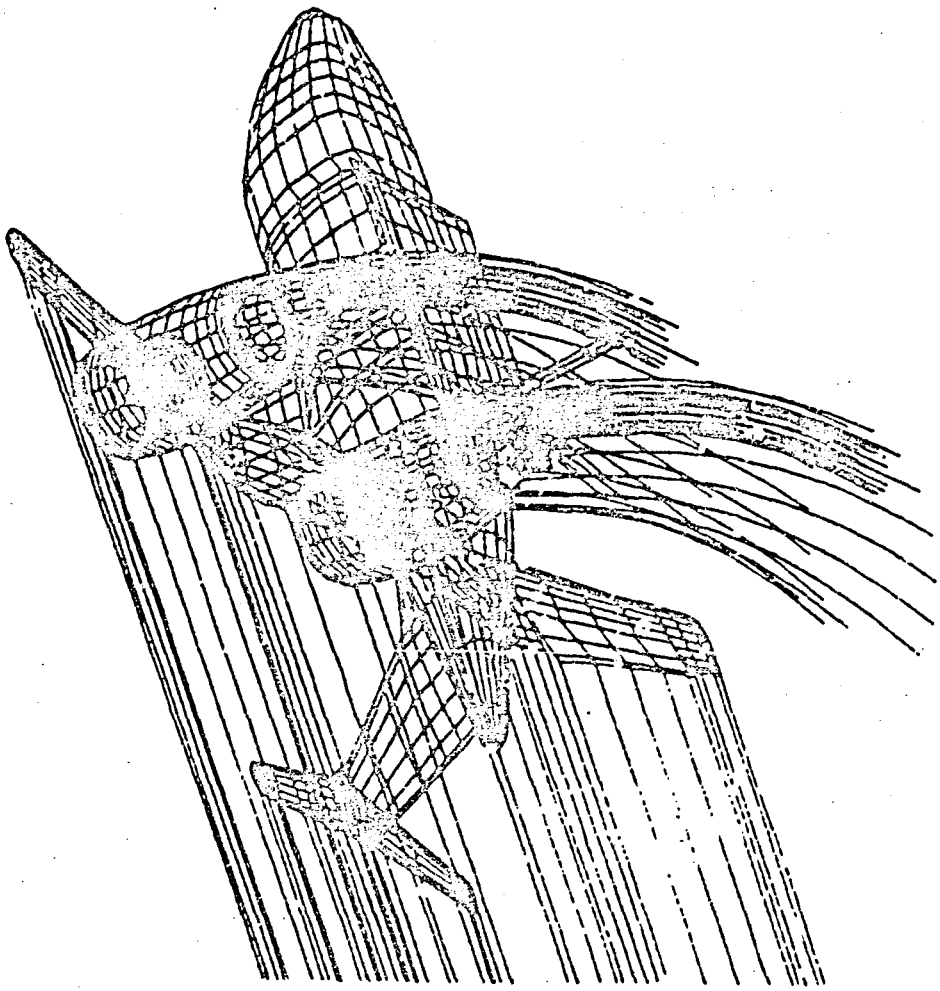

Figure 34. Grumman 698-411 Tilt-Nacelle V/STOL Model.

5.2.2 Results

The operational boundaries of the TF34-100 nacelle as calculated by VSAERO correlate well with the results from wind tunnel tests of the Grumman design 698-411 tilt-nacelle V/STOL model conducted at NASA Ames (27). The operational boundary of the TF34-100 nacelle, which is determined by the onset of separation in the engine inlet, is described in this case by a plot of nacelle absolute angle of attack as a function of engine specific air flow. The VSAERO results for a freestream velocity of 100 knots are presented in Figure 35 along with the appropriate test data.

A possible explanation for the scatter in the experimental data as shown by Figure 35 involves the nacelle/fuselage interference. As previously mentioned the parameter plotted on the ordinate is the "absolute" nacelle angle of attack which consists of the nacelle angle of attack relative to the fuselage reference line (δ_N) and the configuration angle of attack (α). The data scatter, therefore, may be produced by varying both δ_N and α with δ_N being in a sense a measure of the degree of nacelle/fuselage interference. To emphasize this point, the nacelle/fuselage interference effects were "minimized" by setting α to zero and δ_N to 76.5°.(This may not necessarily be a minimum but the fuselage-induced upwash will be reduced relative to a case with α set to, say, 12° and δ_N set to 64.5°.) The inlet boundary layer results indicate only a very slight difference between the nacelle alone and the nacelle installed configurations as indicated by Figure 36, which is a plot of skin friction coefficient (C_{fD}) as a function of streamline length (S) for both cases. The inlet separation zone for both nacelle alone and nacelle installed is presented in Figure 37. These plots indicate the relatively small difference in the inlet flow environments between the isolated and installed nacelle when the fuselage/nacelle interference is minimized in the latter case. This appears to be a likely explanation for the data scatter experienced in the experimental study and indicative of a "family" of inlet performance separation boundaries with varying alpha.

In the potential flow calculations a range of inlet flow conditions is represented by one solution in which the inlet velocity is normalized by the free-stream velocity. By dividing the specific airflow by the free-stream velocity magnitude, the experimental inlet separation boundaries for a range of forward flight velocities were found to collapse onto one plot shown in Figure 38. It may be inferred from this interesting characteristic that the model need not be tested at a full range of free-stream velocities to determine the overall inlet performance envelope. A sampling of wing tunnel data to verify a full analysis with VSAERO would free valuable wind tunnel operation time and thus allow for other important aspects of this configuration to be examined.

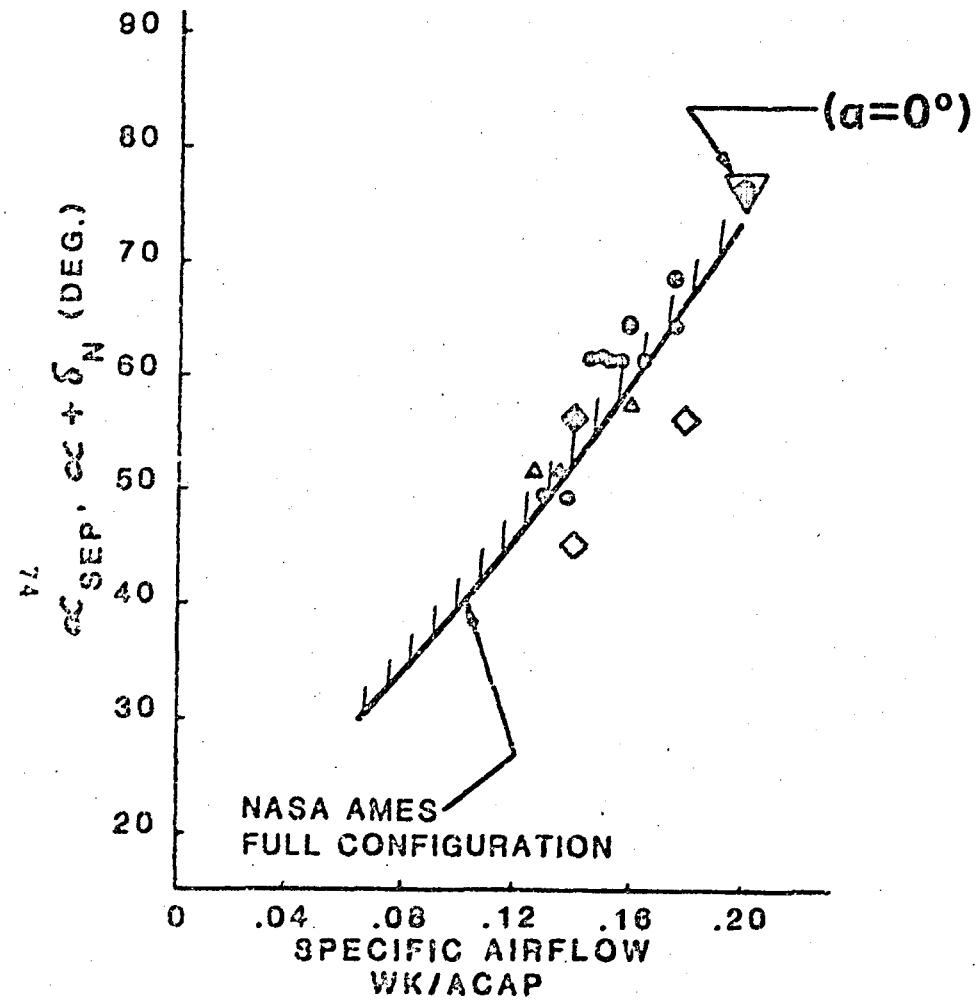

VSAERO ANALYSIS :

TF34 NACELLE ALONE
SEPARATED FLOW ◆
ATTACHED FLOW ◇
FULL CONFIGURATION
SEPARATED FLOW ▽

EXPERIMENTAL RESULTS :
SEPARATED ⊙
INCIPIENT ⊕
ATTACHED △

Figure 35. Experimental Inlet Separation Boundaries with VSAERO Analysis (V_∞ = 100.0 kts.).

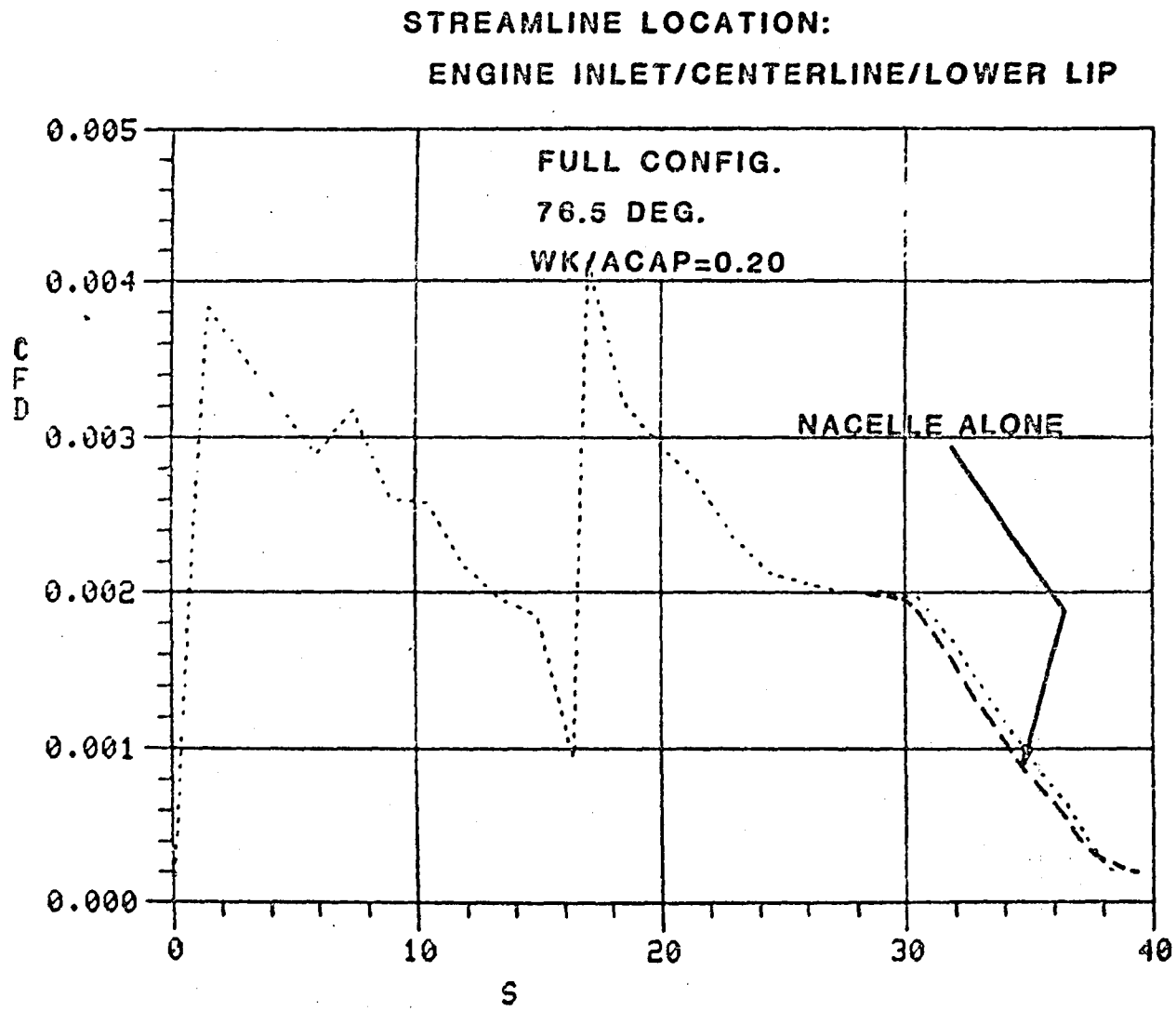

Figure 36. TF-34 Tilt-Nacelle/Streamline and Boundary Layer Analysis; Internal Flow in Nacelle-Alone and Full Configuration; Skin Friction Drag Coefficient, C_{f_D} Versus S.

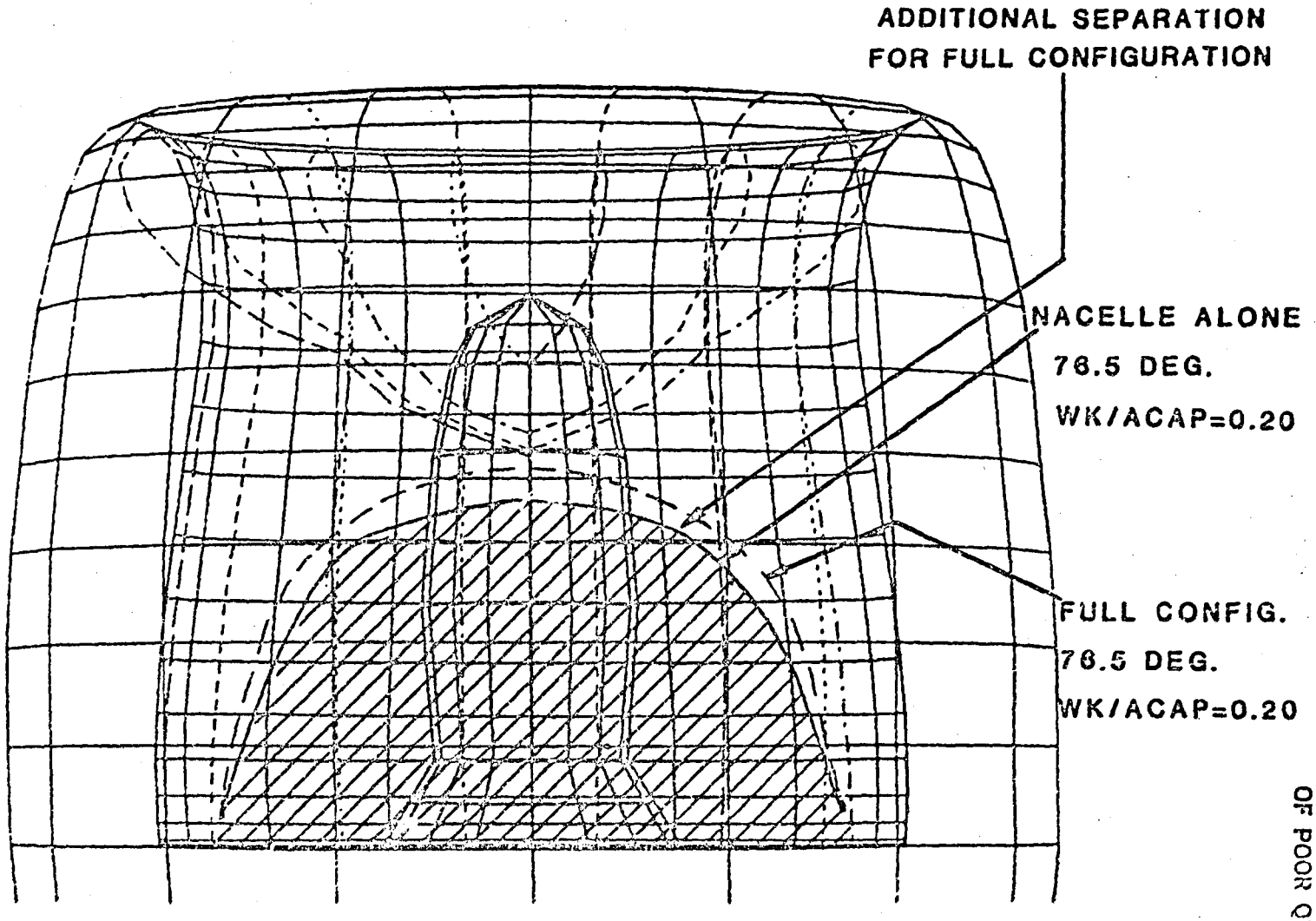

Figure 37. TF-34 Tilt-Nacelle/Streamline and Boundary Layer Analysis; Internal Flow in Nacelle-Alone and Nacelle-Installed; Internal Separation Zone Calculated by VSAERO.

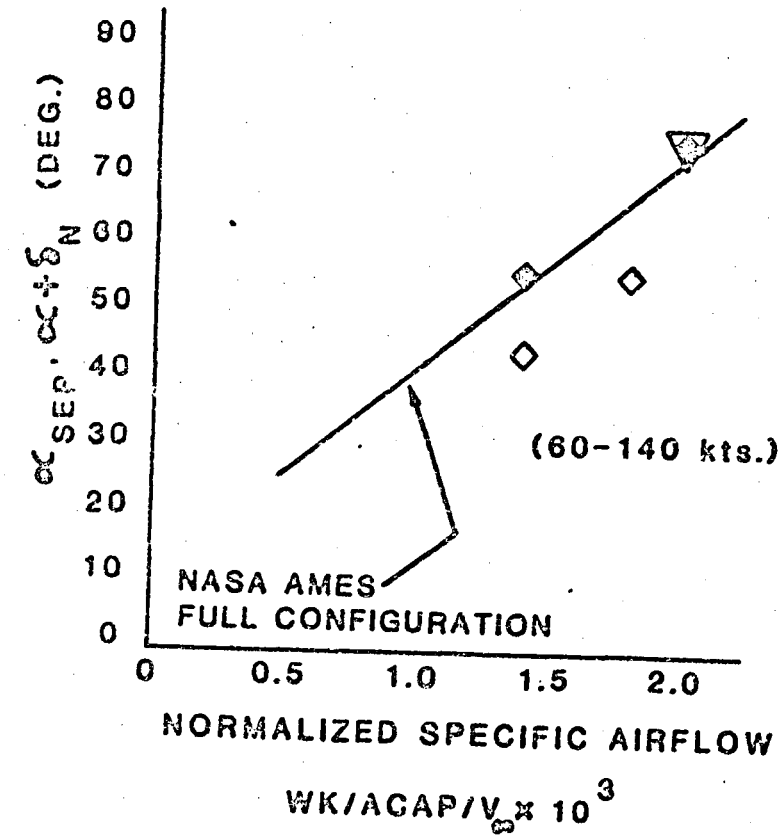

VSAERO ANALYSIS :

TF34 NACELLE ALONE
SEPARATED FLOW ◇
ATTACHED FLOW ◇
FULL CONFIGURATION
SEPARATED FLOW ▽

Figure 38. Experimental Inlet Separation Boundaries in Parametric Form with VSAERO Analysis.

In general a viscous/potential flow iteration tends to result in a boundary layer degradation for the TF-34 nacelle inlet as shown by a plot of C_{fp} as a function of S in Figure 39. The application of VSAERO to external flows such as wings at high angles of attack produced a general improvement in the boundary layer parameters after a viscous/potential flow iteration with convergence reached after an appropriate number of cycles (~3-5). The explanation for the degradation in the inlet flow conditions after the source transpiration/potential flow cycle is apparently associated with inlet flow continuity. A plot of the resultant velocity along the inlet centerline lower lip for both the initial solution as well as the solution with one viscous/potential flow iteration reveals a general slow-down of the inlet velocity in the latter case (see Figure 40). With the fan face velocity constant throughout the calculation (as specified by the user) the introduction of fluid by the source transpiration technique results in a reduction in the inlet flow velocity thus satisfying continuity in the inlet. The boundary layer sees this inlet velocity reduction as an equivalent reduction in mass flow (or a shift to the left on the inlet separation boundary plot with α_{SEP} constant) thus resulting in inlet boundary layer deterioration. This blockage effect may be alleviated by incrementing the fan face velocity based on the amount of additional fluid introduced during the viscous/potential flow cycle. Also requiring further study and related to this analysis phenomenon is the source transpiration modelling beyond separation. Currently the source values are set to zero beyond separation but the feasibility of a source model coupled with the boundary layer parameters at separation should be examined.

The adverse effect of the close coupling between the nacelle and fuselage is clearly shown by the behavior of streamlines on the external engine cowling. In particular, flow asymmetry, a direct consequence of the fuselage induced upwash, was observed in experiment when comparing the inboard and outboard engine cowling as well as being indicated by the VSAERO calculation for the full configuration which is shown in Figure 41. The inboard external streamlines are observed to separate earlier for the nacelle-installed condition as compared to the nacelle-alone environment. Since the streamlines on the inboard side of the engine cowling are in the presence of a crude representation of the dumbbell support structure for this analysis, further insight into the adverse effects of the nacelle/fuselage interaction would require a more accurate panel representation of this nacelle support structure to ensure an accurate analytical environment.

Jet-induced power effects as calculated by VSAERO are clearly shown by observing the behavior of the external streamlines with a change in engine mass flow (see Figure 42). With a 50% increase in mass flow the engine cowling separation zone decreases in size due to the increase in the capture area stream tube and a reduction in spillage.

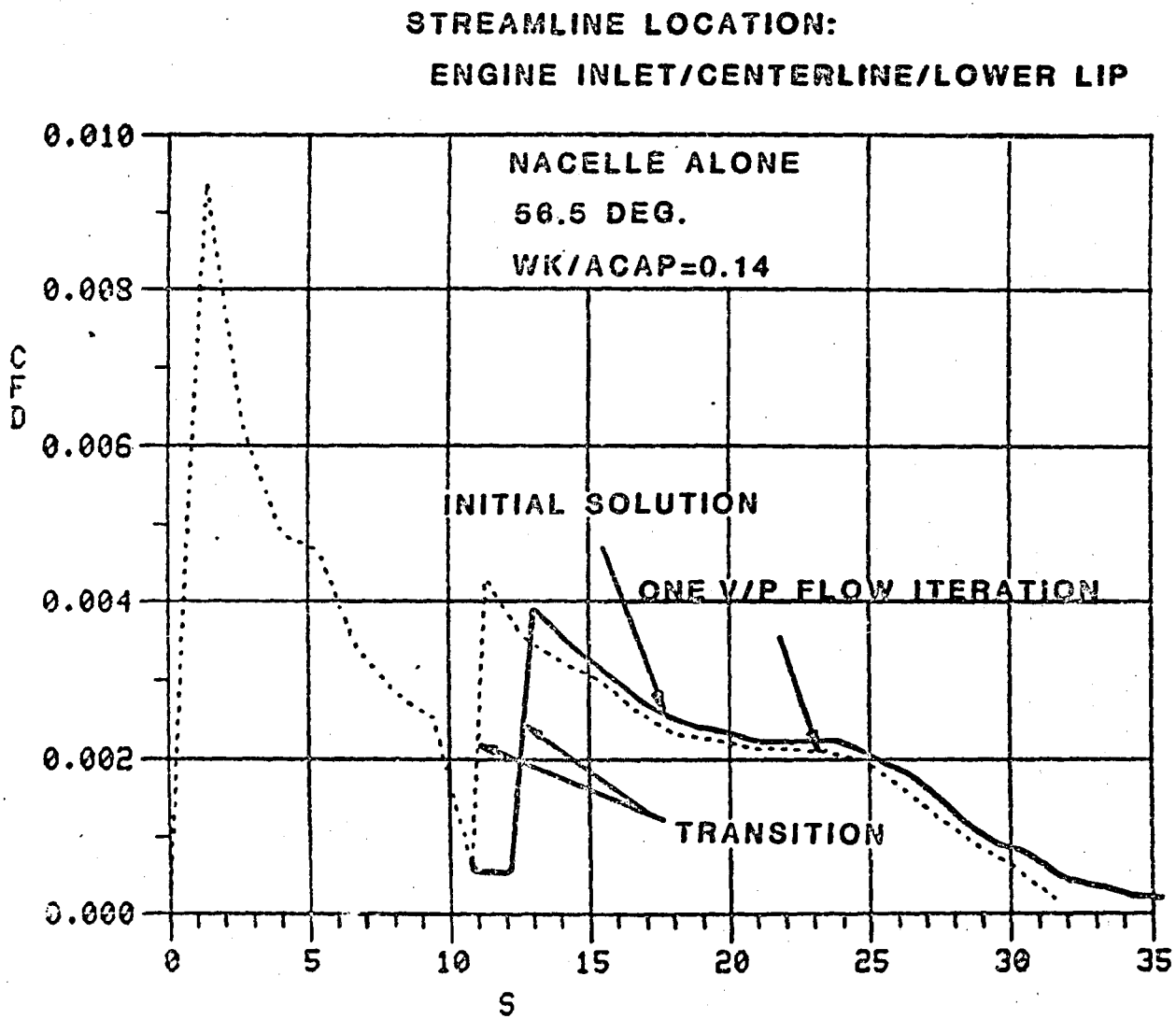

Figure 39. TF-34 Tilt-Nacelle/Streamline and Boundary Layer Analysis; Viscous/ Potential Flow Iteration; Separated Inlet Flow; Skin Friction Drag Coefficient, C_{f_D} Versus S.

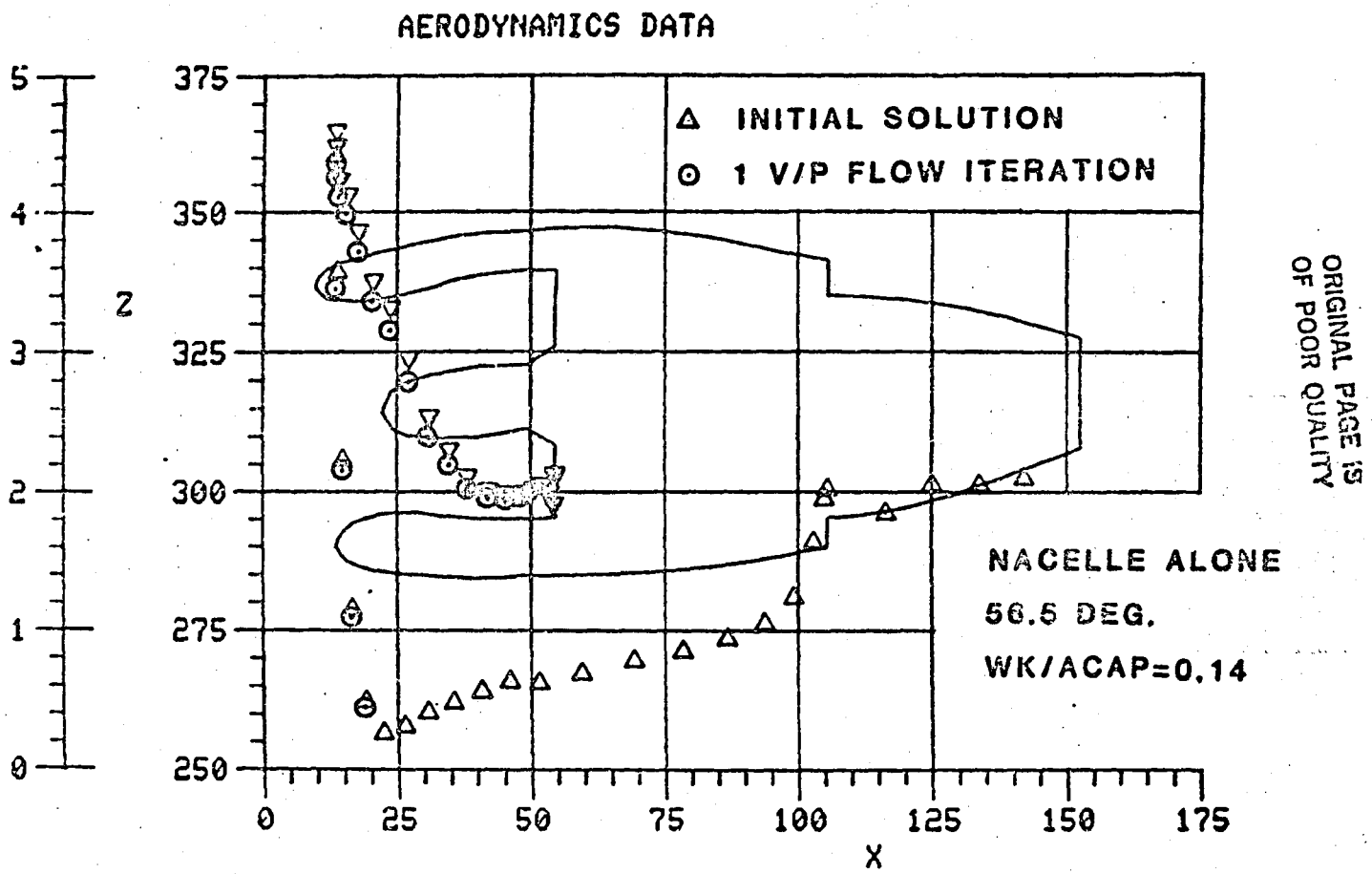

Figure 40. TF-34 Tilt-Nacelle/Streamline and Boundary Layer Analysis; Viscous/Potential Flow Iteration; Separated Inlet Flow; Resultant Velocity along Inlet Centerline--Lower Lip.

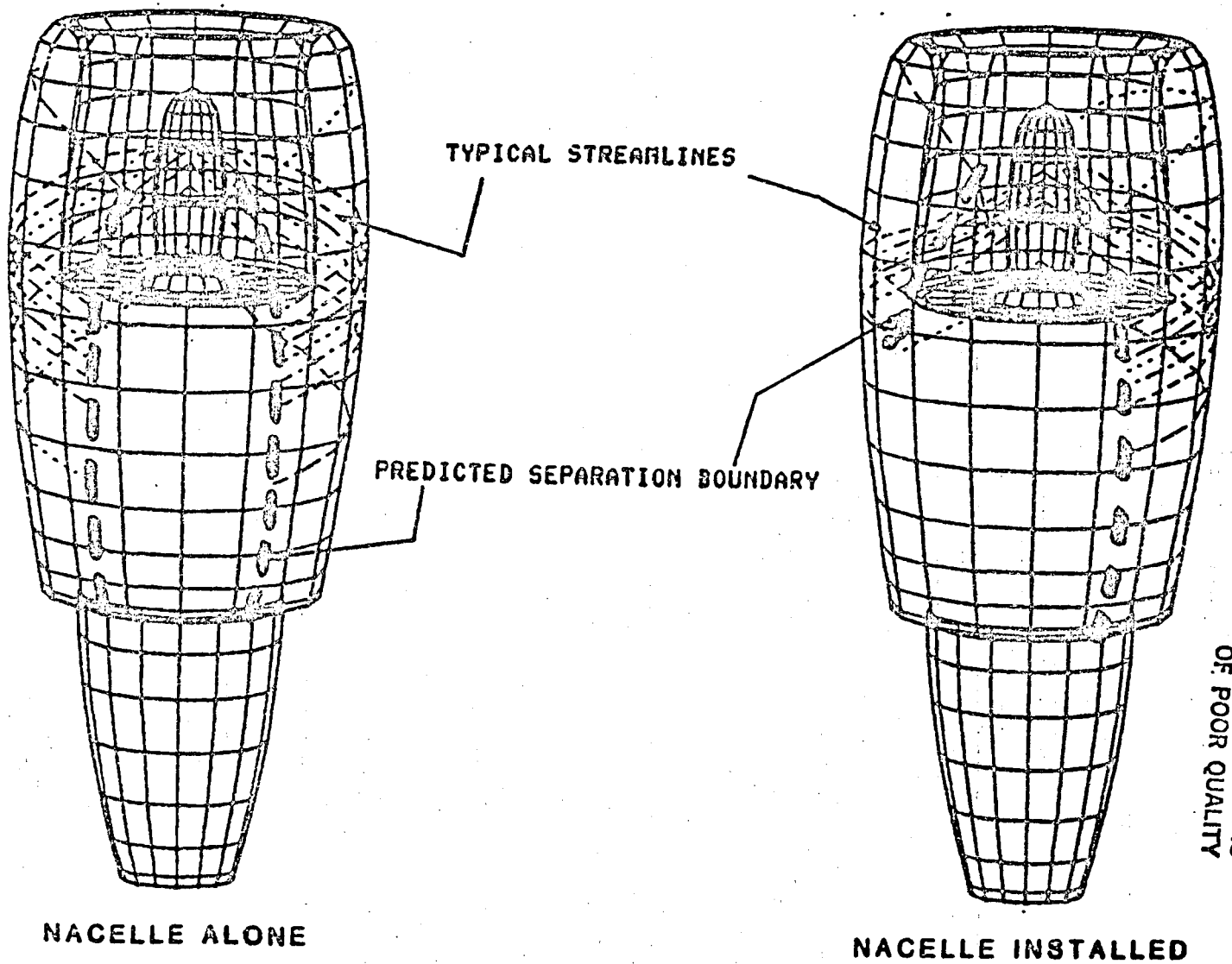

Figure 41. TF-34 Tilt-Nacelle/Streamline and Boundary Layer Analysis; Top View; External Streamlines; Sample Calculation.

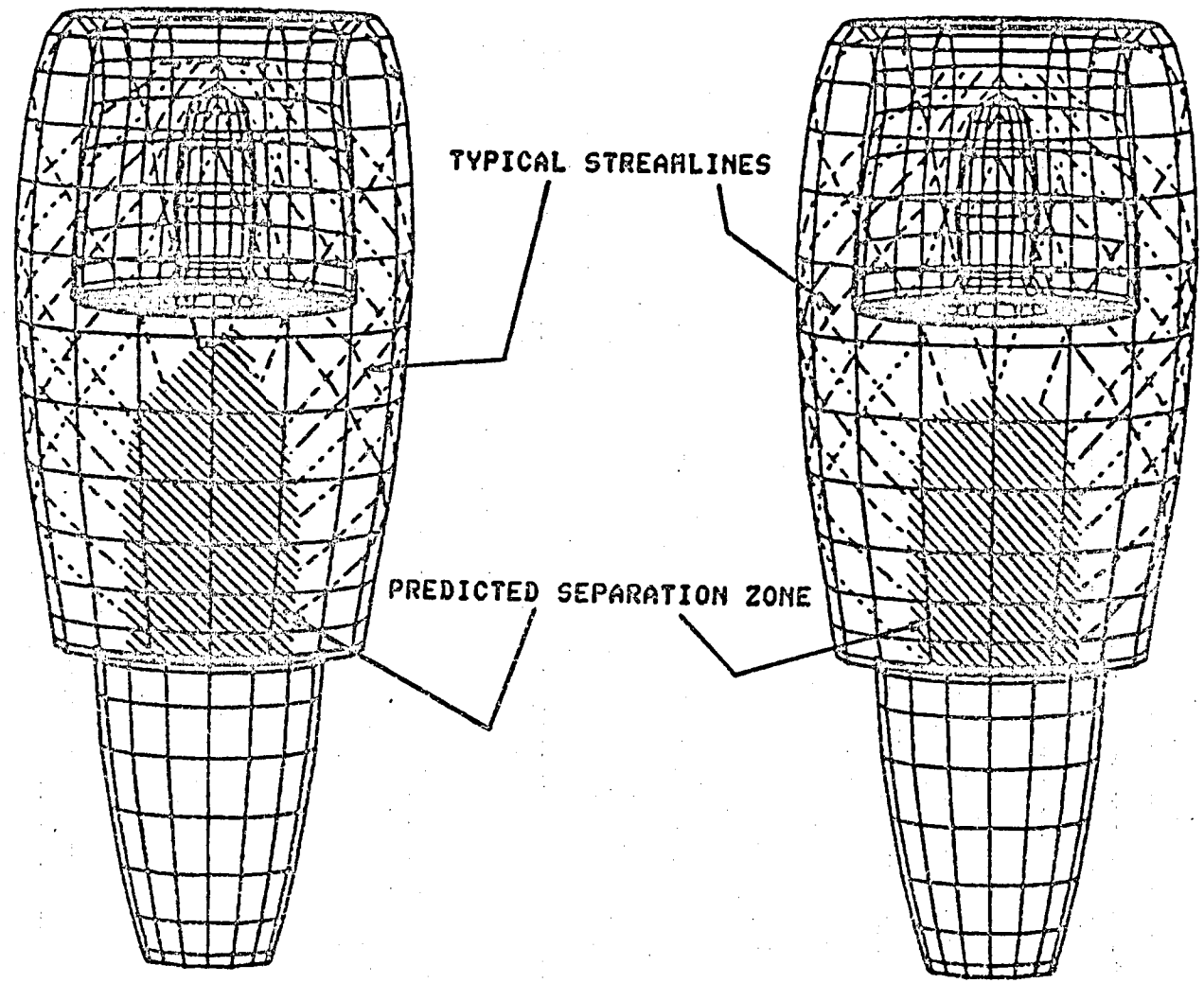

Figure 42. TF-34 Tilt-Nacelle/Streamline and Boundary Layer Analysis; Top View; External Streamlines; Effect of Mass Flow on External Separation Zone.

Typical boundary layer calculations for attached inlet flow conditions are shown in Figure 43(a) and (b) for C_{f_D} and from factor (H) as a function of S.

5.2.3 Summary

Promising results were obtained for the streamline/boundary layer analysis of the TF34-100 tilt-nacelle at a full range of flow conditions with the nacelle at high angles of attack. This study has shown the economy in utilizing VSAERO for the analysis of the full configuration performance characteristics and the results are verified by existing experimental data. The nacelle-alone calculations involved 784 surface panels on one side of the plane of symmetry and included 24 streamline/boundary layer calculations. These calculations were made on a PRIME 550 minicomputer and took 8200 CP seconds, which is equivalent to about 82 seconds on the CRAY.

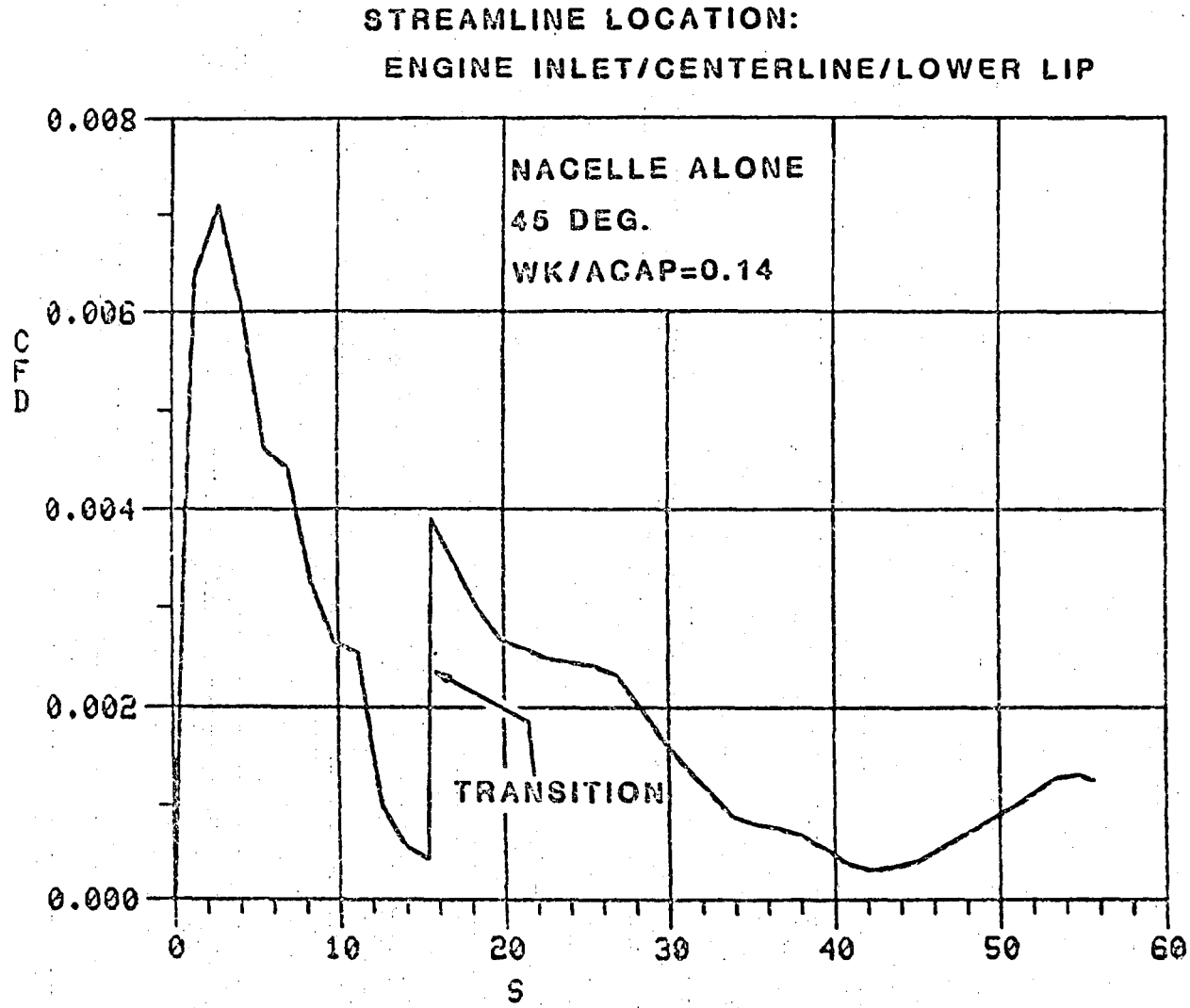

Figure 43. TF-34 Tilt-Nacelle/Streamline and Boundary Layer Analysis; Attached Inlet Flow.

(a) Skin Friction Coefficient, C_{f_D} Versus S.

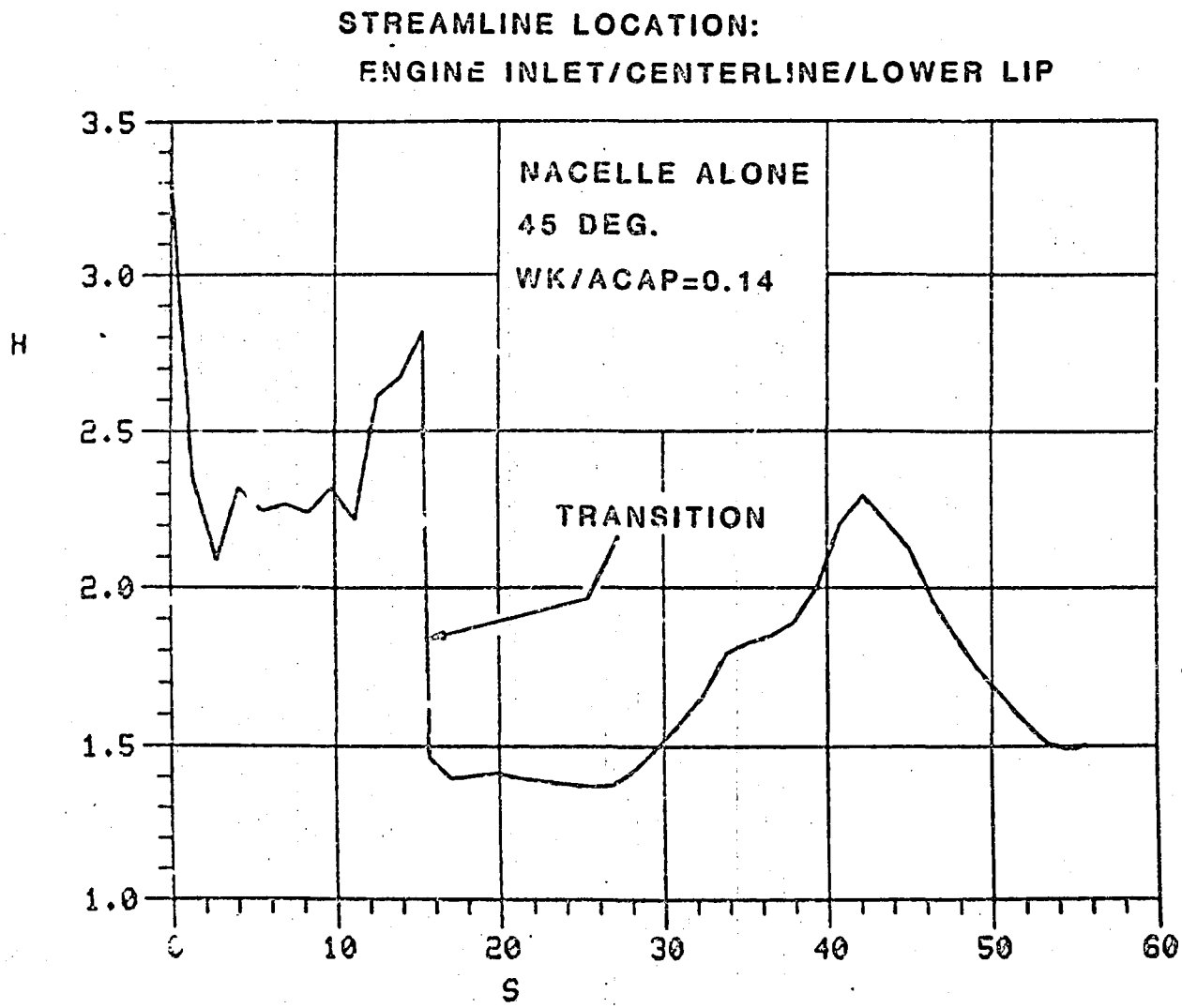

Figure 43. Concluded.
(b) Form Factor, H Versus S.

5.3 The Application of a Simple Jet Model in VSAERO to Analyze a Powered STOL Fighter

5.3.1 Configuration

The STOL (Short Takeoff and Landing) Fighter Model was designed as a 3/4-size representation of a high-performance supersonic fighter aircraft. A drawing of the model is shown in Figure 44. The salient feature of this aircraft is the Vectored-Engine-over-Wing (47) propulsion system. In this concept the engine efflux impinges on the inboard plain flap, leading to a change in the thrust vector whenever the flap is deflected.

Thrust is provided by two General Electric J-97 turbojet engines installed in podded nacelles over the wings. Each engine has a rated thrust of 14,011 N at a nozzle pressure ratio of 2.7 and an exhaust gas temperature of 650 C. The engine nozzles are constructed to simulate the flight configuration during STOL operation. These nozzles, which are illustrated in Figure 45, are two-dimensional, convergent-divergent, wedge nozzles with a throat cross-sectional aspect ratio of eight. The nozzle duct has a throat area of 120 in.2, a fixed diffusion ratio of 1.09, and an exit angle of 25° downward. The primary-nozzle exit plane is located directly above the wing inboard-flap hinge line. Spanwise-blowing nozzles were provided in the sides of the nacelles, but their use will not be considered.

The fuselage is blended into broad fuselage strakes which extend well forward because of their 71° leading-edge sweep. The large nacelles outboard of the strakes house the propulsion system and act as mounts for the canards. The canards have a leading-edge sweep of 45° and could be attached in three positions: forward, intermediate and aft. Figure 44 shows the canards mounted in the forward position. The canards are situated 1.2 ft. above the wing plane. The wings have an aspect ratio of 3.2 and also a moderate leading-edge sweep of 40°. Both wing and canard have thin airfoil sections.

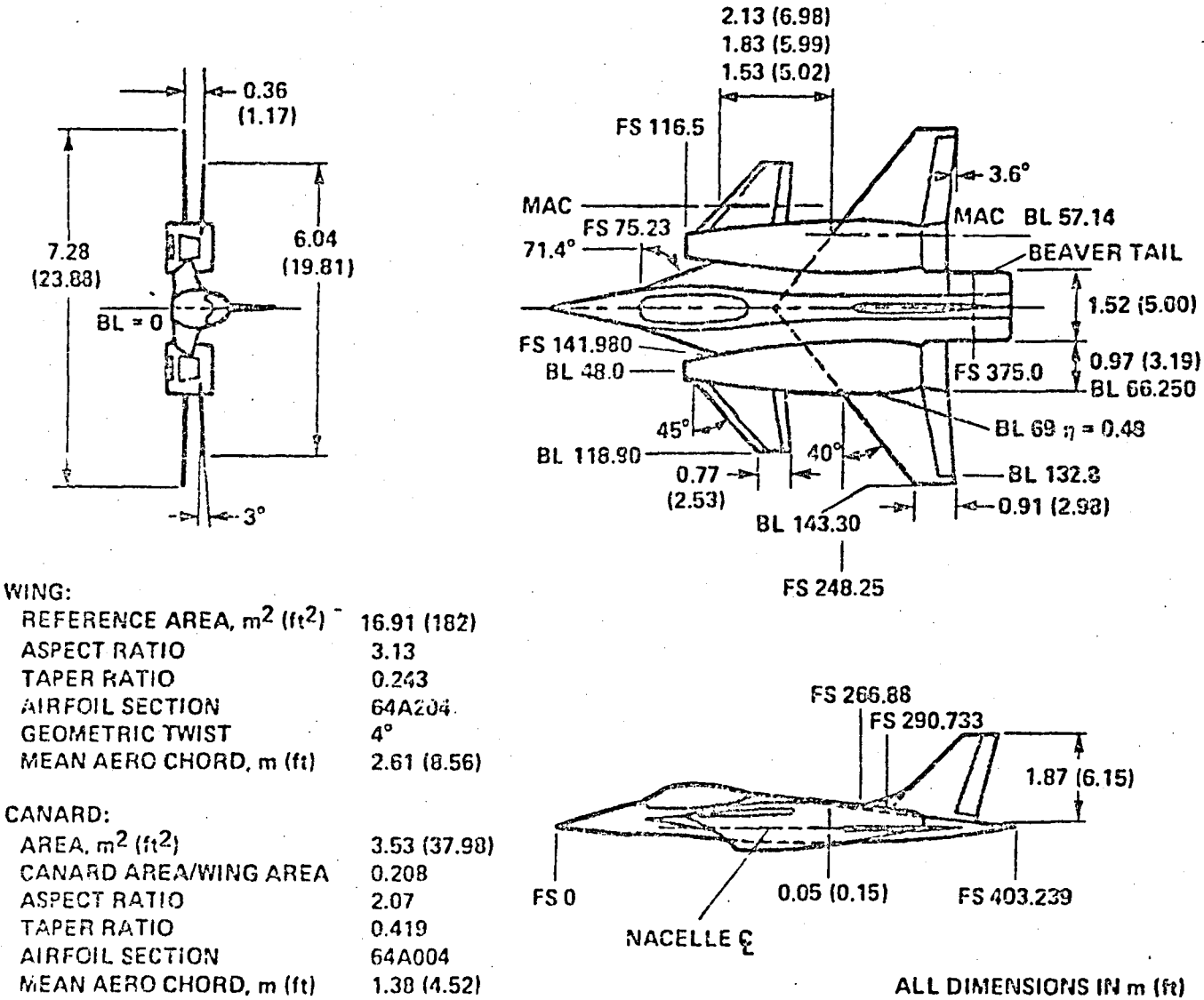

WING:	
REFERENCE AREA, m^2 (ft^2)	16.91 (182)
ASPECT RATIO	3.13
TAPER RATIO	0.243
AIRFOIL SECTION	64A204
GEOMETRIC TWIST	4°
MEAN AERO CHORD, m (ft)	2.61 (8.56)
CANARD:	
AREA, m^2 (ft^2)	3.53 (37.98)
CANARD AREA/WING AREA	0.208
ASPECT RATIO	2.07
TAPER RATIO	0.419
AIRFOIL SECTION	64A004
MEAN AERO CHORD, m (ft)	1.38 (4.52)

Figure 44. Large-Scale Powered STOL Fighter Model.

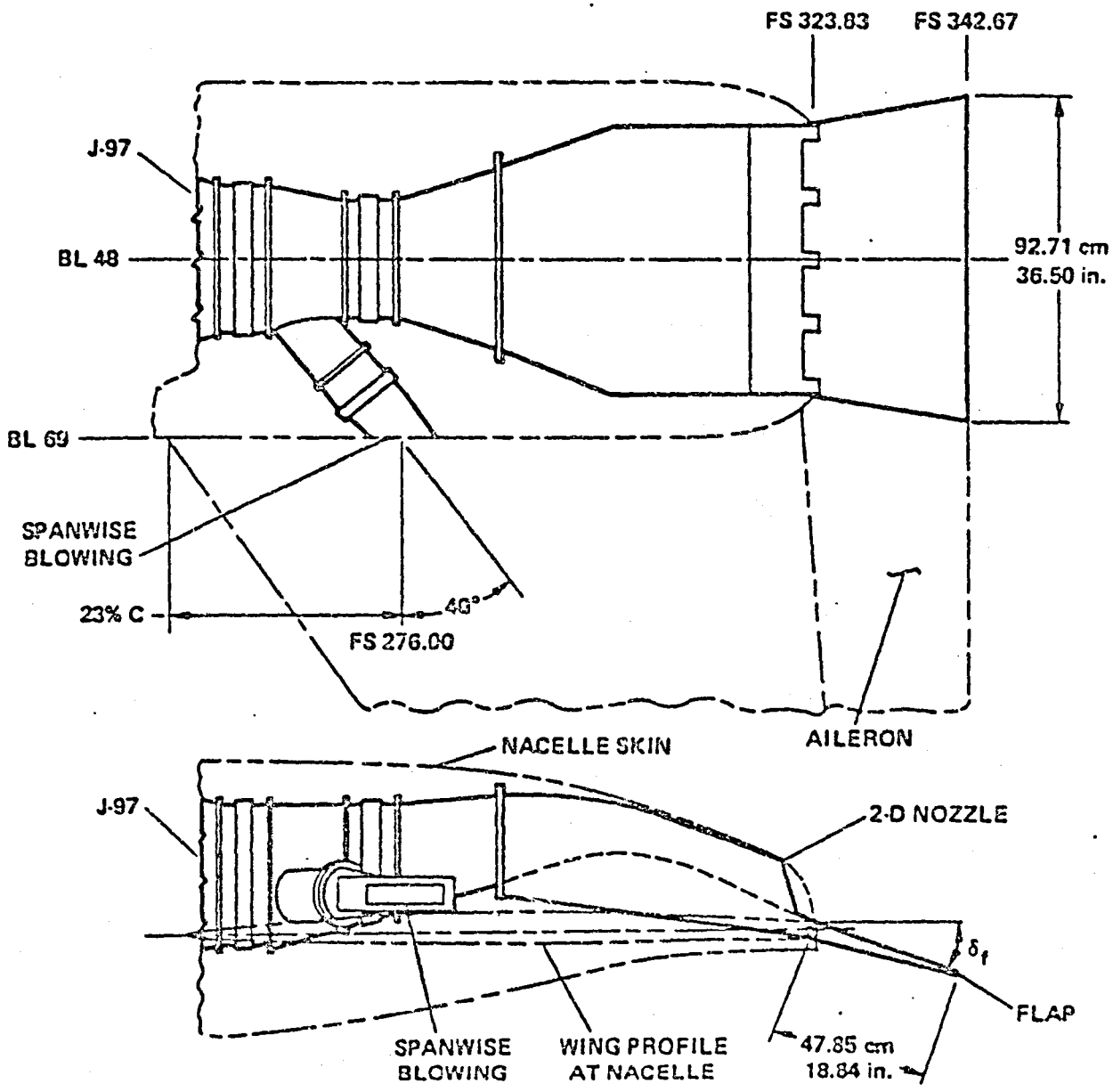

Figure 45. Port Nozzle Geometry.

5.3.2 Wind Tunnel Tests

The STOL Fighter Model was tested in the Ames 40 x 80-foot wind tunnel as reported in Ref. 26. Before proceeding with the results of the analysis a review of the pertinent aspects of the wind tunnel investigation is worthwhile. Summaries are also available in Refs. 48 and 49.

The model was equipped with pressure taps to measure the surface pressures on the port canard, wing, nozzle flap, beaver tail and strake. The location of the taps is presented in Figure 46. Total pressure rakes on the nozzle and flap measured the engine exhaust. Temperature readings were also taken on the beaver tail and wing. The pressure readings indicated that except at very low angles of attack (less than 3°) weak leading-edge vortices existed over the canard and wing. A stronger vortex existed over the strake leading edge. Each separation produced a loss in leading-edge suction, but more negative pressures just behind the leading edge on the upper surface.

Power-on tests were conducted at only two thrust settings, 3370 and 3860 lb (engine pressure ratios of 1.8 and 2.0). The thrust coefficient was varied by changing the tunnel dynamic pressure. The variation in tunnel velocity introduced some effects due to changes in Reynolds number. The effect of Reynolds number was investigated in power-off runs made at the same velocity as the test at C_t=1.4. These power-off tests had the inlets open with engine freewheeling.

The convergent-divergent nozzle at an engine pressure ratio of 2.0 issued the flow in an overexpanded state at a discharge Mach number of 1.35 with oblique shock waves then reducing the flow to subsonic speeds. The static pressure profiles on the flap indicated that the transition to subsonic flow occurred upstream of the first pressure tap.

For angles of attack below 16°, increasing power induced a small but consistent increase in canard lift. On the wing at low angles of attack with the flaps undeflected, adding power increased the upwash slightly. The outboard taps showed little power effects in the region of the aileron but stronger induced upwash with its consequences evident forward on the chord. The spanwise taps indicated there was an almost uniform reduction in pressure over the span due to power at high angles of attack.

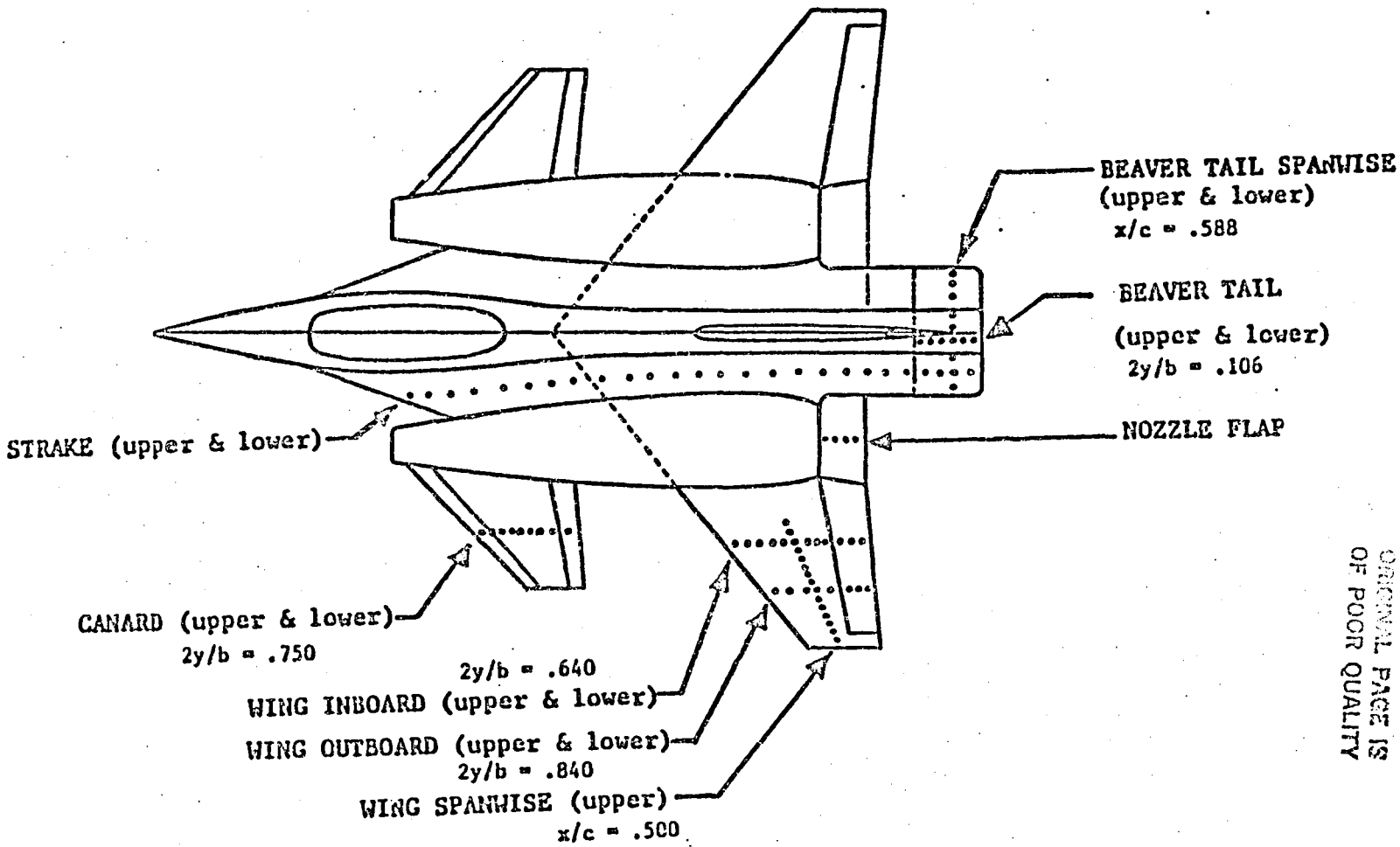

Figure 46. STOL Fighter Pressure Tap Locations.

5.3.3 Aerodynamic Model

The geometry of the STOL Fighter Model was provided to Analytical Methods by the NASA Ames Research Center in the form of the coordinates of the panel corners. The panelling scheme for the model, some 700 panels, is shown in Figure 47. This panelling was used with a few minor changes in VSAERO. The geomecry specified the canard in the aft position, and all control surfaces were undeflected.

The inlet and the nozzle face, that is, those panels which have nonzero normal velocities, are flush with the inlet and nozzle lips. The inlet, designed for supersonic operation, is panelled at an inclination of 60° to the free stream; and, as was stated before, the nozzle directed the exhaust downward at an angle of 25°, while the exit panels are almost vertical. The importance of this is that better results are usually obtained if these panels are aligned perpendicular to the local flow. This requires submerging the inlet and nozzle panels and adding short ducts. For the present study the simpler geometry was retained, but detailed studies of the flow in these regions should be deferred until these improvements are made.

The wakes attached to the model are shown in Figure 48. Normal lifting-type wakes are attached to the trailing edge of the canard, beaver tail and wing. In addition, a jet wake is attached to the trailing edge of the inboard flap and the lip of the nozzle. The jet wake in this case has a constant vorticity distribution on each panel. The vorticity is the difference between the external velocity and the jet velocity. This difference is specified as an input to VSAERO. A rigorous analysis would also include wakes from the leading-edge separations on the wing, canard and strake that were noted in the wind tunnel. These have been omitted in order to concentrate on jet-induced effects.

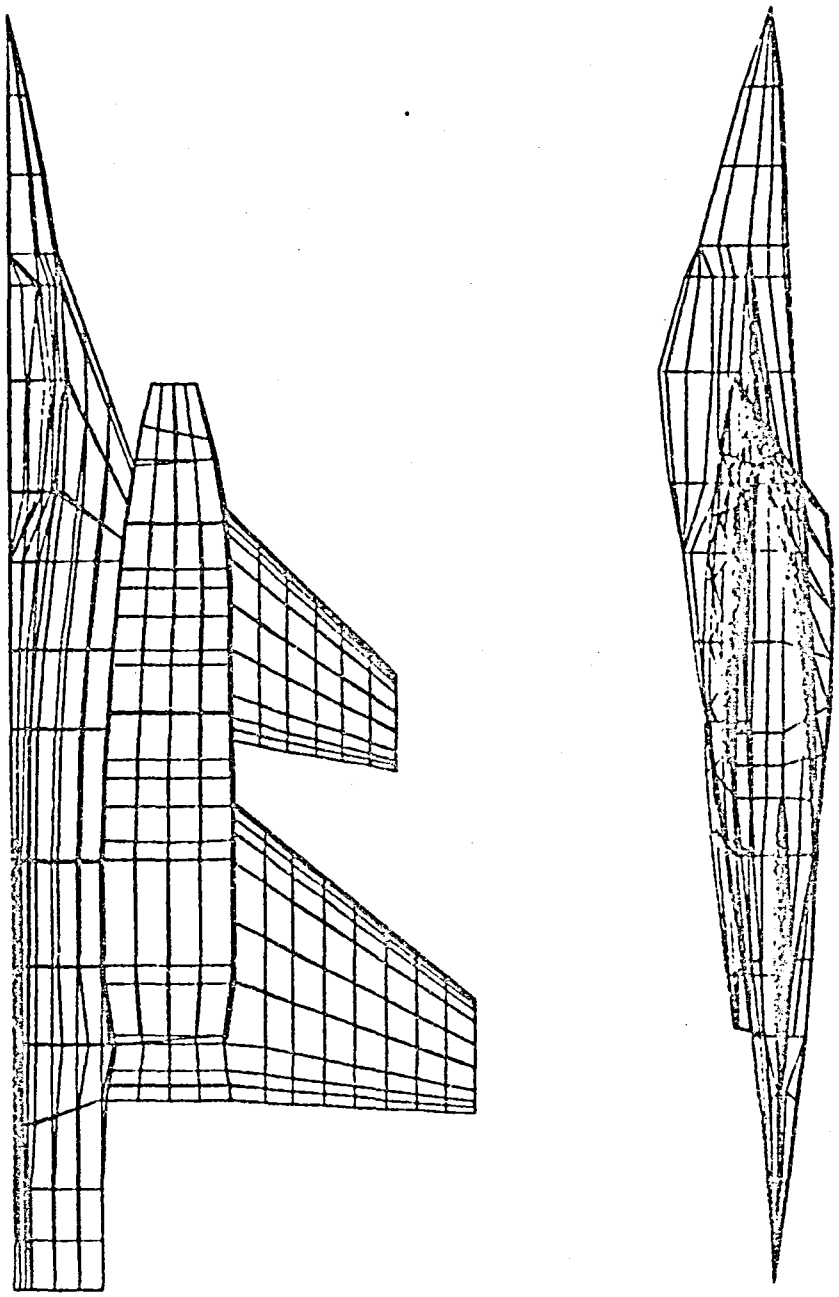

Figure 47. STOL Fighter Panel Distribution.

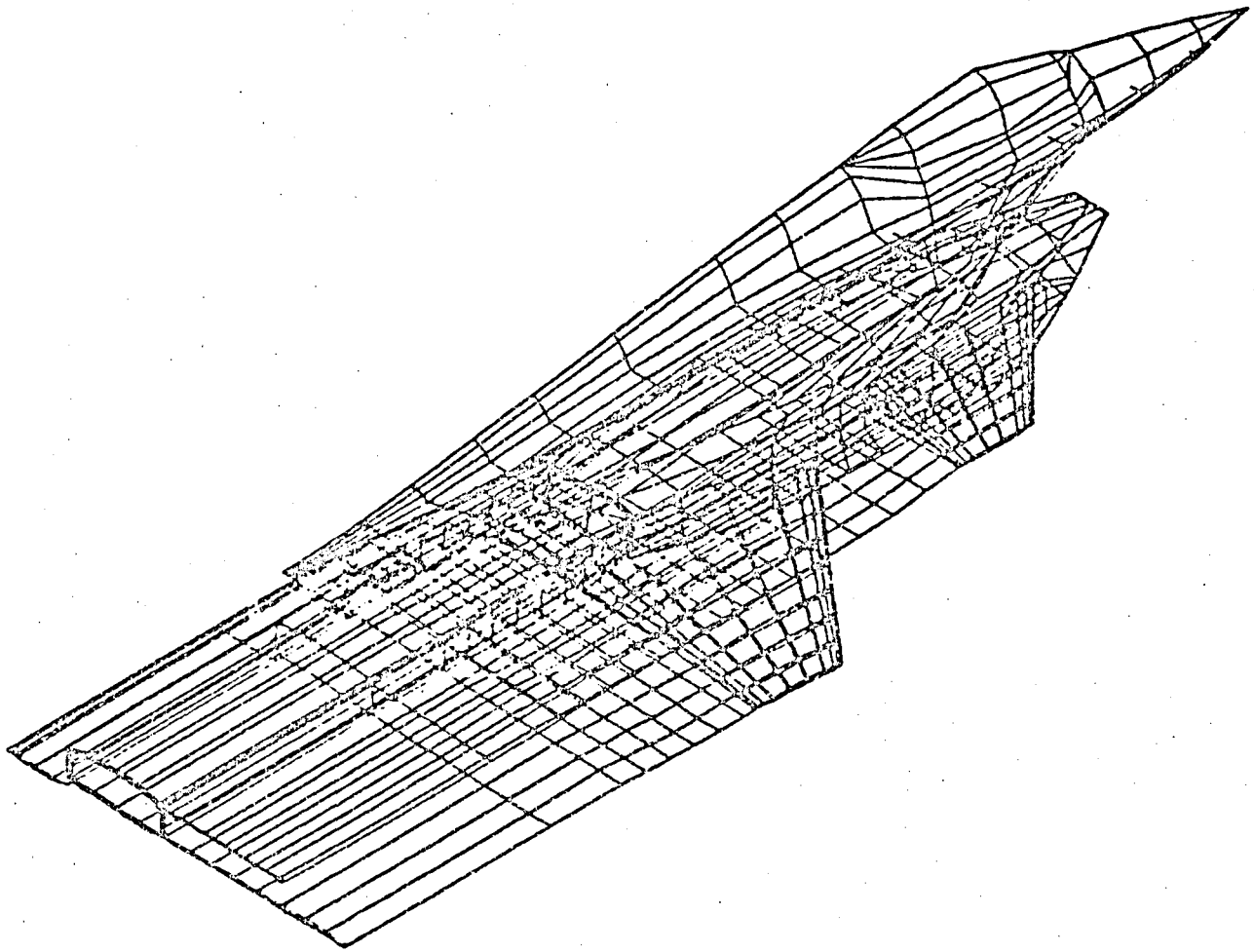

Figure 48. Oblique View of STOL Configuration with Wake.

5.3.4 Derivation of Jet Velocity

The power-on tests as we have seen were run at a constant engine pressure ratio of 2.0 corresponding to a thrust of 3860 lb. The pressure ratio at the nozzle exit will be 1.8 according to the calibrated duct and nozzle losses (50). Assuming the static pressure over the flap is near ambient, the exhaust, once it has compressed from its overexpanded state, will have a Mach number of about 0.9. At a total temperature of 1600 R the exhaust velocity will be some 1500 ft/sec, varying slightly with the thrust coefficient, C_t. This is verified by the effective exhaust velocity,

$$V_e = T/\dot{m}$$

where $\dot{m}$ is the exhaust mass flow, approximately 40 lb/sec/engine.

From the equation

$$C_t = \frac{T}{1/2\rho V_{inf}^2 S_{ref}}$$

the wind tunnel thrust of 3860 lb implies

$$V_{inf} = 133 \text{ ft/sec } \frac{1}{\sqrt{C_t}}.$$

So, the ratio of the exhaust velocity to freestream velocity is

$$V_{jet}/V_{inf} = 11 \sqrt{C_t}.$$

This was the jet velocity used in VSAERO. The velocity external to the jet was estimated to be the velocity on the nacelle just upstream of the jet, which turned out to be slightly higher than freestream.

Certain improvements to this model are obvious. First, the jet velocity and vorticity should vary as the exhaust compresses or turns. Second, the compressible nature of the jet should be represented in the calculations. Entrainment should also be included. Nevertheless, much of the jet effects can be reproduced by this model, as will be seen.

The static calibration of the wedge nozzle measured the exhaust jet thickness at the flap trailing edge. It was found to have the same height, and therefore approximately the same cross-sectional area as the nozzle. This is consistent with a high subsonic Mach number in the exhaust.

It should be pointed out that from the throat area and diffuser ratio we can derive the area of the nozzle exit plane as

$$Ae = \frac{120 \text{ in.}^2 \ (1.09)}{\cos 25^\circ} = 144 \text{ in.}^2$$

The nozzle panels specified in the geometry extend from buttline 30 to BL 66 and from waterline 30 to WL 42 which leads to a cross-sectional area of 432 $in.^2$ This is three times greater than the derived area. Again, further analysis should be preceded by a review of the panel geometry.

5.3.5 VSAERO Results

5.3.5.1 Power-Off Calculations

The first step in the analysis of the STOL fighter was a set of power-off calculations at several angles of attack. When compared to the experiment, Figure 49, the lift slope is about 15% less than experiment. More noticeable is that the predicted angle of zero lift is about 1.8° higher than experiment. The lift versus pitching moment curve, Figure 50, has a very good correlation. This curve, which is independent of the angle of zero lift, tends to indicate that there is an inconsistency between the angle of attack stated in the experimental results and that used for the calculation.

Further arguments for an inconsistency are found in the pressure data. For example, the canard pressure taps in both experiment and calculation were found to be influenced little by power effects (Figure 51). From this it can be inferred that the inlet spillage and, hence, the upwash induced by the nacelle does not affect the canard under this condition. Yet, at zero angle of attack and zero incidence, the experimental pressures around the symmetrical airfoil indicate the canard is generating significant lift; whereas the calculations show almost no lift. When a prediction is made for the canard at an angle of attack which reflects the assumed error, the comparison, Figure 52, is quite good. At angles of attack much larger than the error, Figure 53, the comparison is good, but the calculation is still consistently lower than experiment. Pressures on the wing also compare much better if the angle of attack used in the calculations is 1.8° higher (Figure 54).

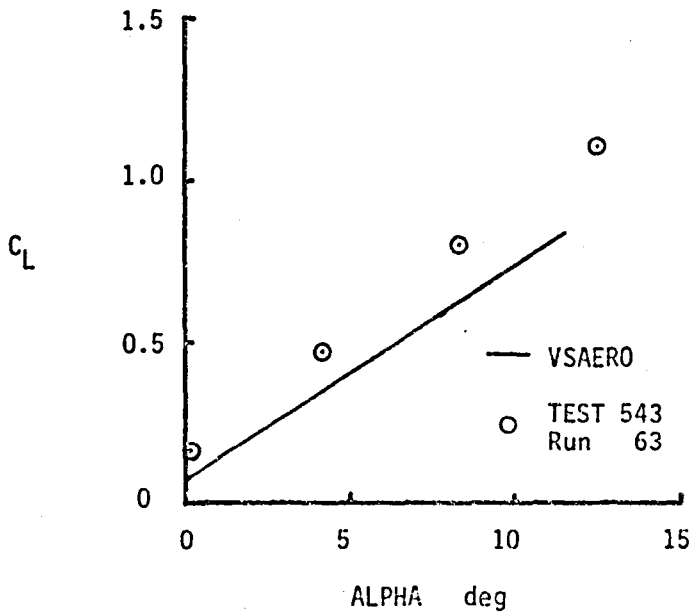

Figure 49. Lift Versus Angle of Attack, Power Off.

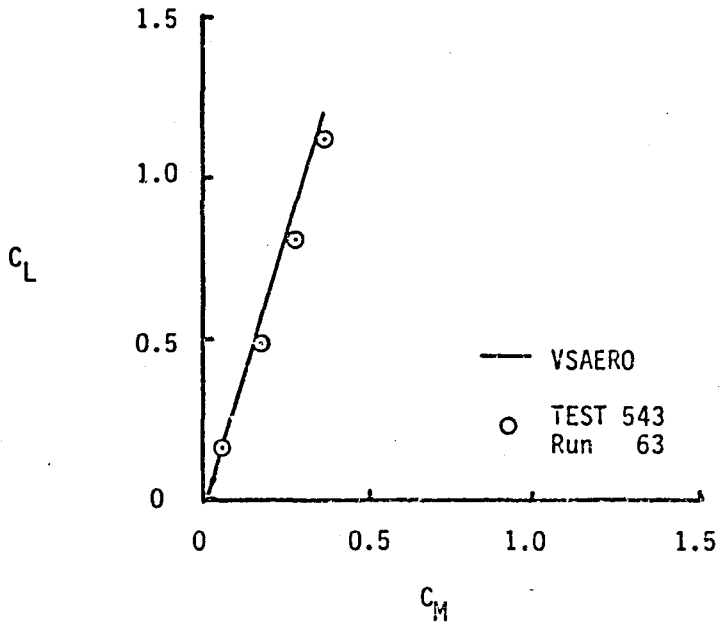

Figure 50. Lift Versus Pitching Moment, Power Off.

SYM	TEST	RUN	ALPHA	CT	ITEF	OTEF	CAN	SWB
⊖	543	63	0.1	0.00	0	0	0	OFF
⊞	543	59	0.1	1.42	0	0	0	OFF
◻	VSAERO		0.0	1.31				

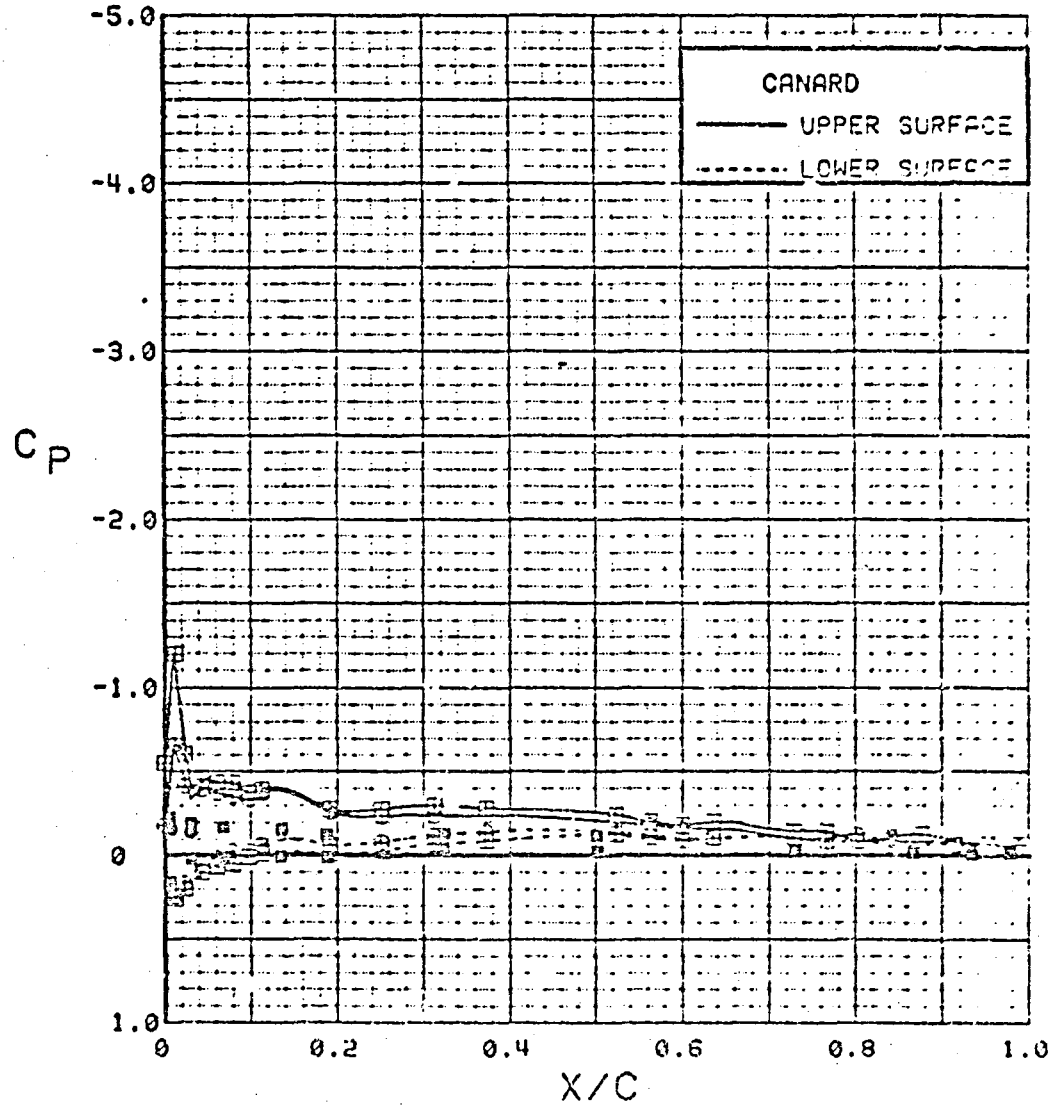

Figure 51. Power-off/Power-on Comparisons, Wing Flaps Neutral, α = 0 deg.

SYM	TEST	RUN	ALPHA	CT	ITEF	OTEF	CAN	SWB
⊕	543	63	0.1	0.00	0	0	0	OFF
⊞	543	59	0.1	1.42	0	0	0	OFF
⊛	VSAERO		1.8	0.15				

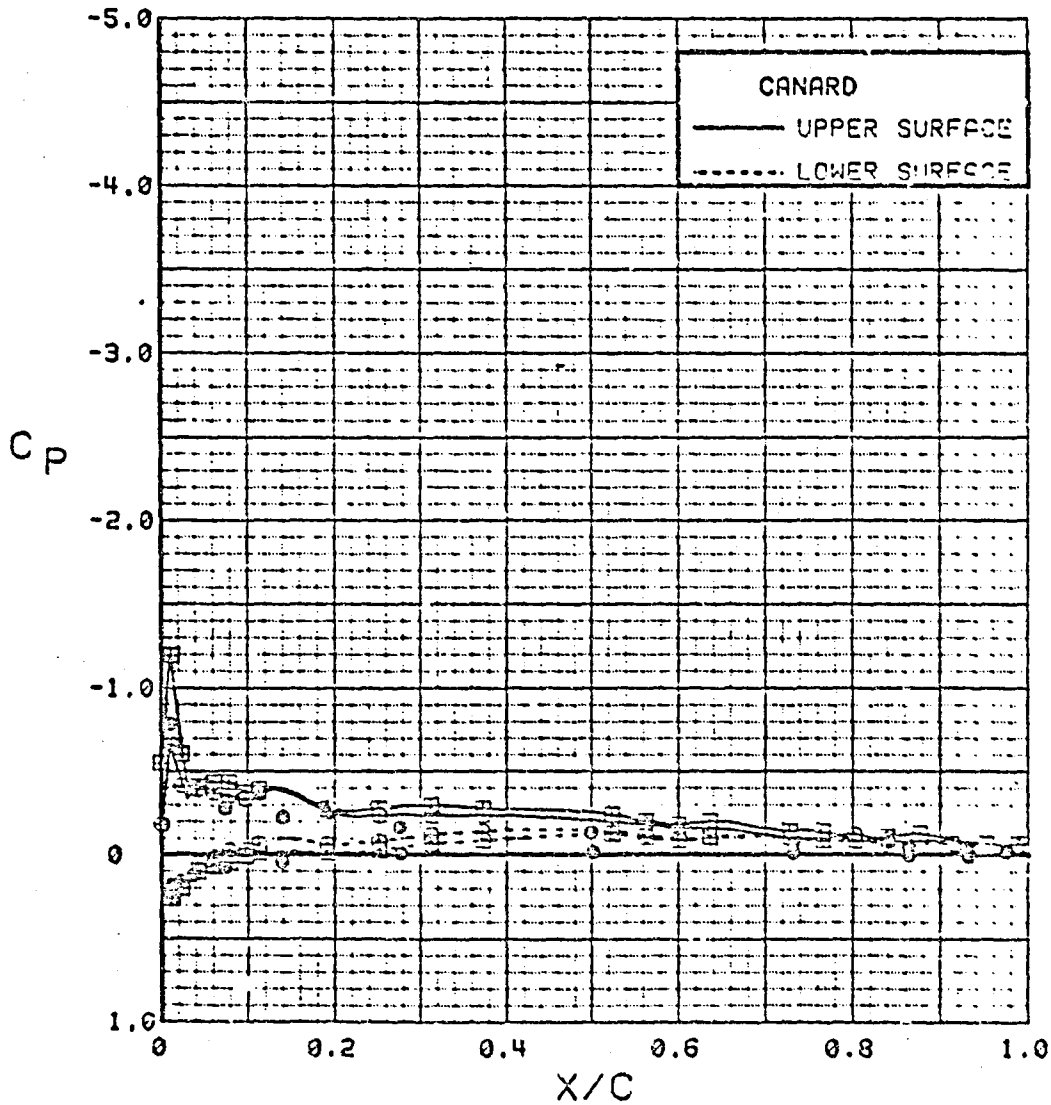

Figure 52. Power-off/Power-on Comparisons, Wing Flaps Neutral, α = 0 deg.

SYM	TEST	RUN	ALPHA	CT	ITEF	OTEF	CAN	SWB
⊖	543	63	4.2	0.00	0	0	0	OFF
⊞	543	64	4.2	0.27	0	0	0	OFF
△	543	62	4.2	0.48	0	0	0	OFF
◈	543	60	4.3	0.93	0	0	0	OFF
✱	543	59	4.3	1.40	0	0	0	OFF
+	543	58	4.3	1.84	0	0	0	OFF
⊙	VSAERO		4.2	1.31				

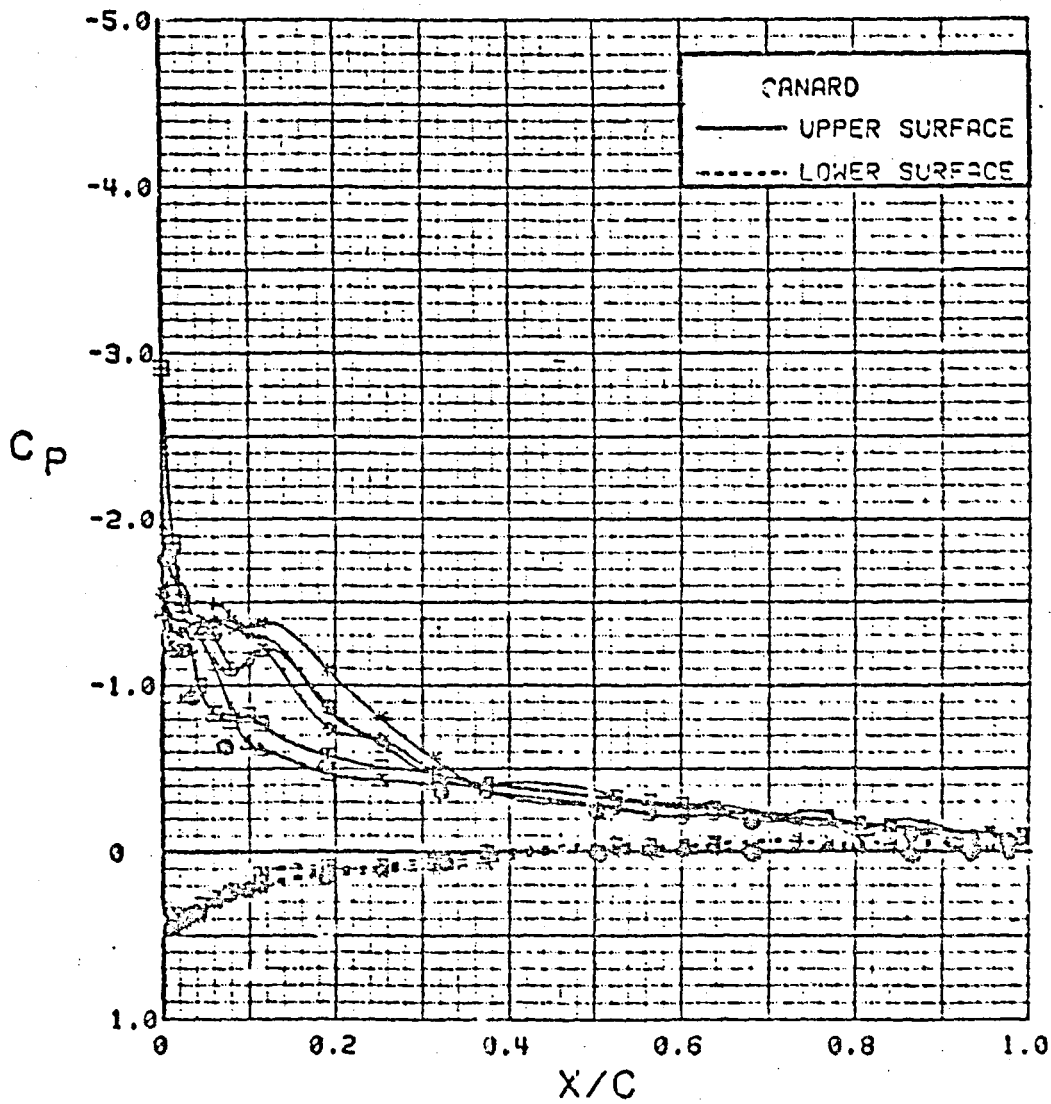

Figure 53. Power Effects, Wing Flaps Neutral, α = 4 deg.

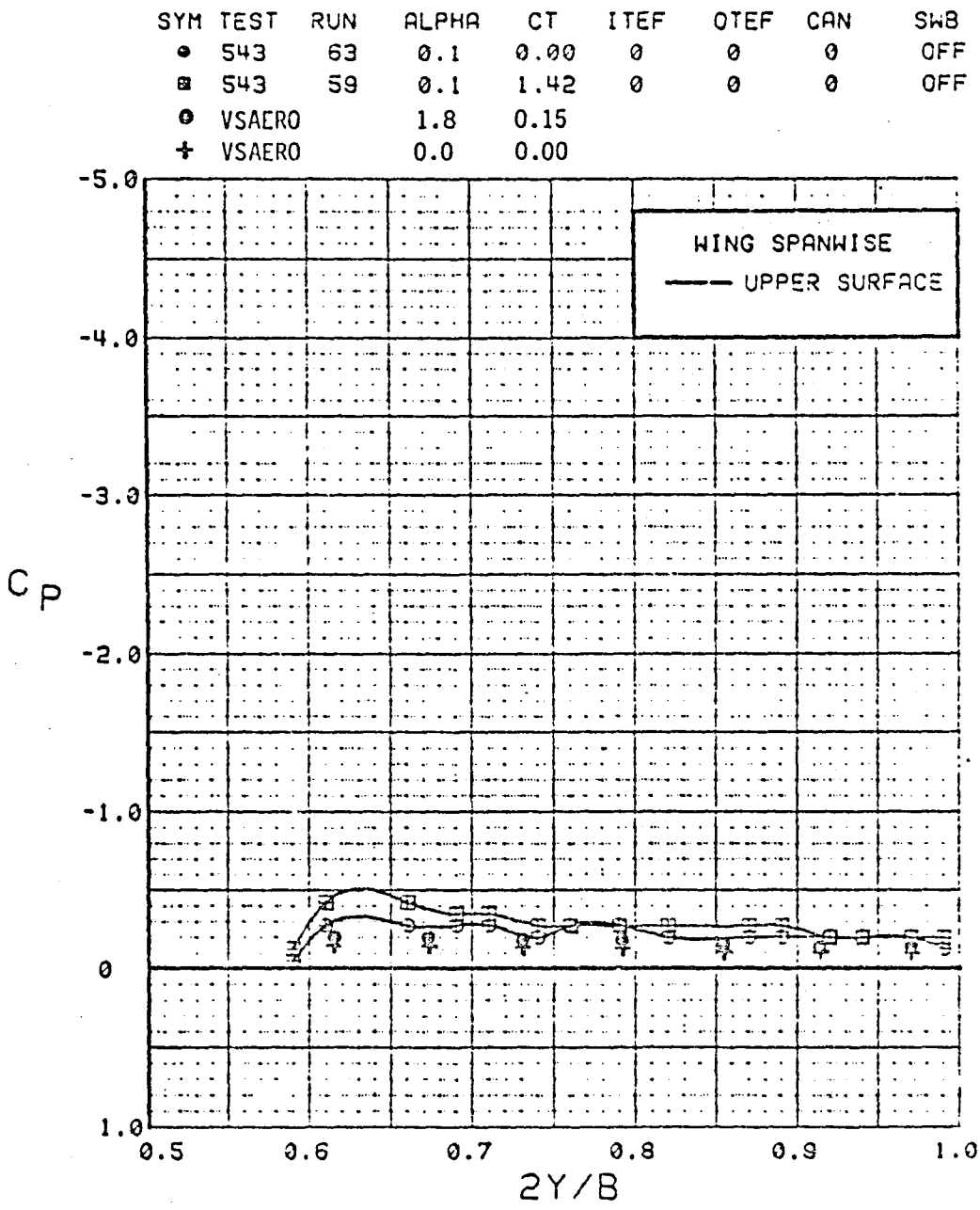

Figure 54. Power Effects, Flaps Neutral, Spanwise, α = 0 deg.

5.3.5.2 Power Effects

Figures 55 through 62 compare the effect of increasing engine thrust on the pressure distribution over the canard, wing and strake. The difficulty in perceiving quantitative effects from the experimental data makes such a comparison difficult, but the qualitative effects predicted in the calculations is virtually the same as experiment.

Figure 55 shows the canard pressure distribution at various power settings. The trend for both experiment and theory is one of small, but consistent increases in lift with increases in power. At this higher angle of attack, the leading-edge separation in the wind tunnel reduces the suction on the upper surface over the leading edge; whereas the analysis maintains a high suction associated with attached flow. The lower-surface pressures compare well.

The calculated pressure trend on the wing outboard station (Figure 56) agrees with the experimental data in indicating a significant effect on the outboard leading edge, but little effect on the aft portion of the airfoil. The greatest influence of the jet is in the inboard wing chord, Figure 57. Power reduces the pressures over the entire chord.

The wing spanwise data (Figure 58) show that the jet influence extends far out on the wing at 8° angle of attack with more effect inboard near the nacelle. The calculated power effect is very close to the measured effect.

The strake calculations predict that only the area near the nozzle exit is influenced by power effects (Figure 59). This is confirmed by the experimental data. The strong leading-edge separation on the strake is very apparent.

At a lower angle of attack the results are much the same. Figure 51 shows the correlation between experiment and theory for the canard pressures. The results for power-off were almost identical to those at Ct=1.3 and have not been graphed. This shows again that power effects had little influence on the canard.

Figures 60 and 61 show the wing chordwise pressures. The lower-surface pressures on the inboard station do not compare favorably with experiment, but the upper-surface pressures appear very good. The spanwise prediction at zero angle of attack (Figure 62) indicates that the power effect is overemphasized. Still, the results show how the jet effect is strongest closest to the nacelle and dies out towards the wing tip. The experimental data support this.

SYM	TEST	RUN	ALPHA	CT	ITEF	OTEF	CAN	SWB
⊕	543	63	8.3	0.00	0	0	0	OFF
⊞	543	64	8.4	0.27	0	0	0	OFF
△	543	62	8.4	0.47	0	0	0	OFF
◆	543	60	8.4	0.94	0	0	0	OFF
✱	543	59	8.4	1.41	0	0	0	OFF
+	543	58	8.4	1.88	0	0	0	OFF
○	VSAERO			0.04				
⊡	VSAERO			1.31				

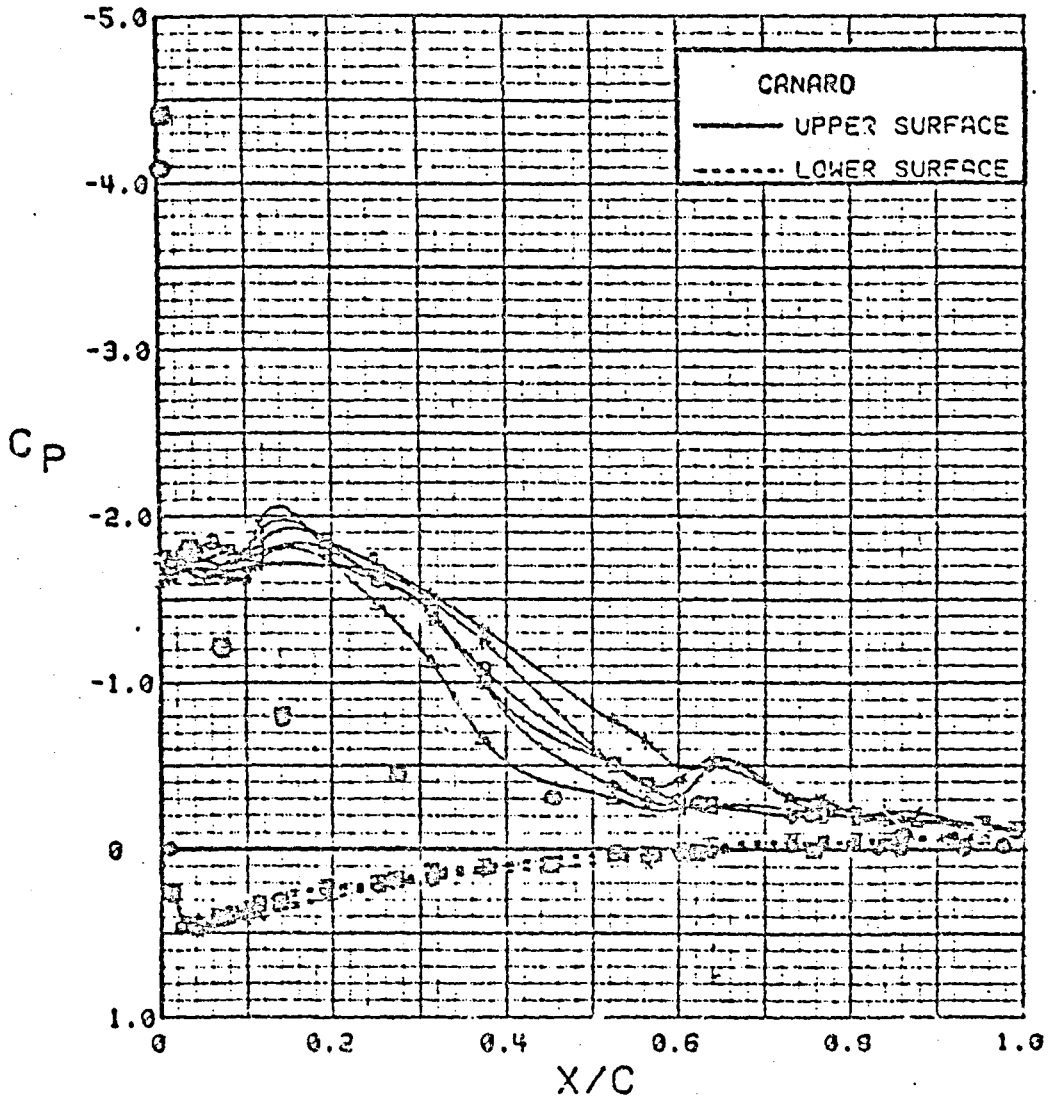

Figure 55. Power Effects, Wing Flaps Neutral, α = 8 deg.

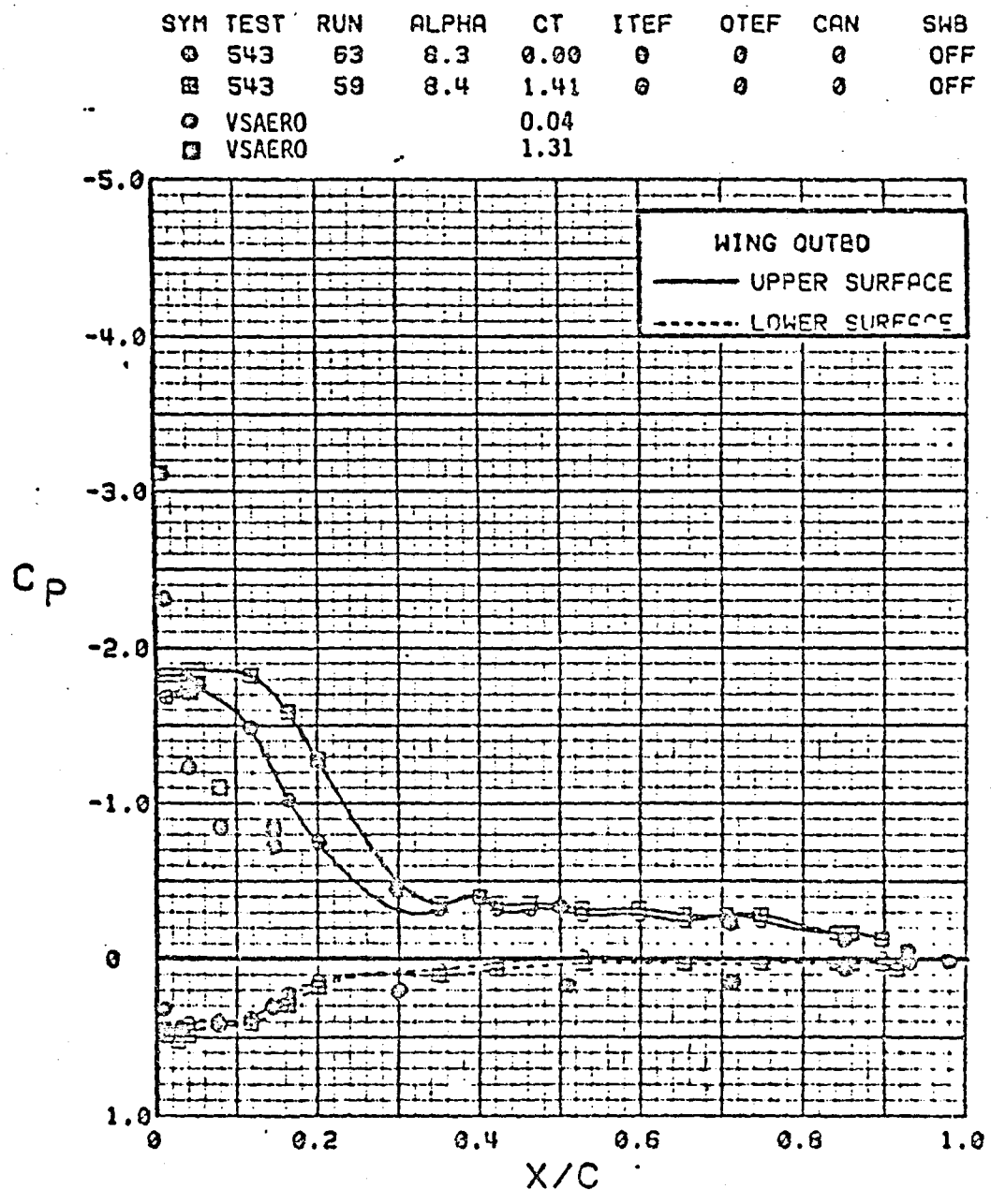

Figure 56. Power Effects, Flaps Neutral, Outboard, α = 8 deg.

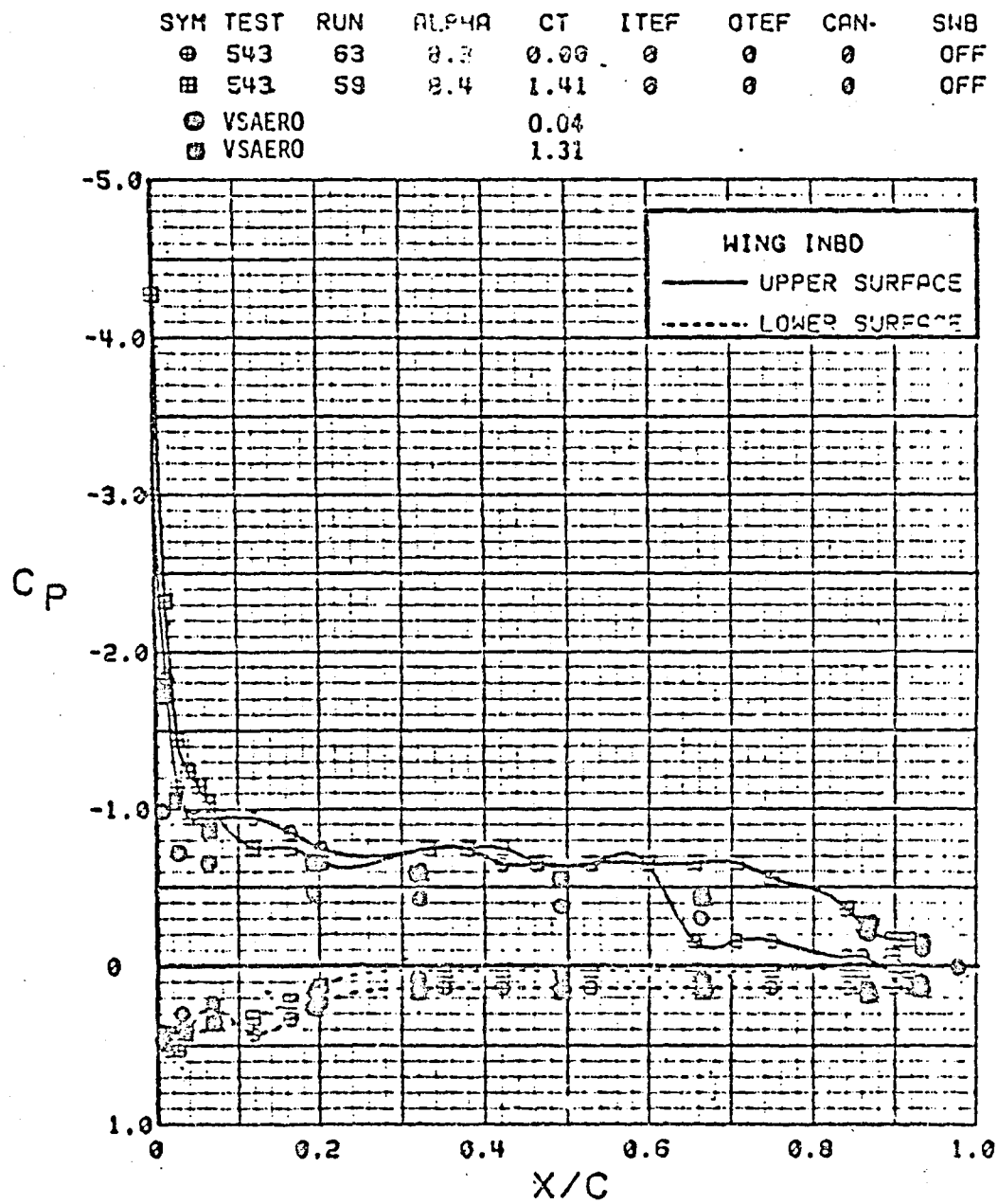

Figure 57. Power Effects, Flaps Neutral, Inboard, α = 8 deg.

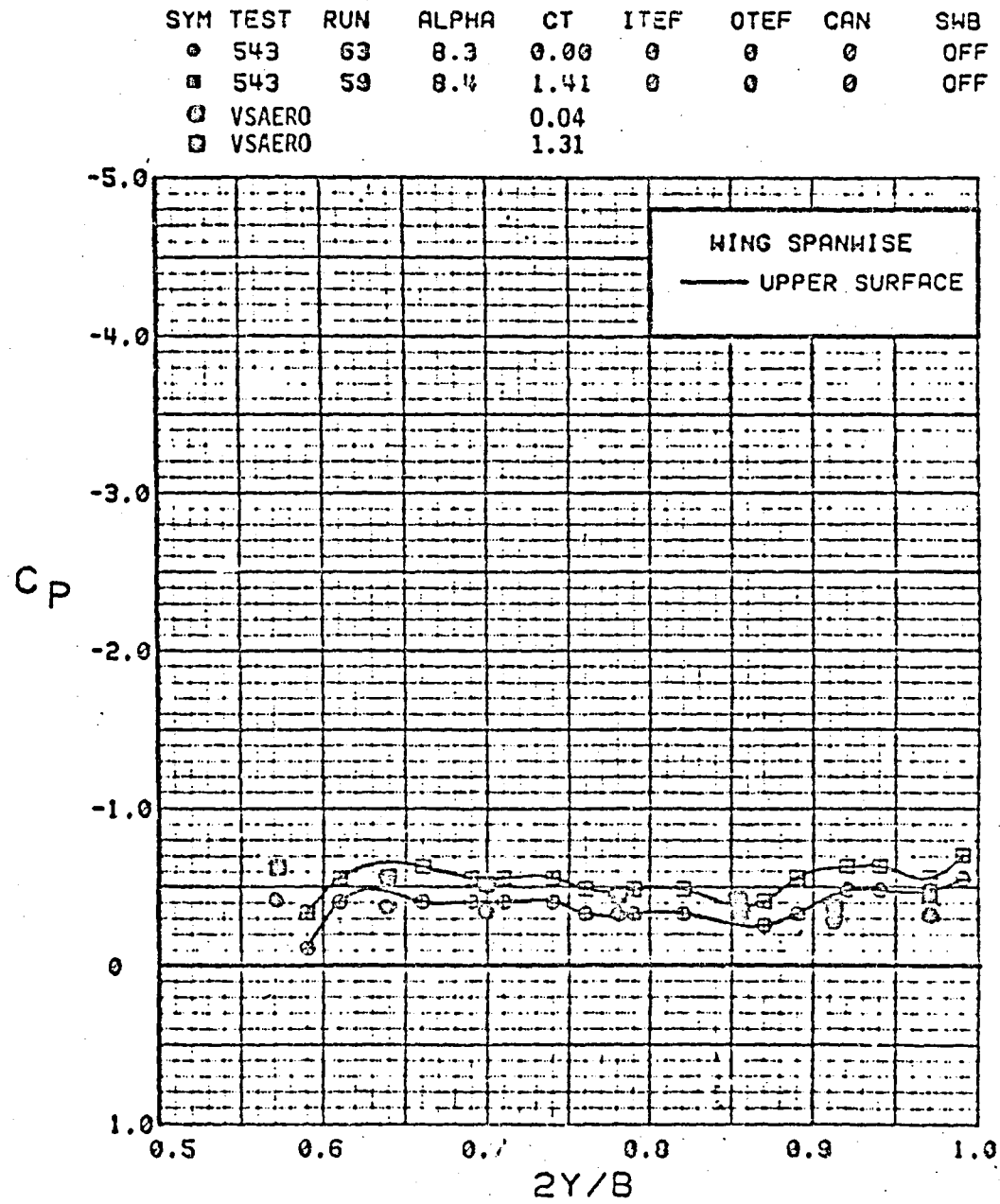

Figure 58. Power Effects, Flaps Neutral, Spanwise, α = 8 deg.

SYM	TEST	RUN	ALPHA	CT	ITEF	OTEF	CAN	SWB
⊖	S43	63	8.3	0.00	0	0	0	OFF
⊞	S43	62	8.4	0.47	0	0	0	OFF
△	S43	60	8.4	0.94	0	0	0	OFF
◆	S43	59	8.4	1.41	0	0	0	OFF
✱	S43	58	8.4	1.90	0	0	0	OFF
○	VSAERO			0.04				
⊡	VSAERO			0.70				

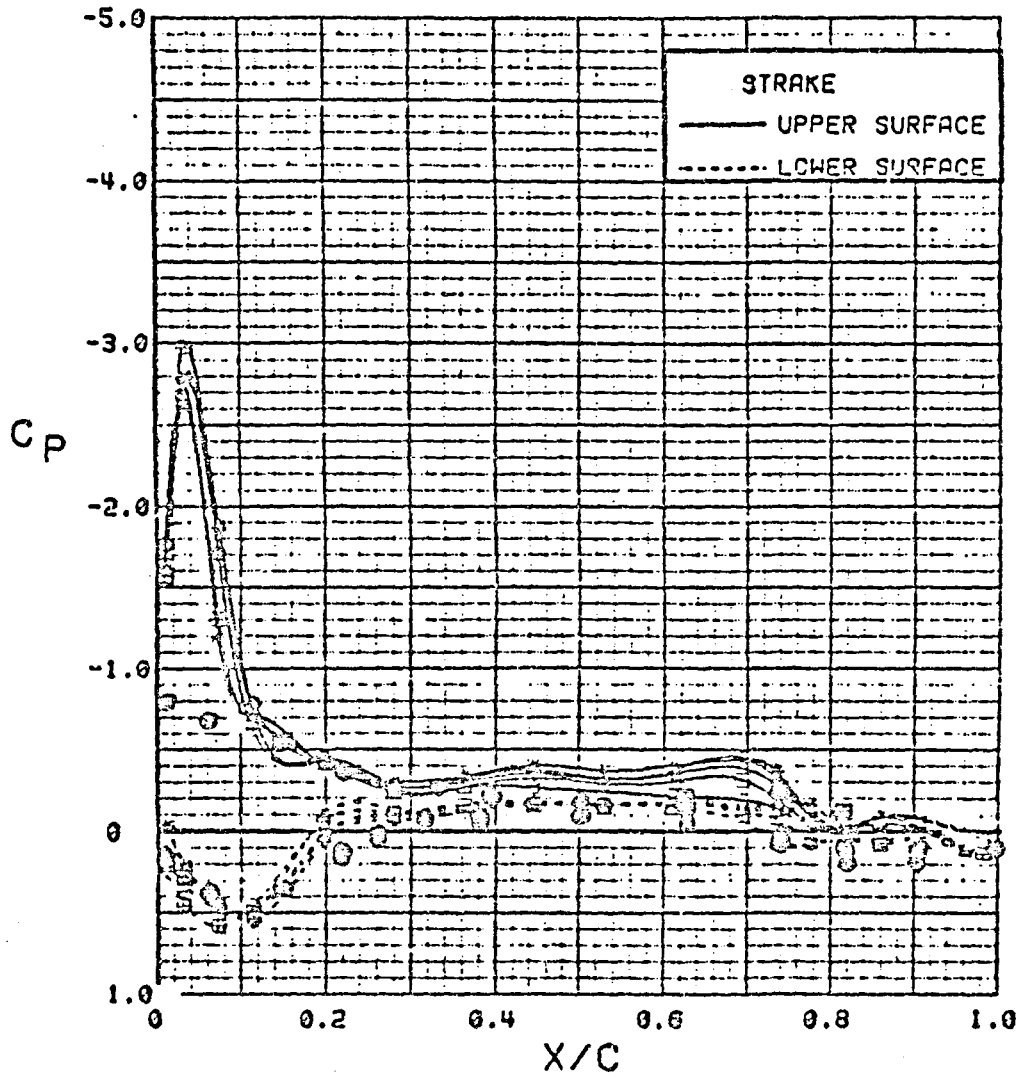

Figure 59. Power Effects on Strake Pressures, Wing Flaps Neutral, α = 8 deg.

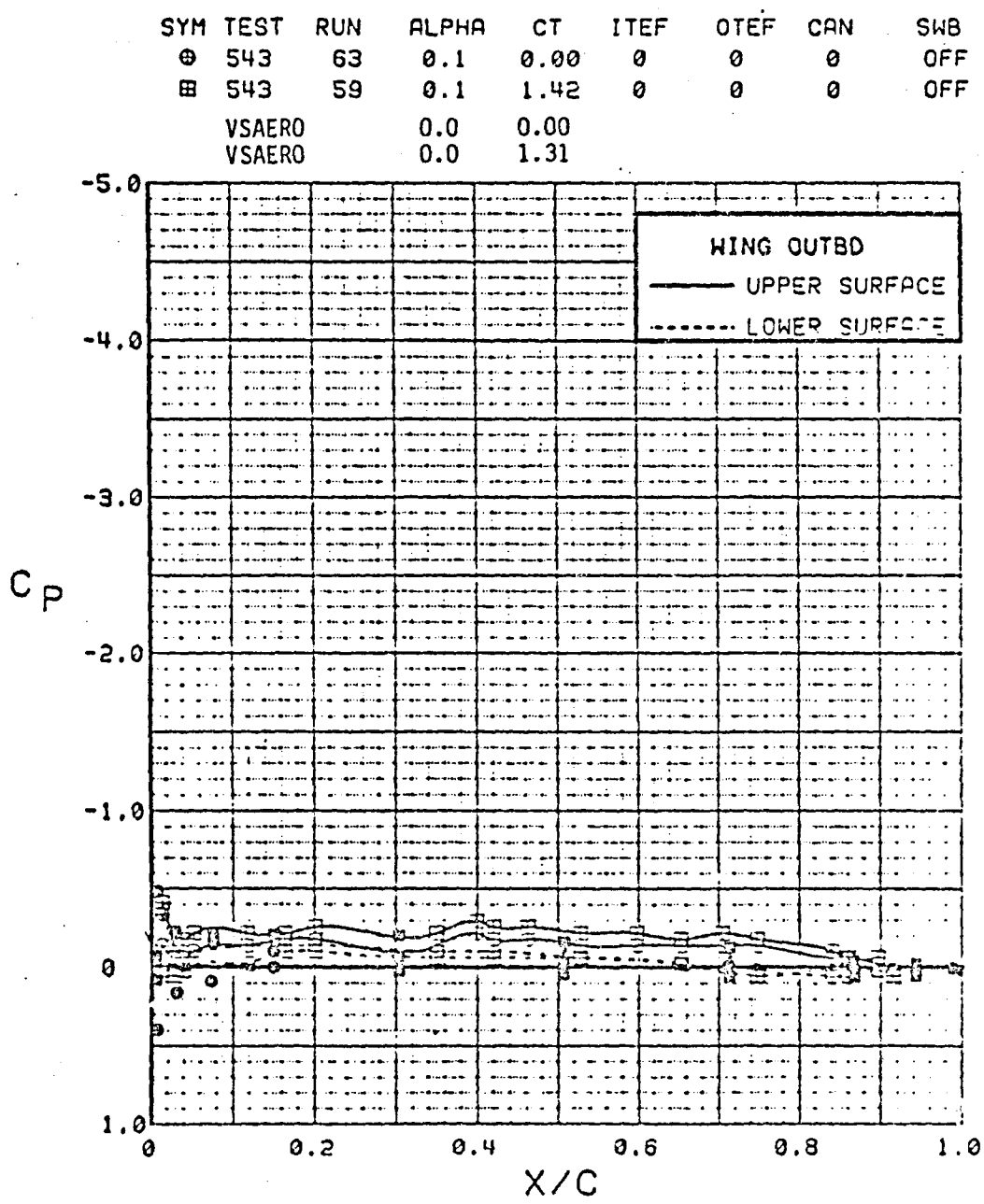

Figure 60. Power Effects, Flaps Neutral, Outboard, α = 0 deg.

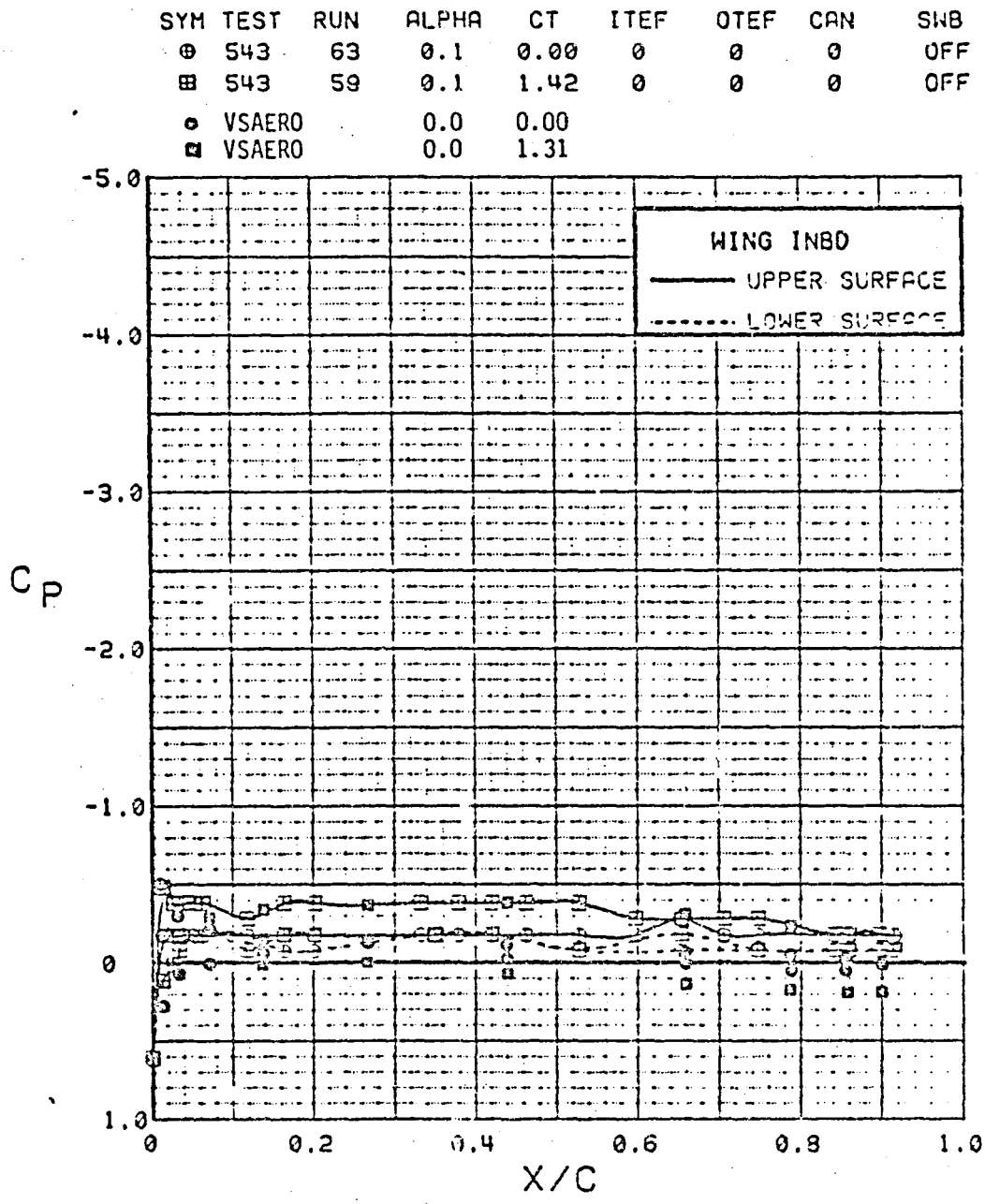

Figure 61. Power Effects, Flaps Neutral, Inboard, α = 0 deg.

ORIGINAL PAGE IS
OF POOR QUALITY

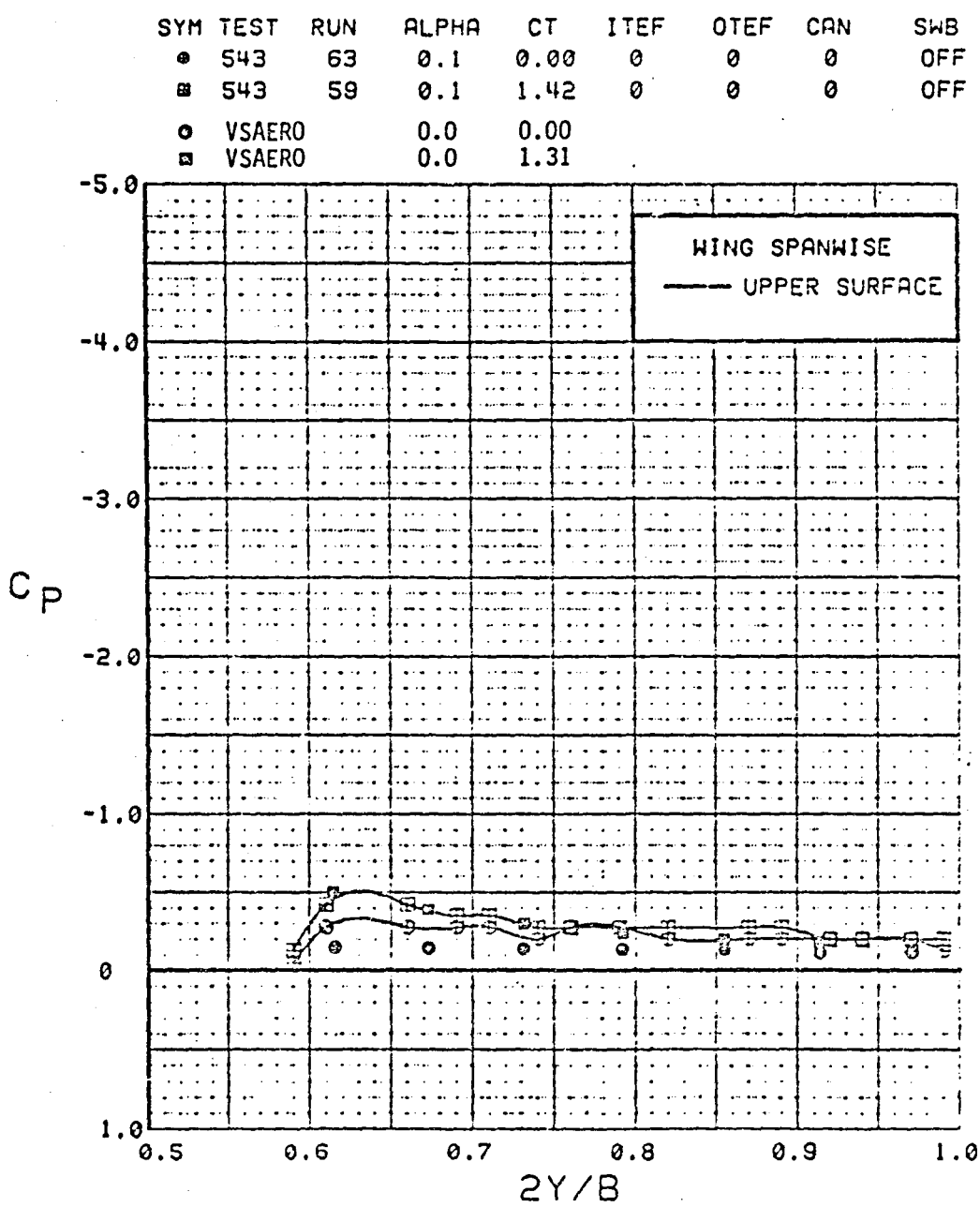

Figure 62. Power Effects, Flaps Neutral, Spanwise, α = 0 deg.

A quantitative comparison is shown in Figure 63 where the predicted and measured lift coefficients have been compared. For much of the angle-of-attack range considered, the power-on predictions appear very good. The angle of attack of the experimental data has been increased to reflect the assumed error in the angle of attack. Qualitatively, VSAERO predicts both the increase in lift and increased lift slope seen in the data.

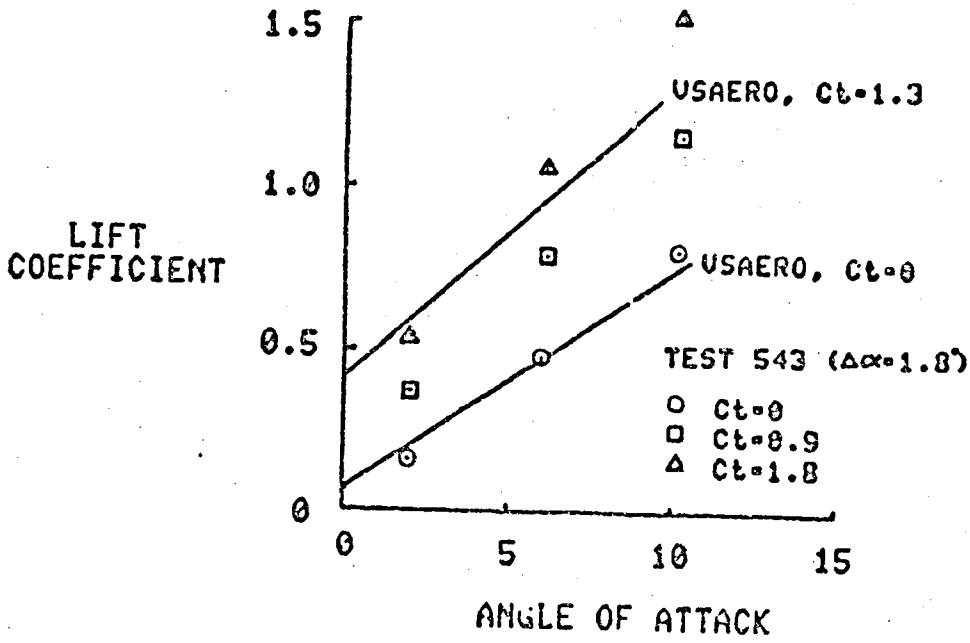

Figure 63. Power Effects on Lift Curve.

5.3.5.3 Wake Relaxation Effects

To further explore the extent to which VSAERO has assimilated the jet model, wake relaxations were made with power applied. Under low-speed flight conditions where the flow perturbations from jets and high-lift devices will be large, wake relaxations can be expected to be important in getting the correct solution. Relaxing the canard wake of the STOL Fighter should be of particular importance based on the results from similar configurations. Figure 64 shows the predicted wake geometry at $C_t = 1.3$ at an angle of attack of 8.4°. The jet presence gave no problems when predicting the shape of the canard wake. Until a variable vorticity jet model is included, relaxation of the jet wake, while possible, is not worthwhile.

Figures 65 and 66 indicate the sensitivity of the wing pressures to the canard wake geometry. The inboard pressures are affected in much the same way as they are by power and to almost the same degree. The spanwise data show that letting the canard-tip vortex roll up can redistribute the lift further outboard. This is closer to the experimental trend, Figure 58.

There were no apparent effects on the canard or strake from relaxing the canard wake.

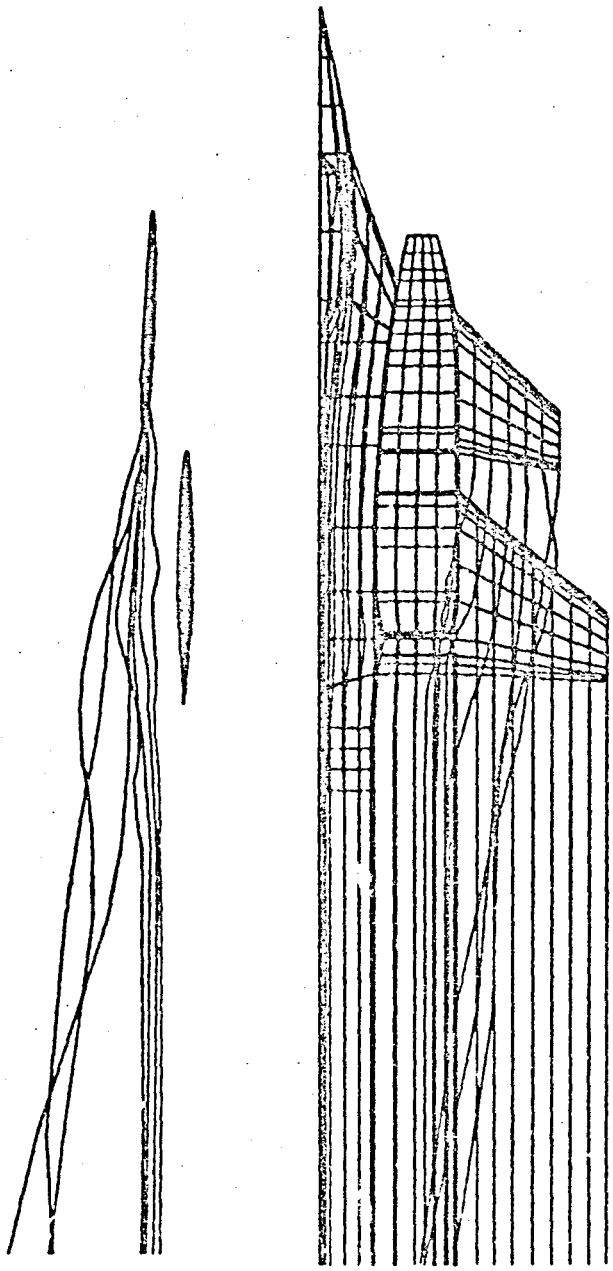

Figure 64. Powered STOL Fighter with Relaxed Canard Wake.

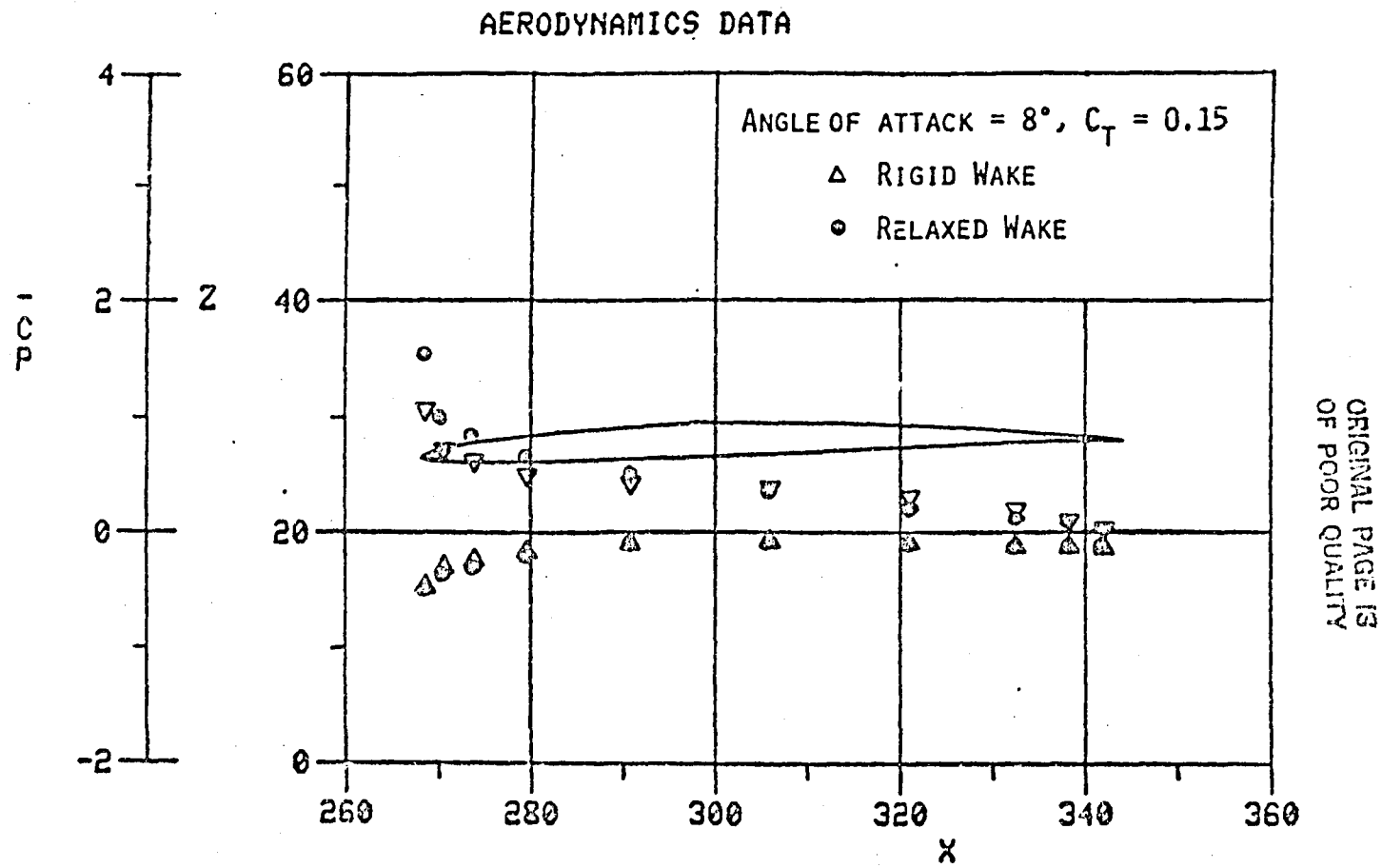

Figure 65. NASA Ames STOL Fighter Model with Canard-Wake Relaxation.

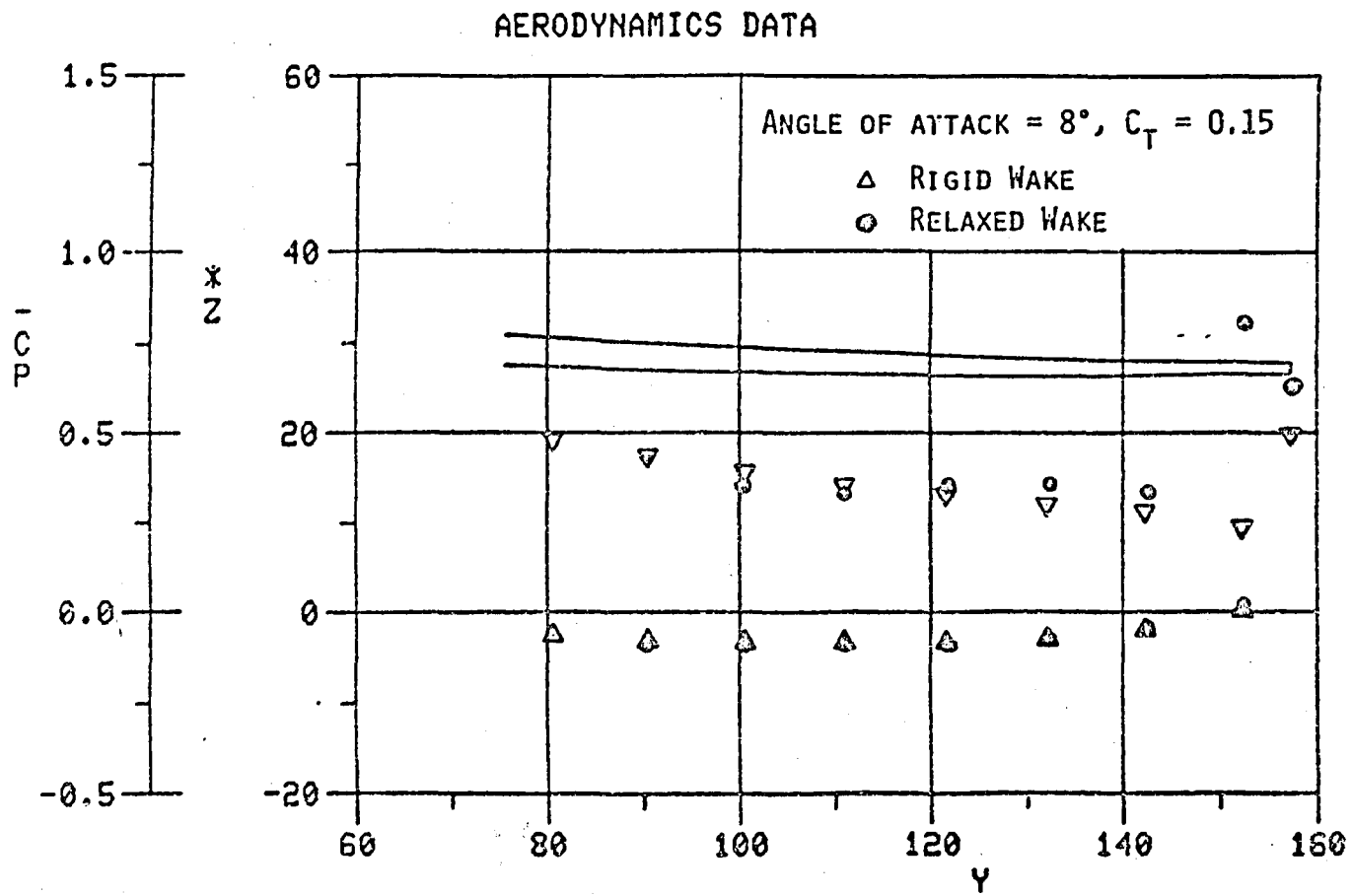

Figure 66. NASA Ames STOL Fighter Model with Canard-Wake Relaxation.

5.3.6 Summary

The jet model used in VSAERO for the analysis of the STOL Fighter has provided quite good overall predictions for power effects. The model predicts more lift at the same angle of attack and higher lift slope with power on as compared to power off. As verified by experimental data, the jet effects at moderate angles of attack are most pronounced close to the nozzle while barely perceptible on the canard.

The jet model does not impair the solution on remote components and is compatible with other VSAERO capabilities such as wake relaxation. Further development is required for a correct analysis of components very close to the jet.

The STOL Fighter configuration was run on the PRIME 550 minicomputer. A case with 700 panels and 350 wake panels on one side of the plane of symmetry took 6,000 CP seconds, which is equivalent to about one minute on the CRAY. A case with one wake relaxation took 10,000 CP seconds on the PRIME 550.

6.0 JET TRAJECTORY CALCULATIONS

6.1 General

The VSAERO program has an iterative wake relaxation scheme based on force-free boundary conditions. Since the jet boundaries are described as special wakes inside the program, in principle, the jet boundary can also be relaxed in the iterative procedure in order to compute the jet trajectory. Such calculations at low jet deflection angles have been very promising. However, at larger deflection angles numerical problems have been encountered. One of the reasons for this is that the wake structure is described in a vertical wake-grid-plane scheme, Figure 67. While this has several advantages for regular wakes it is too restrictive for jets with large deflection angles: numerical problems arise because of the large inclination of the jet axis relative to the wake grid plane.

Although an alternative more general scheme is required for treatment of the jets at large crossflow angles, development of such a scheme was beyond the scope of the present investigation. Even so, numerical studies of the jet trajectory calculation did indicate other areas of improvment. Some modifications were made to the code in the off-body velocity calculation and in the wake relaxation subroutines. The main change involved the integration process for proceeding from one wake grid plane to the next. Numerical stability problems were traced to an extrapolation procedure, which for regular wake relaxation calculations accelerated the convergence. The more rapid action in the jet vortex pair calculation caused some divergence. The procedure was therefore simplified to an Euler-Gauss scheme. While this slowed down the movement from iteration to iteration, the procedure is much more stable.

6.2 Results

The 6:1 simple body configuration shown in Figures 68 through 71 was utilized to examine the modified relaxed jet wake procedure available in VSAERO. The wake relaxation resulted in the characteristic kidney-shaped cross section for a jet to freestream velocity ratio of 2.0 and an angle of attack of 20 o. The pressure coefficient as a function of x along a buttline cut at the vertical plane of symmetry as presented in Figure 71 indicates a well behaved solution.

A flat plate configuration similar to the one described in Section 4.1 was employed to examine the effectiveness of the VSAERO streamwise linear vorticity jet wake model subsequent to a wake relaxation (see Figure 72). The configuration is modelled after the one used by Fearn and Weston (Ref. 24) in an extensive experimental investigation which concentrated on the characteristics of the pair of contrarotating vortices. The flat plate is at zero degrees angle of attack with the jet issuing at 900 with respect to the plate surface. A solid potential core model of

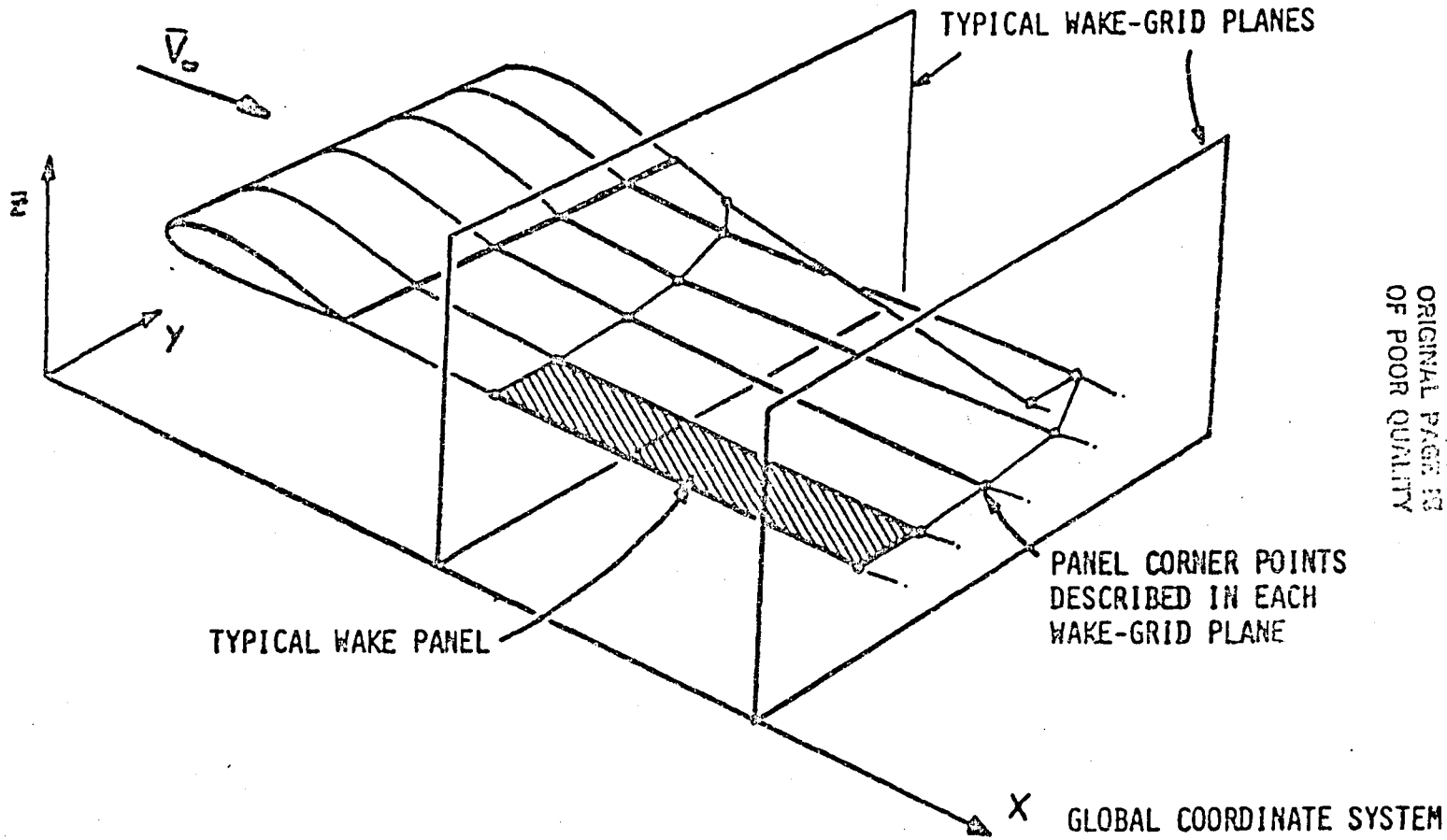

Figure 67. Wake-Grid-Plane Scheme.

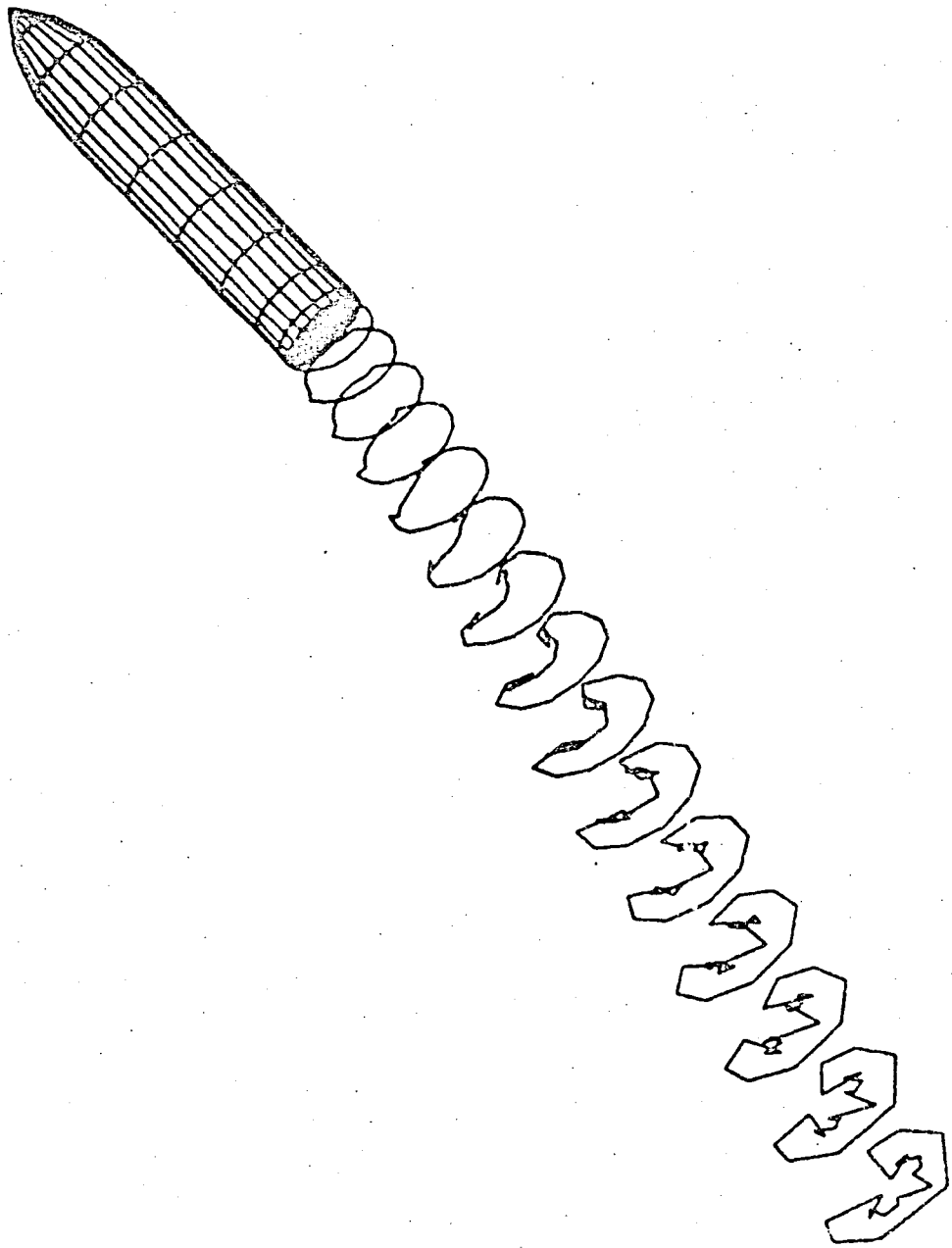

Figure 68. Type-4 Wake Test Body.

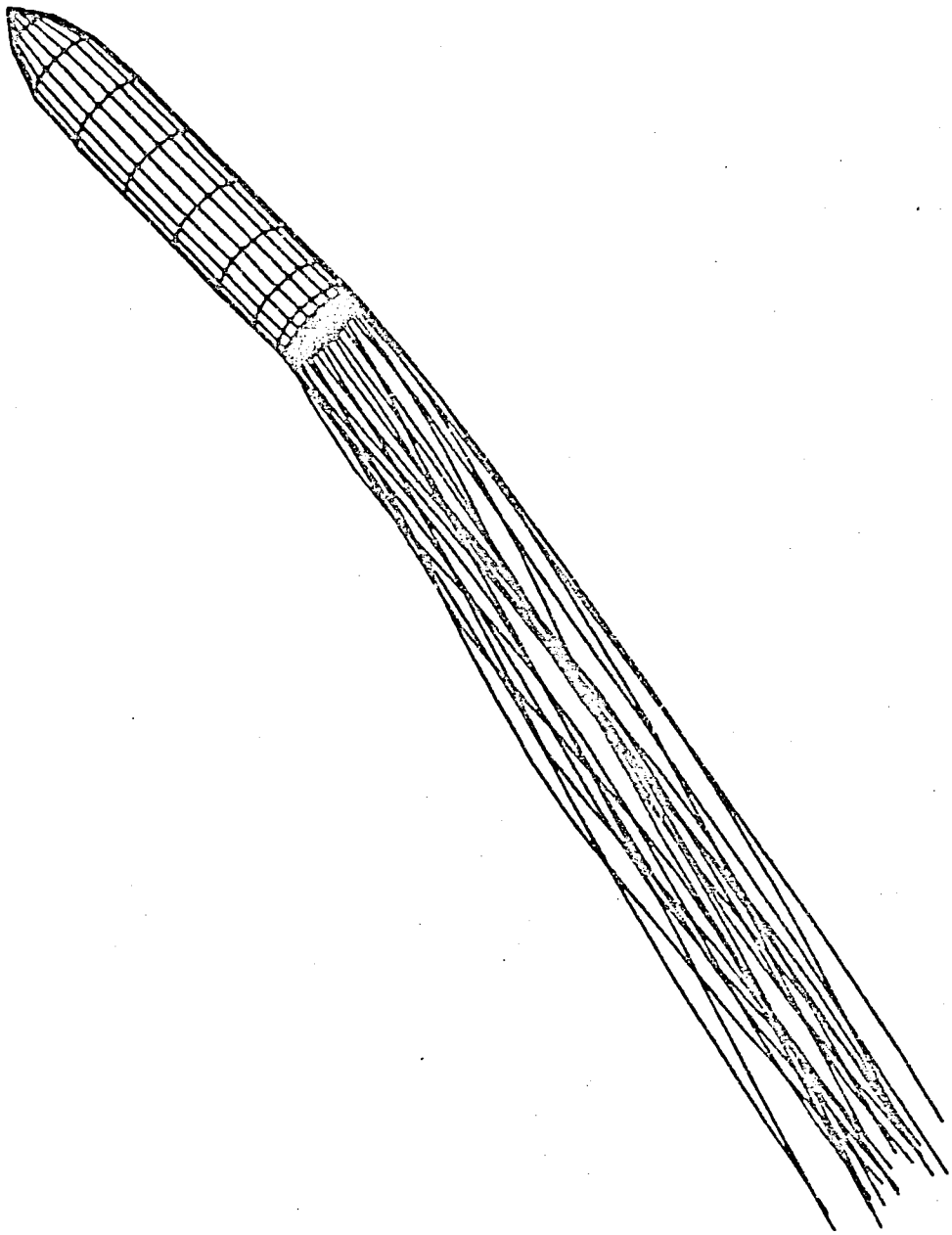

Figure 69. Type-4 Wake Test Body.

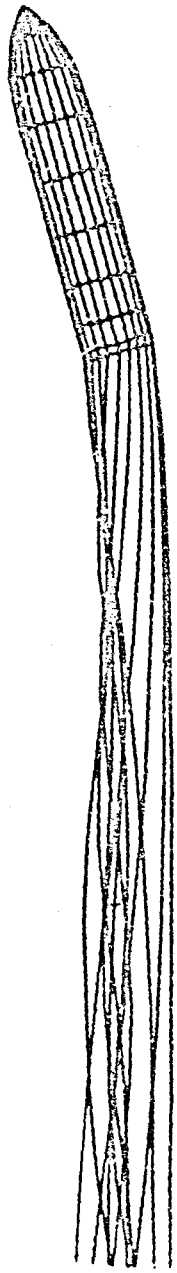

Figure 70. Type-4 Wake Test Body.

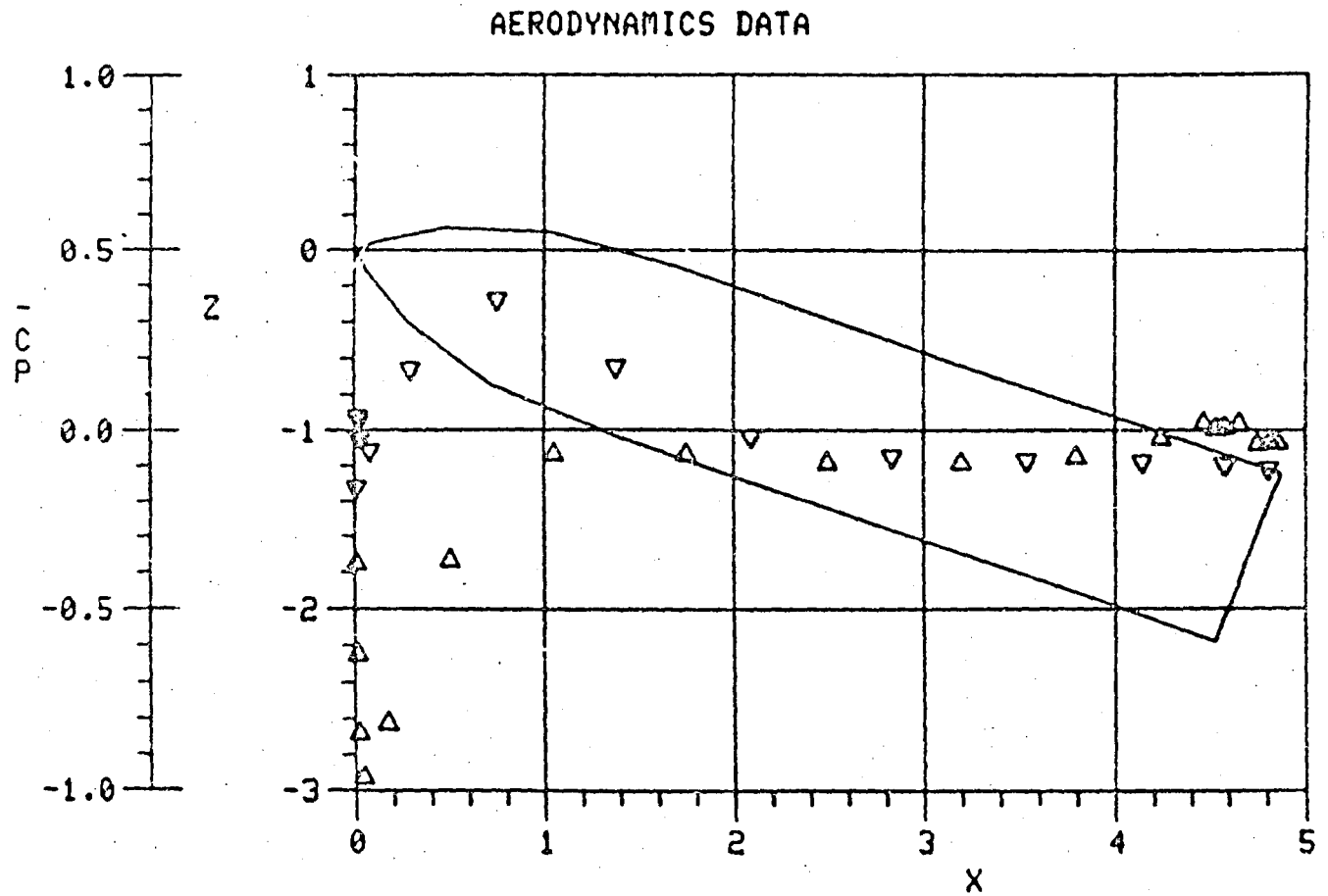

Figure 71. Type-4 Wake Test Body.

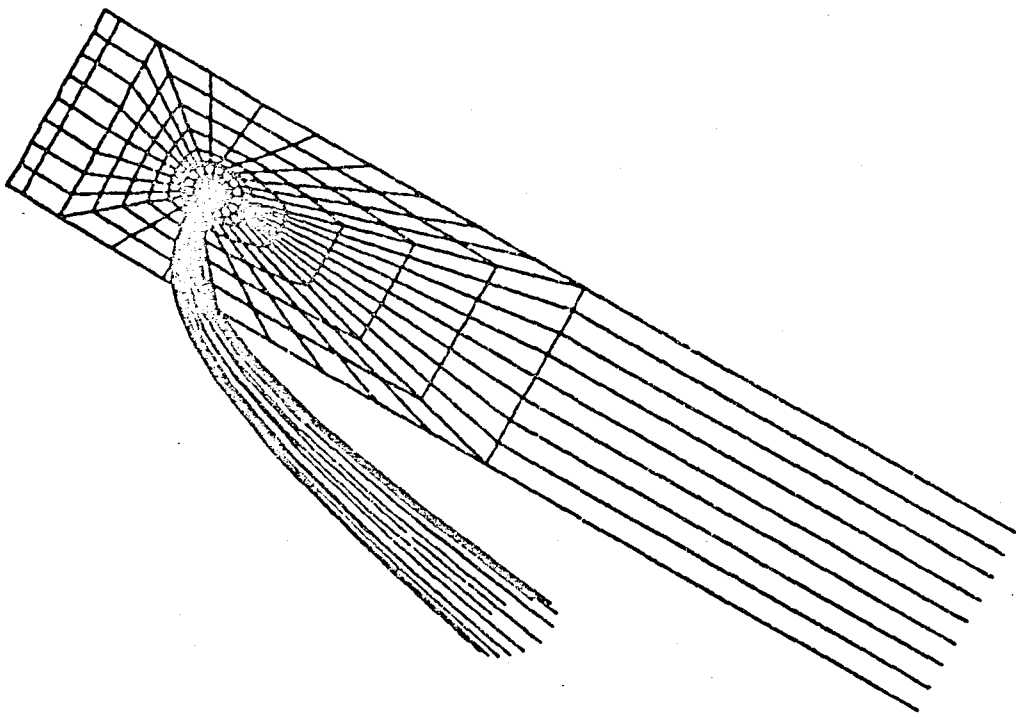

Figure 72. Flat Plate Configuration; $V_j/V_\infty = 8.0$, $\delta_j = 90$; Prescribed Jet Trajectory.

one jet diameter in height is utilized to turn the flow through 90° in the initial stages of jet development. This height is about one third as high as indicated by experiment for a jet velocity ratio of 8.

The relaxed wake geometry is compared to the prescribed jet trajectory in Figure 73 which includes the orientation of a VSAERO velocity scan plane. The scan plane was utilized to compare critical aspects of the vortex pair as calculated by VSAERO to experimental measurements and thus assess the effectiveness of the VSAERO jet model. As indicated by this figure, the entire configuration was rotated (as well as the onset flow) by 45° in order to conform to the present vertical wake-grid-plane structure.

This wake-grid-plane structure is a critical aspect of the wake geometry definition in VSAERO. In the present example the wake-grid-plane structure intersects the jet wake at angles other than the optimum of 90°, thus resulting in a distorted wake panel definition which in turn introduces numerical tabilities during the jet trajectory calculation. The jet tra ctory after one VSAERO relaxed wake calculation has deviated from the specified geometry (as generated by Margason's empirical equation), throughout the initial stages of jet development with a recovery at about 10 jet diameters downstream as indicated by Figure 73. The geometry of the cross section as shown in Figure 74 for the relaxed wake, indicates a general distortion of the jet although the characteristic kidney shape is present indicating the presence of the vortex pair. A more general scheme for the jet trajectory calculation is now being developed for the VSAERO program. This should alleviate the above dificiencies, thereby giving a more accurate relaxed jet wake geometry for cases with the wake at large angles to the crossflow.

Regardless of the deficiencies in the relaxed wake geometry, the results from the velocity scan plane are promising and support the assertion that the current VSAERO jet model contains the critical aspects present in the jet-in-crossflow problem; specifically, the swirl produced by the pair of contrarotating vortices and the strong axial velocity component of the basic jet (see Section 2.6.1). Accepting the fact that the jet trajectory has deviated from experimental results due to the wake-grid-plane structure, for comparison purposes the VSAERO scan plane results were shifted vertically to coincide with the experimental results as presented in Figures 75 and 76. Contours of constant axial velocity ratioed by the maximum centerline value at that station (V/V_{CLMAX}) are presented in Figure 75(a) in a mirror image format with respect to the experimental results. In Figure 75(b) the cross components of velocity are presented in vector form indicating the swirl activity produced by the pair of contrarotating vortices. The upper half of the VSAERO cross-component vector plot compares very well with experiment but the correlation tends

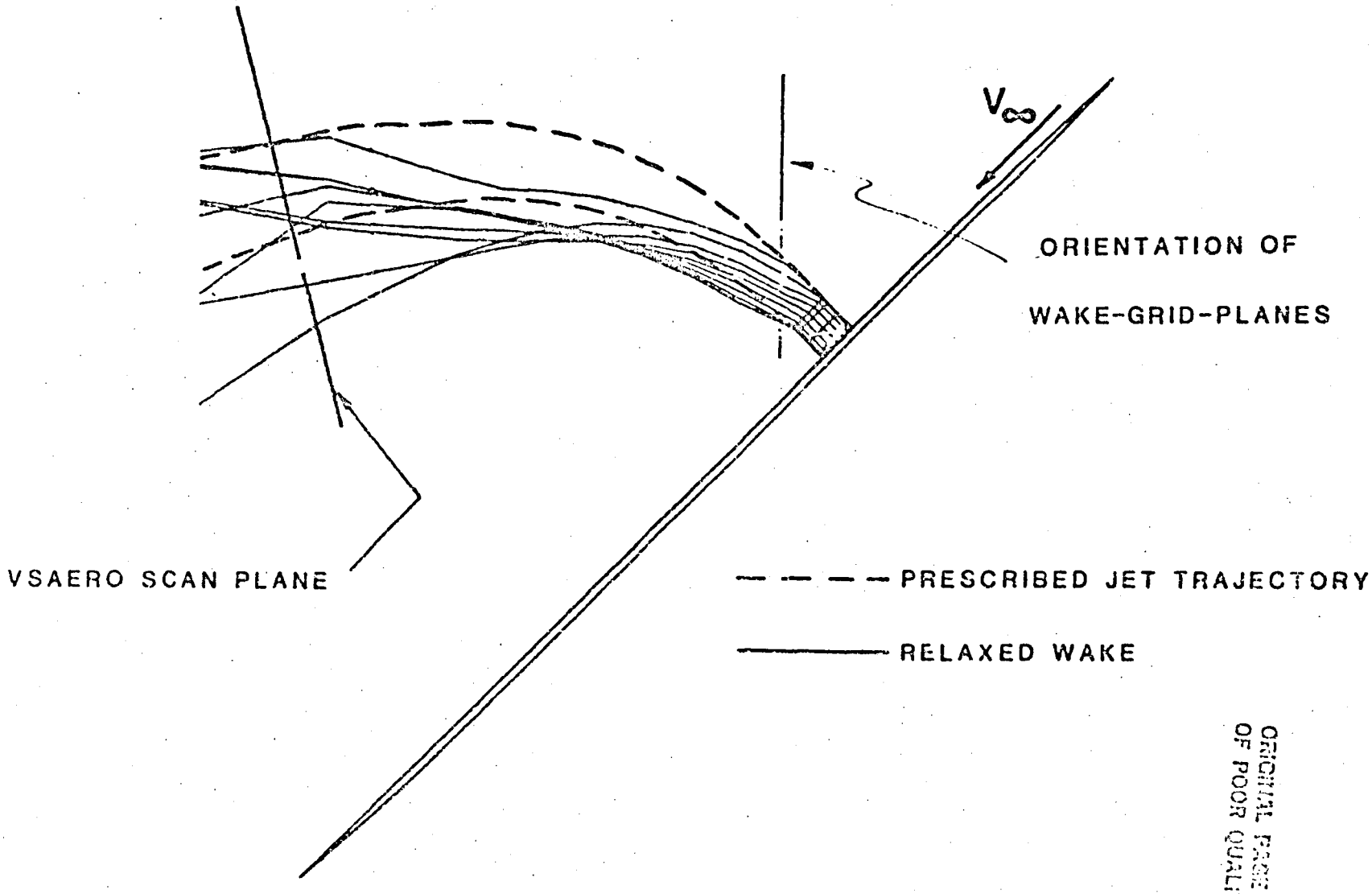

Figure 73. Flat Plate; Relaxed Wake Analysis.

Figure 74. Flat Plate Configuration; $V_j/V_\infty = 8.0$, $\delta_j = 90$; VSAERO Relaxed Wake Calculation.

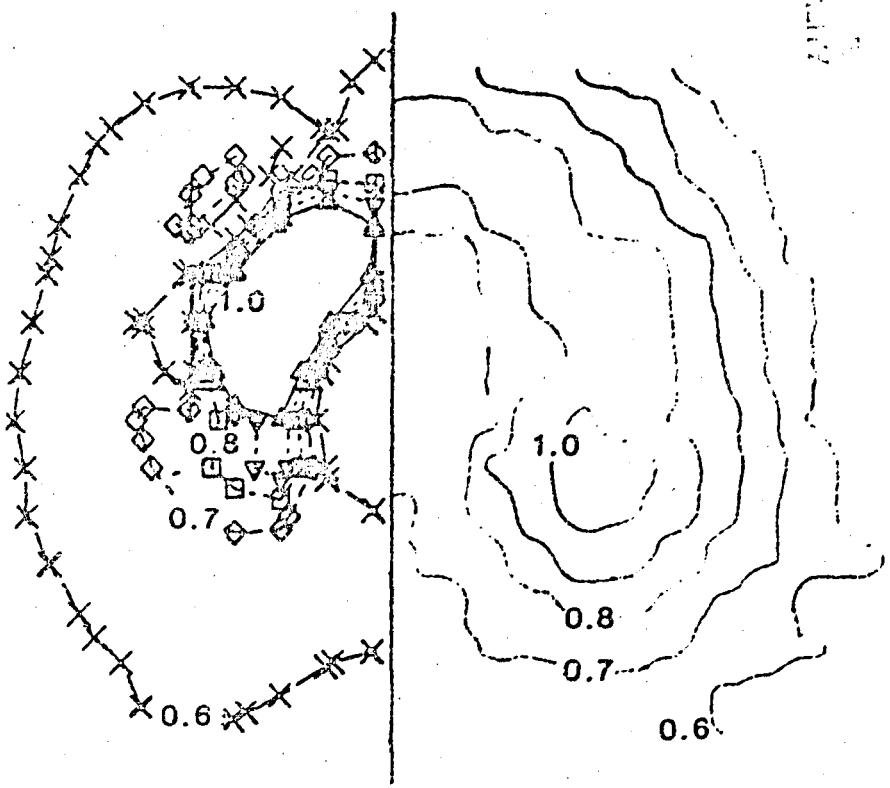

(a) Contours of Constant Axial Velocity.

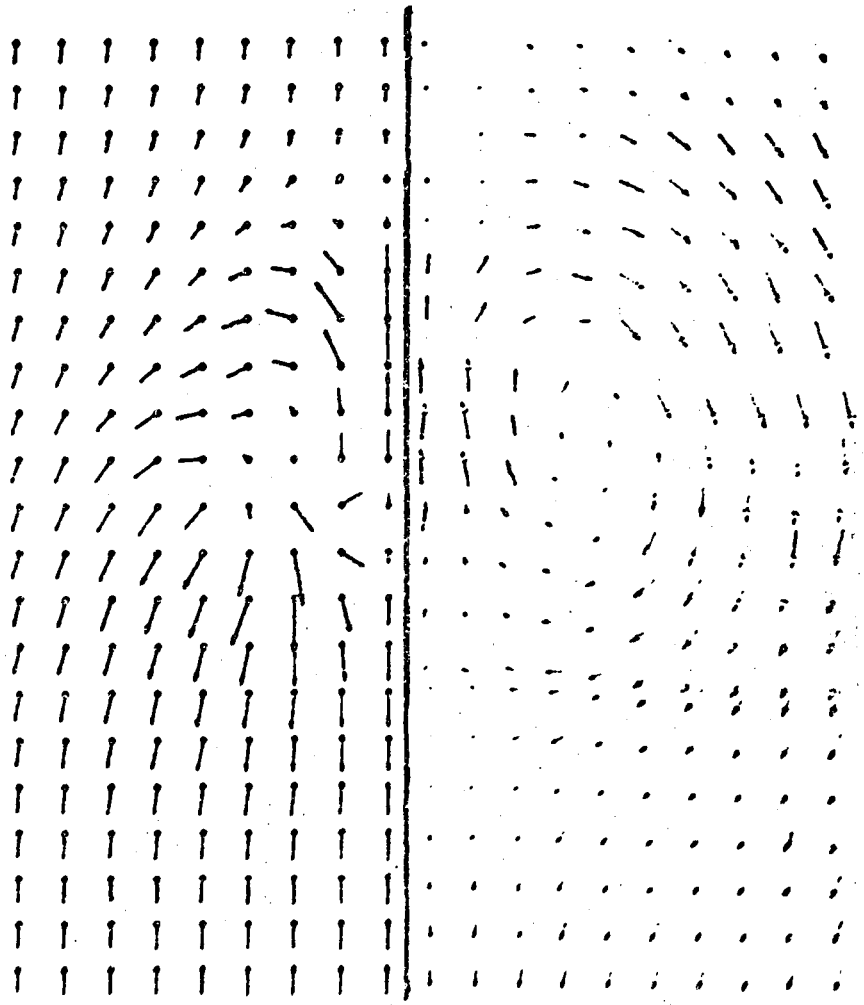

(b) Cross Components of Velocity in Vector Form.

Figure 75. Velocity Characteristics in VSAERO Scan Plane with Corresponding Experimental Results.

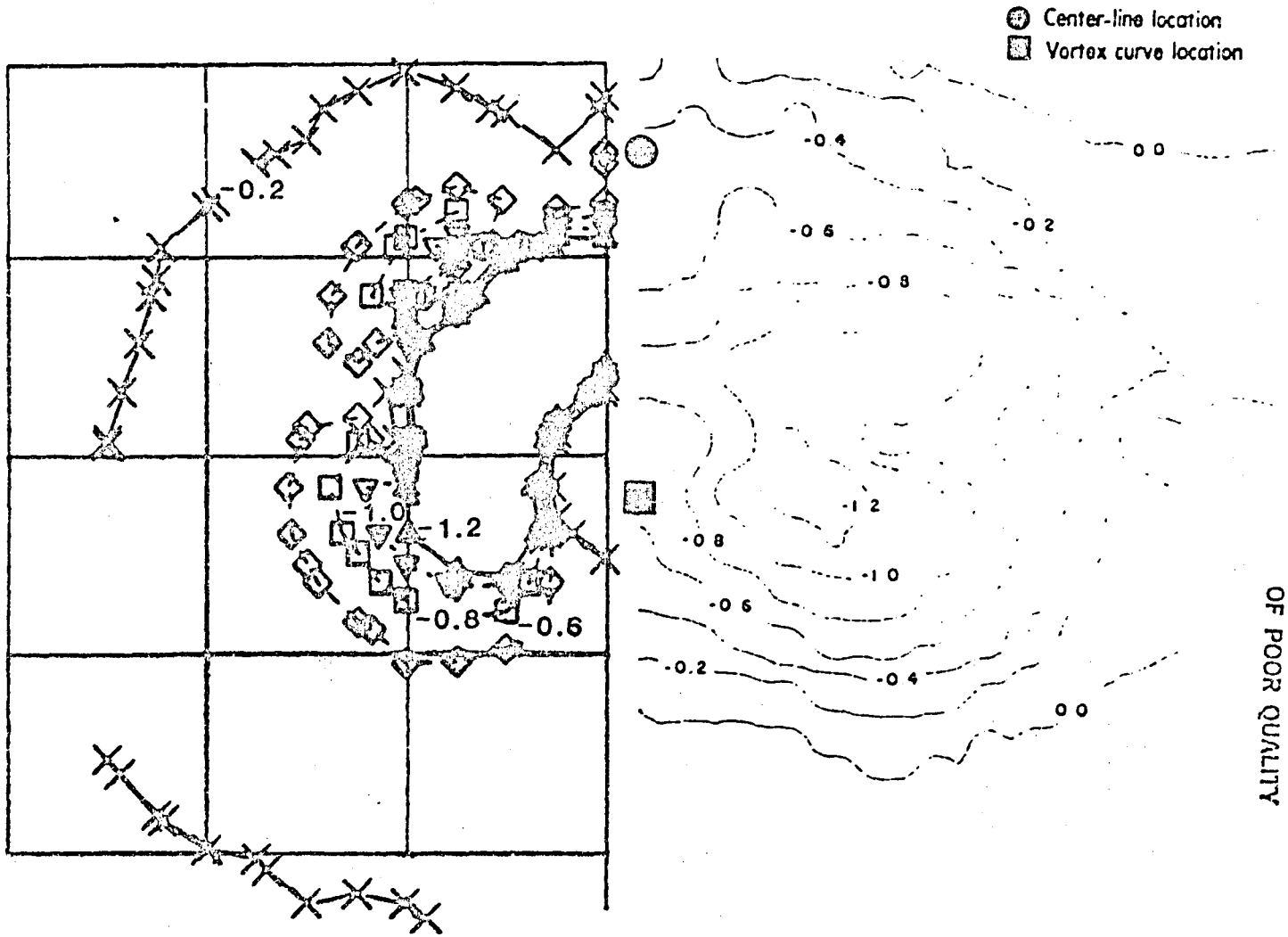

Figure 76. Flat Plate Configuration; Static Pressure Contours.

to deviate in the lower half of the plane due to the distortion of the jet cross section shown in Figure 74. Contours of constant static pressure coefficient are presented in Figure 76.

The application of VSAERO to the TF34-100 nacelle at 46.5° angle of attack and at a specific airflow setting of 0.092 (Figure 77) resulted in a realistic jet relaxation calculation as shown in Figures 78(a) and 78(b). The relaxed jet wake calculation appears to have performed very well for this rather complex coaxial jet configuration. The intersection of the coaxial jets as shown by Figure 78(b) does not appear to have adversely affected the numerical stability of the wake relaxation procedure. This wake intersection, which is apparently a consequence of the relative magnitude of the jet velocities with the inner primary jet having a larger jet velocity magnitude than the outer secondary jet, requires further study to examine the feasibility of merging the primary and secondary jets at the point of intersection.

6.3 Summary

The application of VSAERO to a series of V/STOL related configurations which exhibit the jet-in-crossflow phenomenon has resulted in the following conclusions. The vertical wake-gridplane scheme is too restrictive for jets at or near 90° with respect to the crossflow. This wake geometry definition results in a more shallow penetration of the jet into the freestream than indicated by empirical results. A more general wake geometry definition is under current study. The critical aspects of the jet-in-crossflow problem, namely the pair of contrarotating vortices and the strong axial component of velocity for the basic jet are effectively simulated by the VSAERO jet wake model.

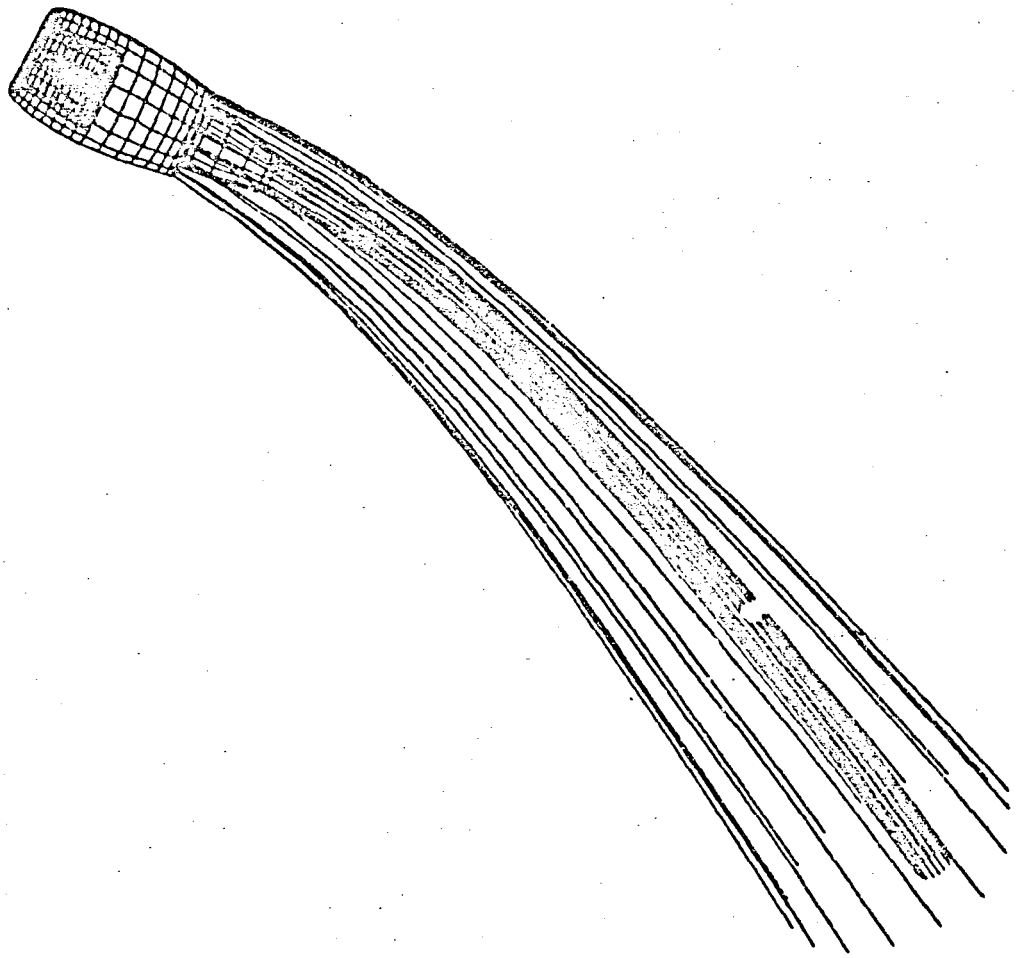

Figure 77. TF-34 Nacelle; Specified Geometry.

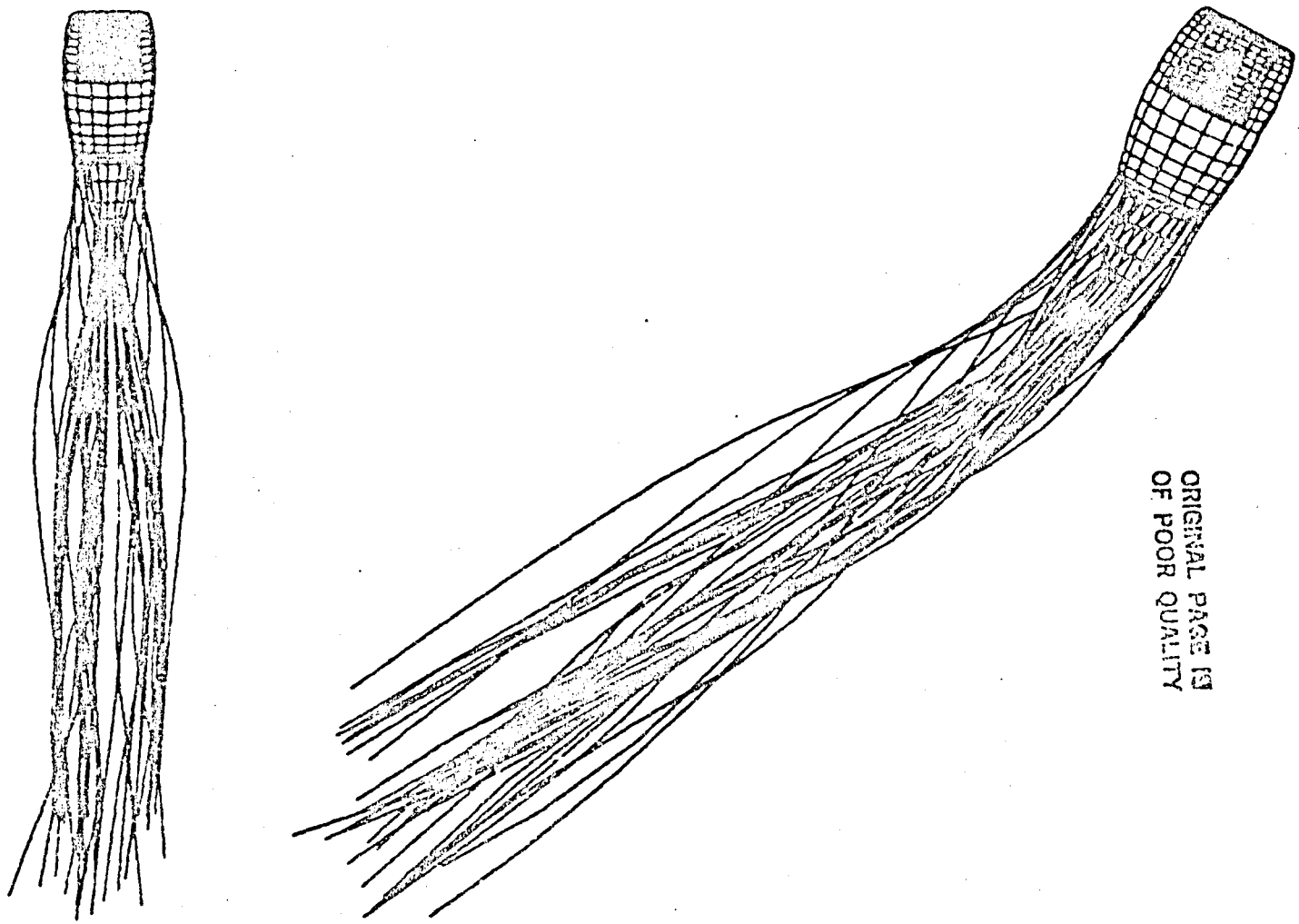

Figure 78. VSAERO Relaxed Wake Calculation with the TF-34 Nacelle at 46.5° and $W_K/A_{CAP} = 0.092$.

(a) General Views.

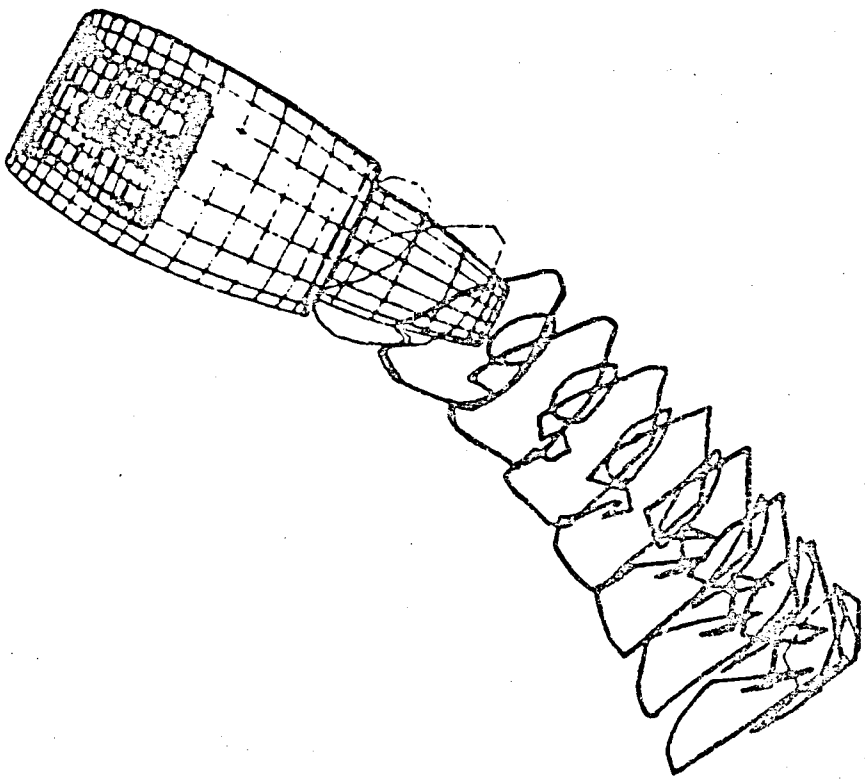

Figure 78. Concluded.

(b) Coaxial Jet Wake Cross Sections.

7.0 CONCLUSIONS

Modifications to the vortex-tube jet model in the VSAERO code have resulted in improved correlation with experimental surface pressures in the presence of a round jet leaving the surface into a cross flow. These modifications included a simple treatment of the initial "solid" core and empirical entrainment. Further, significant improvements in the correlation were obtained using a simple free vortex sheet representation of the separation behind the jet.

The jet model now in the VSAERO program provided good overall prediction of power effects on the STOL Fighter configuration. Lift increments, lift curve slope increments and pressure distribution changes due to power agreed very closely with experimental data up to 8 angle of attack covered in the calculation. The basic lift curve slope predicted by the program was lower than experiment primarily because the calculation excluded the effect of the leading-edge vortices which occur at moderate to high angles of attack on this configuration. Any future calculation beyond 8 should include leading-edge vortex modelling.

The jet model in the code is compatible with other VSAERO capabilities such as wake relaxation. The latter capability was especially important in obtaining good correlation with experimental wing pressure distributions in the presence of the canard wake on the STOL Fighter configuration. Further refinements in the jet model, particularly with respect to entrainment, is required for correct analysis of surfaces in close proximity to the jet. At that time detailed changes should be made to the panelling of the inlet and exhaust regions using inset inflow/outflow surfaces submerged in inlet/exhaust ducts and oriented normal to the local flow.

Applications of the program to the Grumman 698-411 tilt-nacelle design proved very successful. The program accurately predicted the pressure distribution inside the inlet for a range of flight conditions up through a nacelle angle of attack of 62 . Furthermore, coupled viscous/potential flow calculations gave very close correlation with experimentally determined operational boundaries dictated by the onset of separation inside the inlet. Experimentally observed degradation of these operational boundaries between nacelle-alone tests and full configuration tests were also indicated by the VSAERO calculation.

The VSAERO relaxed wake analysis for a series of V/STOL related configurations indicated that the critical aspects of the jet-in-crossflow problem, namely, the pair of contrarotating vortices and the axial component of velocity for the basic jet, are effectively simulated by the VSAERO jet wake model. Further improvements related to the VSAERO wake geometry scheme are deemed necessary when analyzing jets at large angles to the freestream.

Overall, these initial applications of the VSAERO program to V/STOL configurations have been most successful and promise further potential improvement in these aerodynamic predictions in the future. Furthermore, the exercise has demonstrated that these V/STOL calculations are both practical and economical: many of the cases were run on a PRIME 550 minicomputer while the larger cases, i.e., the full Grumman tilt-nacelle configuration, took about 2 1/2 minutes on the CRAY computer.

8.0 REFERENCES

1. Margason, R.J., "Review of Propulsion-Induced Effects on Aerodynamics of Jet/STOL Aircraft", NASA TN D-5617, February 1970.

2. Wooler, P.T., Kao, H.C. and Schwendemann, M.F., "V/STOL Aircraft Aerodynamic Prediction Methods Investigation", AFFDL TR-72-26, Vol. I-IV, January 1972.

3. Platzer, M.F., "Prediction Methods for Jet V/STOL Propulsion Aerodynamics", Naval Air Systems Command, AD-A024-023, July 1975.

4. Platzer, M.F. and Margason, R.J., "Prediction Methods for Jet V/STOL Propulsion Aerodynamics", J. Aircraft, Vol. 15, No. 2, February 1978.

5. Chapman, D.R., "Computational Aerodynamics Development and Outlook", AIAA J., Vol. 17, No. 12, December 1979.

6. Hickey, D.H., "V/STOL Aerodynamics: A Review of the Technology", Conference Proceedings on V/STOL Aerodynamics, AGARD-CP-143, April 1974.

7. Taylor, A.E. and Mann, W.R., Advanced Calculus, John Wiley and Sons, Inc., New York, 1972.

8. Hess, J.L., "Calculation of Potential Flow about Arbitrary Three-Dimensional Lifting Bodies", Douglas Aircraft Co., Report MDC J5679-01 (Contract N00019-71-C-0524), 1972.

9. Maskew, B., "Prediction of Subsonic Aerodynamic Characteristics: A Case for Low-Order Panel Methods", J. Aircraft, Vol. 19, No. 2, February 1982.

10. Magnus, A.E. and Epton, M.E., "PAN AIR--A Computer Program for Predicting Subsonic or Supersonic Linear Potential Flows about Arbitrary Configurations Using a Higher-Order Panel Method", NASA CR-3251, April 1980.

11. Boppe C.W., "Transonic Flow Field Analysis for Wing-Fuselage Configurations", NASA CR-3243, May 1980.

12. Spence, D.A., "The Lift Coefficient of a Thin, Jet-Flapped Wing", Proceedings of the Royal Society, Ser. A, Vol. 238, 1956, pp. 46-68.

13. Shollenberger, C.A., "Analysis of the Interaction of Jets and Airfoils in Two Dimensions", J. Aircraft, Vol. 10, May 1973, pp. 267-273.

14. Shollenberger, C.A., "Three-Dimensional Wing/Jet Interaction Analysis Including Jet Distortion Influences", J. Aircraft, Vol. 12, No. 9, September 1975.

15. Wooler, P.T., Burghart, G.H. and Gallagher, J.T., "Pressure Distribution on a Rectangular Wing with a Jet Exhausting Normally into an Airstream", J. Aircraft, Vol. 4, No. 6, Nov.-Dec. 1967.

16. Margason, R.J., "The Path of a Jet Directed at Large Angles to a Subsonic Free Stream", NASA TN D-4919, November 1968.

17. Fearn, R. and Weston, R.P., "Vorticity Associated with a Jet in a Cross Flow", AIAA J., Vol. 12, No. 12, December 1974.

18. Kuhlman, J.M. and Ousterhout, D.S., "Experimental Investigation of Effect of Jet Decay Rate on Jet-Induced Pressures on a Flat Plate", NASA CR-2979, April 1978.

19. Nash, J.F. and Patel, V.C., "Three-Dimensional Turbulent Boundary Layers", SBC Technical Books, 1972.

20. Peyret, R. and Viviand, H., "Computation of Viscous Compressible Flows Based on the Navier-Stokes Equations", AGARD-AG-212, 1975.

21. Wirz, H.H., "Computational Fluid Dynamics", AGARD Lecture Series No. 86, 1977.

22. Graves, R.A., Jr., "Computational Fluid Dynamics, The Coming Revolution", Aeronautics and Astronautics, March 1982.

23. Keffer, J.F., "Analysis of a Jet in a Subsonic Crosswind", NASA SP-218, Symposium held at Langley Research Center, Hampton, VA, September 9-10, 1969.

24. Fearn, R.L. and Weston, R.P., "Induced Velocity Field of a Jet in a Cross Flow", NASA TP-1087, 1978.

25. Aoyagi, K. and Snyder, P.K., "Experimental Investigation of a Jet Inclined to a Subsonic Cross Flow", AIAA/NASA Ames V/STOL Conference, Palo Alto, CA, AIAA-81-2610, December 7-9, 1981.

26. Howell, G.A., Crosthwait, E.L. and Witte, M.C., "Evaluation of Pressure and Thermal Data from a Wind Tunnel Test of Large-Scale Powered STOL Fighter Model", NASA CR-166170, June 1981.

27. Grumman Aerospace Corporation, "Full-Scale Tests of Grumman Design 698-411 Tilt-Nacelle V/STOL Model at the NASA Ames Research Center", NASA CR-166170, December 1981.

See also:

Dudley, M., Falarski, M., Pisano, A. and Hill, W., "Ground Effect Hover Characteristics of a Large-Scale Twin Tilt Nacelle V/STOL Model", AIAA/NASA Ames V/STOL Conference, AIAA-81-2609, December 1981.

Falarski, M.D., Dudley, M.R., Buchman, W. and Pisano, A., "Aerodynamic Characteristics of a Large-Scale Two Tilt-Nacelle V/STOL Model", AIAA 19th Aerospace Sciences Meeting, St. Louis, MO, AIAA-81-0150, January 1981.

28. Stoll, F. and Minter, E., Large-Scale Wind Tunnel Tests of a Sting Supported V/STOL Fighter Model at High Angles of Attack", AIAA/NASA Ames V/STOL Conference, Palo Alto, CA, AIAA-81-2621, December 7-9, 1981.

29. Minter, E.A. and Yates, R.W., "Wind Tunnel Test of a 0.4-Scale Fighter Model at High Angles of Attack--Analysis of Pressure Data", Vought Corporation, NASA CR-166-198, July 1981.

30. Abramovich, G.N., The Theory of Turbulent Jets, The M.I.T. Press, Boston, Mass., 1963.

31. Dietz, W.E., Jr., "A Method for Calculating the Induced Pressure Distribution Associated with a Jet in a Cross Flow", M.S. Thesis, Florida University, 1975.

32. Margason, R.J., Yip, L.P. and Gainer, T.G., "Recent Developments in Propulsive-Lift Aerodynamic Theory", Conference at Langley Research Center, Aerodynamic Analysis of Requiring Advanced Computers, Parts I and II, NASA SP-347, March 1975.

33. Margason, R.J., "Effects of Jets, Wakes and Vortices on Lifting Surfaces", NASA TMX-73974, November 1976.

34. Tulinius, J.R. and Margason, R.J., "Aircraft Aerodynamic Design and Evaluation Methods", AIAA Paper 76-15, Washington, D.C., 1976.

35. Fearn, R.L. and Weston, r.P., "Induced Pressure Distribution of a Jet in a Cross Flow", NASA TND-7616, 1975.

36. Kamotani, Y. and Greber, I., "Experiments on a Turbulent Jet in a Cross Flow", NASA CR-72893, June 1971.

37. Oustcchout, D.S., "An Experimental Investigation of a Cold Jet Emitting from a Body of Revolution into a Subsonic Free Stream", NASA CR-2089, August 1972.

38. Ricou, F.P. and Spalding, D.B., "Measurements of Entrainment of Axisymmetrical Turbulent Jets", J. Fluid Mech., Vol. 11, 1961, pp. 25-32.

39. Monical, R.E., "A Method of Representing Fan-Wing Combinations for Three-Dimensional Potential Flow Solutions", J. Aircraft, Vol. 2, No. 6, Nov.-Dec. 1965.

40. Ziegler, H. and Wooler, P.T., "Multiple Jets Exhausting into a Cross Flow", J. Aircraft, Vol. 8, No. 6, July 1971.

41. Kamotani, Y. and Greber, I., "Experiments on a Turbulent Jet in a Cross Flow", AIAA J., Vol. 10, No. 11, November 1972.

42. Keffer, J.F. and Baines, W.D., "The Round Turbulent Jet in a Crosswind", J. Fluid Mech., Vol. 15, 1963, pp. 481-496.

43. Pratte, B.D. and Baines, W.D., "Profiles of the Round Turbulent Jet in a Cross Flow", J. Hydraulics Div., Proceedings of the ASCE, Vol. 92, No. HY6, November 1967, pp. 53-64.

44. Mikolowsky, W. and McMahon, H., "An Experimental Investigation of a Jet Issuing from a Wing in Cross Flow", J. Aircraft, Vol. 10, No. 9, September 1973.

45. Dvorak, F.A., Maskew, B., and Woodward, F.A., "Investigation of Three-Dimensional Flow Separation on Fuselage Configurations", USAAMRDL-TR-77-4", Eustis Directorate, U.S. Army Air Mobility Research and Development Laboratory, Fort Eustis, VA, 23604, March 1977.

46. Vaidyanathan, T.S., "A Flow Field Analysis Procedure Based upon Velocity Potentials", Paper submitted for presentation at the AIAA Applied Aerodynamics Conference, Danvers, Mass., July 13-15, 1983.

47. Bradley, R.G., Jeffries, R.R., and Capone, F.J., "A Vectored-Engine-Over-Wing Propulsive Lift Concept", AIAA Paper No. 76-917, September 1976.

48. Falarski, M.D., Whitten, P.D., and Haris, J.J., "Aerodynamic Characteristics of a Large-Scale Model of a Highly Manerverable Supersonic V/STOL Fighter: STOL Configuration", AIAA 80-0234, January 1980.

49. Falarski, M., Dudley, M. and Howell, G., "Analysis of Data from a Wind Tunnel Investigation of a Highly Maneuverable Supersonic V/STOL Fighter: STOL Configuration", AIAA/NASA Ames V/STOL Conference, AIAA-81-2620, December 1981.

50. Harris, M.J. and Falarski, M.D., "Static Calibration of a Two-Dimensional Wedge Nozzle with Thrust Vectoring and Spanwise Blowing", NASA TM-81161, 1980.

1. Report No.	2. Government Accession No.	3. Recipient's Catalog No.
NASA CR-166479		

4. Title and Subtitle	5. Report Date
INVESTIGATION OF ADVANCE PREDICTION TECHNIQUES OF THE LOW-SPEED AERODYNAMICS OF V/STOL AIRCRAFT	February 1983
	6. Performing Organization Code
7. Author(s)	8. Performing Organization Report No.
B. Maskew, D. Strash, J. Nathman and F. A. Dvorak	8302
	10. Work Unit No.
9. Performing Organization Name and Address	T-5520
Analytical Methods, Inc. 2047 - 152nd Avenue N.E. Redmond, WA 98052 (206) 643-9090	11. Contract or Grant No. NAS2-11169
	13. Type of Report and Period Covered
12. Sponsoring Agency Name and Address	Contract Report
NASA Ames Research Center Moffett Field, CA 94035	14. Sponsoring Agency Code 505-43-01

15 Supplementary Notes

Point of Contact: Technical Monitor, Michael R. Dudley, MS 247-1
Ames Research Center, Moffe-t Field, CA 94035
(415) 965-5046 or FTS 448-5046

16 Abstract

A computer program, VSAERO, has been applied to a number of V/STOL configurations with a view to advancing prediction techniques for the low-speed aerodynamic characteristics. The program couples a low-order panel method with surface streamline calculation and integral boundary layer procedures The panel method--which uses piecewise constant source and doublet panels--includes an iterative procedure for wake shape and models boundary layer displacement effect using the source transpiration technique. Certain improvements to a basic "vortex tube" jet model were installed in the code prior to evaluation.

Very promising results were obtained for surface pressures near a jet issuing at 90° from a flat plate. A solid core model was used in the initial part of the jet with a simple entrainment model. Preliminary representation of the downstream separation zone significantly improved the correlation

The program accurately predicted the pressure distribution inside the inlet on the Grumman 698-411 design at a range of flight conditions. Furthermore, coupled viscous/potential flow calculations gave very close correlation with experimentally determined operational boundaries dictated by the onset of separation inside the inlet. Experimentally observed degradation of these operational boundaries between nacelle-alone tests and tests on the full configuration were also indicated by the calculation.

Application of the program to the General Dynamics STOL fighter design were equally encouraging. Very close agreement was observed between experiment and calculation for the effects of power on pressure distribution, lift and lift curve slope. In an absolute sense the basic lift curve slope predicted by the program was lower than experiment, primarily because the leading-edge vortices, which occur at the higher angles of attack were not modelled at this stage. The wake-relaxation capability in the VSAERO code was especially important in obtaining good correlation with experimental wing pressure distributions in the presence of the canard wake.

Overall, these initial applications of the VSAERO program to the prediction of aerodynamic characteristics of V/STOL configurations has been most successful and promise further potential improvements in the future. Furthermore, it has been demonstrated that these V/STOL calculations are both practical and economical in computing time.

17. Key Words (Suggested by Author(s))	18. Distribution Statement
None	[illegible] ors

19. Security Classif. (of this report)	20. Security Classif. (of this page)	21. No. of Pages	22. Price*
Unclassified	Unclassified	141	

[illegible]

END

DATE

FILMED

JUL 1 1986

End of Document